Thermodynamics of the carbon dioxide plus argon (CO_2 + Ar) system: An improved reference mixture model and measurements of vapor-liquid, vapor-solid, liquid-solid and vapor-liquid-solid phase equilibrium data at the temperatures 213 to 299 K and pressures up to 16 MPa

Sigurd Weidemann Løvseth[a,*], Anders Austegard[a], Snorre Foss Westman[a], Hans Georg Jacob Stang[a]

Stefan Herrig[b], Tobias Neumann[b], Roland Span[b]

[a]*SINTEF Energy Research, Postboks 4761 Torgarden, NO-7465 Trondheim, Norway*

[b]*Thermodynamics, Ruhr-Universität Bochum, Universitätsstr. 150, 44780 Bochum, Germany*

Abstract

Phase equilibrium behavior of the carbon dioxide and argon system has been investigated at the temperatures 213, 223, 243, 263, 273, 283, and 299 K. The full vapor-liquid equilibria phase envelope has been measured at all temperatures using an analytical technique where the compositions of both the liquid and vapor phase have been measured. In addition, the fluid compositions at the three-phase line and phase equilibria involving solids at 213 K have been measured. The three-phase line was determined at 213 K with an estimated uncertainty of 2 kPa. Otherwise, the estimated uncertainty is better than 13 mK for the temperature measurements, 3.2 kPa for the pressure measurements, and 0.12 % in total combined uncertainty in terms of mole fraction for all the 107 measured data points. The new data have been compared with existing models, and estimates for the critical points of the 7 isotherms have been made. Together with recently established experimental results for homogeneous density, speed of sound, and dew-point pressure, the vapor-liquid-equilibrium data were used to develop an improved Helmholtz-energy-explicit mixture model. This new model enables the calculation of highly-accurate data for all types of thermodynamic properties. Its development is part of the ongoing work on setting up an extended multi-fluid mixture model for the description of carbon-dioxide-rich mixtures with various impurities as relevant for CCS applications.

Keywords:

phase equilibrium, measurements, fundamental equation of state, carbon dioxide, argon, CO_2 capture and storage

1. Introduction

The properties of CO_2 with impurities have received interest over the last decade, primarily due to the desire to realize CO_2 capture, transport, and storage (CCS) as a major mitigation measure against anthropic global warming. According to the IEA, as much as 6.4 Gt CO_2 should be captured annually in 2050 in order to fulfil the 2 degree / 450 ppm scenario [1]. Cost is a major barrier to realize CCS. At the same time, unforeseen breakdown of vital components, or, worse, accidents in early phases could bar further deployment of CCS. Hence, both design and operation of a range of CCS processes should be optimized in robust manner, which requires accurate thermodynamic property data at all relevant conditions.

Impurities will be present in all processes of CCS [2]. In capture, impurities will result from e.g. the exhaust to be enriched in CO_2 or absorbents. Depending on the level of purification of the CO_2 product, some of these impurities will be transported and injected into the storage site, where the CO_2 product interacts with the fluids already present in the reservoir. It is well known that impurities can have a range of negative impacts on CCS transportation, injection, and storage. For instance, relatively small concentrations of water, in particularly in presence of other impurities [3-5], can cause corrosion [6] or formation of

* Corresponding author.

E-mail address: Sigurd.W.Lovseth@sintef.no

hydrates [7-9], whereas non-condensable gases generally cause an increase in the compression costs due to lower density and higher required pressure to avoid two-phase flow [10, 11]. In principle, impurities can be purified to a level where their impact on CO_2 transport is negligible, but this is not likely to be economical optimal, and, as mentioned, impurities will in any case have to be taken into consideration during CO_2 capture and injection / storage.

Thus, fluid models for CO_2-rich mixtures with relevant components are crucial to provide the thermodynamic state properties needed to realize CCS. The most accurate models for mixtures with such a highly non-ideal mixing behavior are empirical multiparameter equations of state explicit in the reduced Helmholtz energy. The development of a first reference CCS-mixture model based on this approach was completed in 2013. The model was later on presented by Gernert and Span [12] as the "equation of state for combustion gases and combustion gas like mixtures" (EOS-CG). Its mathematical structure enables the calculation of multicomponent-mixture properties by modelling each binary combination of the components. Hence, data on binary mixtures are particularly important in order to fit the binary interaction terms. Nevertheless, the models also have to be verified through measurements of multicomponent mixtures.

As recent reviews have revealed, the data situation is far from satisfactory for a number of properties and mixtures relevant for CCS [12-15]. Hence, SINTEF Energy Research has constructed, in cooperation with partners of the CO_2Mix project [11, 16], a facility to accurately measure phase equilibria of CO_2-rich mixtures with compositions and at conditions relevant for CCS [17]. The focus has so far been on vapor-liquid equilibria (VLE) of binary mixtures between CO_2 and non-condensable gases such as nitrogen [18], oxygen [19], methane[20], and carbon monoxide [21].

In this work, new experimental phase equilibria data on binary mixtures of carbon dioxide and argon are presented. Argon is an important impurity from various capture processes, in particularly in oxy-fuel plants, where there can be several percent of Ar in the CO_2 product prior to additional purification steps [22]. Most of the data are on VLE, but, in addition, phase equilibria involving dry ice have been measured at 213 K. More specifically, new data are provided for frost points or vapor-solid equilibria (VSE), freezing points or liquid-solid equilibria (LSE), and three-phase line at vapor-liquid-solid equilibria (VLSE). Knowing the limit at which dry ice forms is very important for optimized design and operation of liquefaction and low temperature separation processes, as freeze-out may plug equipment. Knowledge of the freeze-out behavior is also very important in order to build models for intentional or accidental depressurization of for instance pipelines [23]. The amount of thermodynamic data of solid CO_2 is very limited [24]. Most of the data on phase equilibria between dry ice and binary mixtures with CO_2 is for CO_2 methane mixtures with low CO_2 content in the fluids and hence at lower temperatures than would be relevant for CCS [23]. No previous freeze-out data for CO_2 + Ar mixtures have been found in the public domain, except two data points below 116 K [25], which is far below the temperatures expected in CCS systems.

Based on the new VLE data an improved Helmholtz-energy-explicit mixture model for CO_2 + Ar has been developed at Ruhr-University Bochum (RUB). This new model replaces the existing binary correlation within the EOS-CG. The refit of the model for CO_2 + Ar is part of the ongoing work to extend and update the EOS-CG, which is considered as the reference model for CCS-relevant mixtures. The quality of the model presented here is additionally enhanced by accurate new measurements of homogeneous densities, speeds of sound, and dew-point pressures [26-30].

In Section 2 of this article the experimental methods are presented, before the experimental results, including data and related uncertainty analysis, are presented in Section 3. In Section 4, analysis of the new data and a comparison with existing literature data and models are provided. This Section includes estimation of critical points using a scaling law model as well as fitting a Peng-Robinson cubic equation of state with mixing rules by Wong and Sandler to the new phase equilibrium data. In Section 5, the new multiparameter mixture model for CO_2 + Ar is presented, taking into account all known thermodynamic data for the system.

2. Experimental methods

The measurements have been performed using an accurate setup designed specifically for mixtures and conditions relevant for CCS, illustrated in Fig. 1. An analytical isothermal method has been employed. The equilibrium cell consists of a sapphire tube between two titanium flanges. The temperature of the equilibrium cell of the 100 ml cell is controlled using thermostatic baths and measured using standard platinum resistance thermometers (SPRTs) located in the top and bottom flange. The cell contents and the total composition are controlled using pumps for injection and valves at the bottom and top of the cell. The resulting pressure is measured using and array of pressure sensors separated from the cell content by a membrane and a differential pressure sensor. To

accelerate the relaxation towards equilibrium, the cell is equipped with a magnetic stirrer. Fluid phase compositions at nominal equilibrium conditions are measured by sampling and analysis using a gas chromatograph (GC) with thermal conductivity detector (TCD), using purpose specific integration and calibration methods.

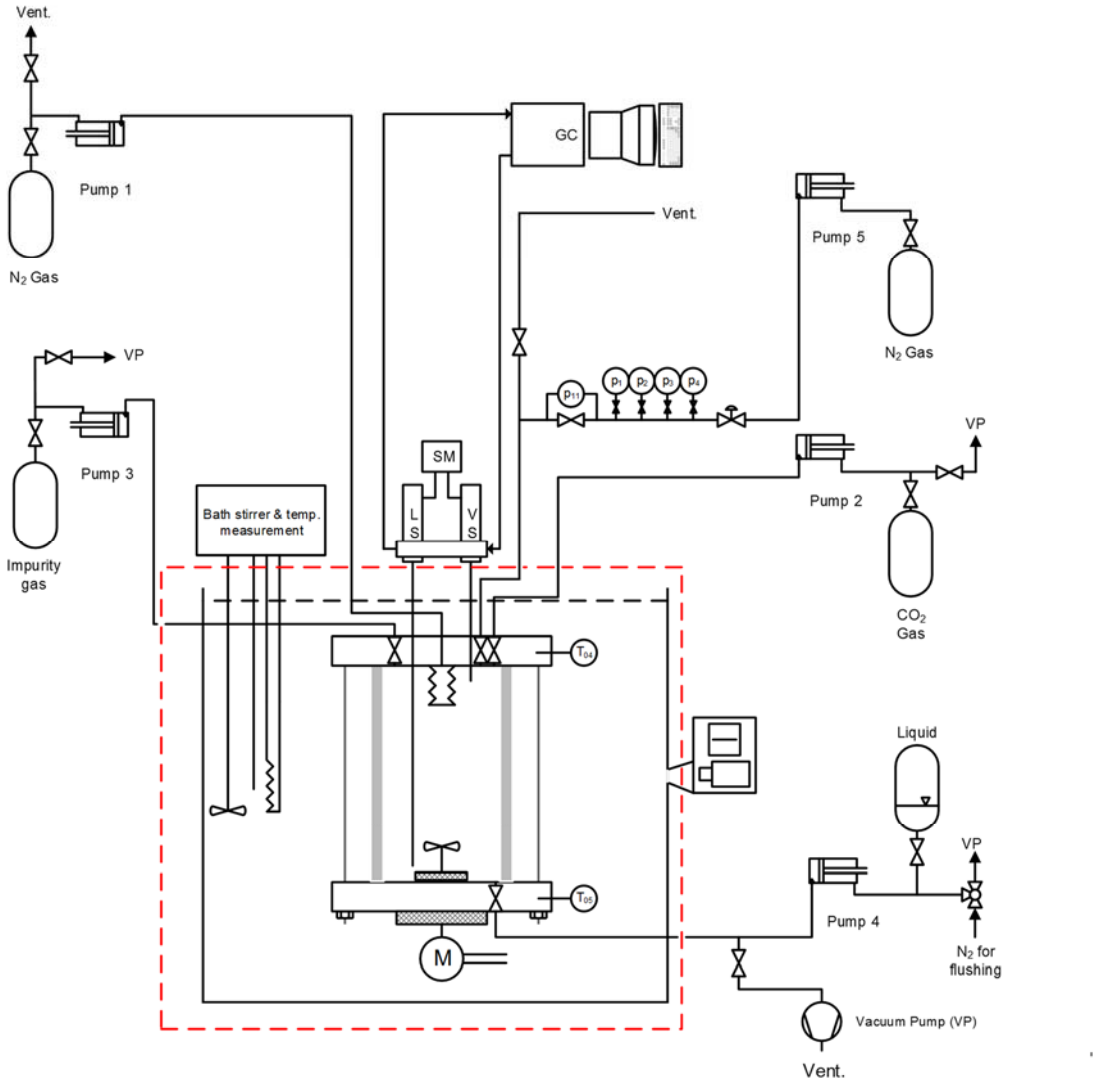

Fig. 1: Schematic diagram of experimental setup [18, 19]

The setup and methods used to produce the vapor-liquid equilibrium (VLE) data and calibration of the various systems of the current work are identical to what have been described in [17-19], and further details will not be repeated here, with a few notable exceptions to be discussed in the following Sections 2.1-2.4. The same setup was also used to measure vapor-solid (VS), vapor-liquid-solid (VLS), and liquid-solid (LS) equilibria, requiring some additional procedures described in Section 2.5.

2.1. Pressure control

A favorable feature of the setup is, however, the ability to avoid pressure loss due to sampling using a 1 ml bellows. Unfortunately, the bellows broke for a period, and the isotherms at 223 and 273 K and most data points at 213 K were measured without pressure compensation, during which the bellows was substituted with a plug.

2.2. Sampling procedure

The sampling procedures were slightly modified compared to previously reported work [18, 19]. After the isothermal temperature has been reached, and cell content injected, the cell is stirred until the pressure has stabilized within experimental uncertainty. The stabilization period was normally around 30 minutes, but was as high as 100 hours at the three-phase line, as will be discussed in Section 3.3.3. The samplers are then flushed, followed by another, but shorter, stabilization period before the extraction of flushing and

measurement samples following the routine described in [18, 19]. The first extra flushing step, which was used in most of the measurements in the current work, was not included in the earlier published measurements using this setup [18, 19]. The advantage is increased safety margin in the latter two flushing samples as the composition in the sampler already would be similar.

The number of measurement samples for each temperature and pressure point for the isotherms at 273, 223, and for most data points at 213 K was increased to 8 in order to partly compensate for the lack of pressure compensation at these temperatures.

2.3. Source gases

The gases used to make the calibration mixtures and used in the VLE measurements are listed in Table 1. Helium was used as carrier gas for the GC. No further purification or treatment of the source gases was performed

2.4. Calibration of composition measurements

The VLE measurements of CO_2 + Ar followed immediately after the measurements of $CO_2 + O_2$ were completed, and no additional calibration were performed on the temperature and pressure measurement systems. These systems have been proven fairly stable, and as will be discussed in Section 3.3.2, the impact of temperature and pressure measurement uncertainty generally is significantly smaller than the impact of the uncertainty in composition.

The calibration of the composition measurements was carried through in a similar manner to what was described in [18]. 6 binary CO_2 + Ar calibration mixtures spanning the composition range of interest were gravimetrically prepared with high accuracy. The GC response of these calibration gases were investigated by extracting a number of samples of each mixture from the cell. The areas of the resulting chromatogram peaks of the two components were recorded using a carefully designed integration technique. The various samples varied in mass, and hence areas, covering the range estimated for the phase equilibrium measurements. These data were used to fit a calibration function of identical functional form to what was used in [18]:

$$k\hat{n}_{\mathrm{CO_2}} = A_{\mathrm{CO_2}} + 0.001c_1(A_{\mathrm{CO_2}})^{c_2}, \quad (1a)$$

$$k\,\hat{n}_{\mathrm{Ar}} = c_3 A_{\mathrm{Ar}} + 0.001c_4(A_{\mathrm{Ar}})^{c_5}, \quad (1b)$$

$$\hat{y}_{\mathrm{CO_2,cal}} = \frac{\hat{n}_{\mathrm{CO_2}}}{\hat{n}_{\mathrm{CO_2}} + \hat{n}_{\mathrm{Ar}}}. \quad (1c)$$

The parameters c_i with $i = 1 \ldots 5$ were fitted by performing a weighted least squares minimization of the objective function described by Eq. (A.32) in [18]. Separate fits were made for the liquid and vapor phase samplers.

Table 1: Specifications of single component mixtures used in the experiments.

Chemical name	CAS #	Source	Purification method	Final mole fraction purity	Analysis method
Carbon dioxide	124-38-9	AGA	None	0.999993	None
Argon	7440-37-1	AGA	None	0.999999	None
Helium	7440-59-7	AGA	None	0.999999	None

2.5. Equilibria with solid phase present and their investigation

One of the isotherms measured was at 213 K, which is below the triple point of pure CO_2. Hence, at this temperature, dry ice will occur at most pressures with high enough CO_2 content. However, according to Gibbs phase rule, all degrees of freedom are spent if gas, liquid, and solids phases are present simultaneously, and hence this condition can only occur at a single pressure per isotherm, the three-phase line pressure. Below this pressure, only gas phase and solid phase can occur at equilibrium. At higher pressures, only liquid phase can coexist with the solid phase. In the current work, the three-phase pressure and compositions were determined at 213 K. Above the three-phase line pressure, vapor-liquid equilibria were measured using similar procedures as in the VLE measurements of the other isotherms. In addition, two melting points (LSE), i.e. liquid in equilibria with dry ice, were measured. Unlike VLE, the liquid phase in this case was sampled using the sampling capillary normally used for the vapor phase located in the upper flange. Below the 213 K three-phase pressure frost points (VSE), i.e. vapor in equilibrium with dry ice, were measured.

The equilibria measurements with solids were greatly aided by the ability to inspect the cell content using a borescope in the thermostatic bath. Prior to these measurements, CO_2 was

injected a few Kelvin above the triple point temperature until a small amount of liquid formed inside the cell. The stirrer was running while the cell subsequently was cooled down to 213 K. This procedure ensured that the stirrer did not become stuck in dry ice. For all measurements of solids, the presence or absence of solids was confirmed by visual inspection using the borescope before sampling was initiated. The composition measurement of the fluid phases followed the routines used for VLE, although, the time needed to stabilize the pressure was longer for measurements involving solids compared with other states. As will be further discussed in Section 3.3.3, this was particularly true at the three-phase line.

3. Experimental results and uncertainty

3.1. Summary of data

Phase equilibria have been measured at seven different temperatures in this work, at the temperatures at 213, 223, 243, 263, 273, 283, and 299 K, and up to 16 MPa. The VLE and LSE liquid mixture data are provided in Table 2 and 3, respectively, whereas the VLE and VSE vapor data are provided in Table 4 and 5. The three-phase line data at 213 K are provided both in Table 2 and 3 for the liquid phase and Table 4 and 5 for the vapor phase, as all the fluid phase curves investigated end there. Finally, in Table 6, the vapor pressure of pure CO_2 is provided for the investigated temperatures. In total 49 liquid and 58 vapor phase equilibrium points are provided. For each data point, the temperature, $\bar{T}_f$, pressure, $\bar{p}_f$, and CO_2 mole fraction of the fluid phases, $\bar{x}_{CO_2}$ for the liquid phases and $\bar{y}_{CO_2}$ for the vapor phases, are provided. In addition, the uncertainties for the different measurands, as well as the total uncertainty in terms of composition, $u_{tot}(\bar{x}_{CO_2})$ or $u_{tot}(\bar{y}_{CO_2})$ are provided. The nomenclature is identical to Refs. [18, 19] except for composition uncertainties to be discussed in 3.3 and some new terms in Table 6 to be discussed in Section 3.4.

The tabulated data are plotted per isotherm in Figs. 2–8. As seen, for all the 7 VLE isotherms the VLE full phase envelopes have been well covered. At 213 K, the frost point curve of the VSE below the three-phase line has been fully covered. Two SLE freezing points have been covered, up to a maximum pressure of 16 MPa.

As mentioned in Section 2.1, the pressure was controlled during sampling for most of the phase equilibrium measurements using a bellows, but not for the isotherms at 232 and 273 K and most data points at 213 K. It has been indicated in the data tables when the bellows have not been used.

In general, the selection of data points for VLE have been performed such that the parts of the isotherm VLE that are most difficult to model and describe have received most attention. That means there for each isotherm is a higher density of data points close to the critical point and in the region with largest curvature, i.e. in the region of the phase envelopes with lowest CO_2 content / retrograde condensation.

3.2. Composition measurement calibration

3.2.1. Reference gas mixtures

The estimated mole fractions of 6 gravimetrically prepared reference gas mixtures sampled from the VLE in order to calibrate composition measurements of this work are provided in Table 7. In the same table, uncertainty contributions and combined uncertainties of these estimated compositions are provided as well. $y_{CO_2,cal}$ is the estimated composition, $u(y_{CO_2,cal}, m)$ is the uncertainty in mole fraction due to the gravimetric preparation, $u(y_{CO_2,cal}, M_{eff})$ is the uncertainty in mole fraction due to uncertainty in molar mass. $u(y_{CO_2,cal}, \text{ads.})$ is the uncertainty in mole fraction due to the stronger tendency of CO_2 than Ar to adsorb at the walls of the VLE cell and gas cylinders, calculated from:

$$u(y_{CO_2,cal}, \text{ads.}) \approx \frac{1}{2}\left[\frac{\Delta n_{CO_2,\text{max.ads.,cyl.}} n_{Ar,cyl.}}{(n_{CO_2,cyl.} + n_{Ar,cyl.}) n_{CO_2,cyl.}} + \frac{\Delta n_{CO_2,\text{max.ads.,cell}} n_{Ar,cell}}{(n_{CO_2,cell} + n_{Ar,cell}) n_{CO_2,cell}}\right]. \quad (2)$$

Table 2: Experimental liquid phase VLE and VLSE data for CO_2 + Ar at mean temperature $\bar{T}_f$, mean pressure $\bar{p}_f$, and mean liquid phase mole fraction $\bar{x}_{CO_2}$, with estimated total compounded standard uncertainty of phase equilibrium measurements in terms of mole fraction, $u_{tot}(\bar{x}_{CO_2})$.[a,b]

	Data point				Temperature			Pressure			Composition		
ID	$\bar{T}_f$ / K	$\bar{p}_f$ /MPa	$\bar{x}_{CO_2}$	$u_{tot}(\bar{x}_{CO_2})$	$s(\bar{T}_f)$ / K	$\bar{u}_c(\bar{T})$ / K	$u_c(\bar{T}_f)$ / K	$s(\bar{p}_f)$ /MPa	$\bar{u}_c(\bar{p})$ /MPa	$u_c(\bar{p}_f)$ /MPa	$s(\bar{x}_{CO_2})$	$\bar{u}_c(x_{CO_2})$	$u_c(\bar{x}_{CO_2})$
L1 [c,d]	213.146	6.8455	0.86621	1.7E-04	5.0E-05	4.6E-03	4.6E-03	2.1E-03	1.2E-03	2.4E-03	7.7E-05	1.5E-04	1.7E-04
L2	213.139	9.0302	0.80825	1.5E-04	1.2E-04	5.0E-03	5.0E-03	1.0E-05	1.4E-03	1.4E-03	1.2E-05	1.5E-04	1.5E-04
L3 [c,e]	213.145	10.9113	0.75037	1.7E-04	1.8E-04	4.4E-03	4.4E-03	-	2.7E-03	2.7E-03	6.5E-06	1.5E-04	1.5E-04
L4 [c,e]	213.146	12.9654	0.66989	2.1E-04	1.2E-04	4.5E-03	4.5E-03	-	3.2E-03	3.2E-03	2.0E-05	1.5E-04	1.5E-04
L5 [c,e]	213.147	14.4608	0.58309	2.9E-04	8.4E-05	4.7E-03	4.7E-03	-	3.1E-03	3.1E-03	5.6E-05	1.5E-04	1.6E-04
L6 [c,e]	213.145	15.0971	0.51738	6.0E-04	2.3E-04	4.1E-03	4.1E-03	-	3.2E-03	3.2E-03	3.4E-05	1.5E-04	1.5E-04
L9 [c]	223.146	5.0573	0.91098	1.5E-04	5.0E-05	2.7E-03	2.7E-03	-	1.1E-03	1.1E-03	1.2E-05	1.5E-04	1.5E-04
L10 [c]	223.146	9.0439	0.80927	1.5E-04	7.2E-05	2.6E-03	2.6E-03	-	1.4E-03	1.4E-03	1.7E-05	1.5E-04	1.5E-04
L11 [c,e]	223.147	13.0070	0.66075	2.1E-04	1.1E-04	2.6E-03	2.6E-03	-	2.7E-03	2.7E-03	7.8E-05	1.5E-04	1.7E-04
L12 [c,e]	223.148	14.8864	0.49163	1.1E-03	9.8E-05	2.6E-03	2.6E-03	-	2.8E-03	2.8E-03	9.4E-05	1.5E-04	1.8E-04
L13	243.122	2.5399	0.97800	1.6E-04	1.0E-04	1.1E-02	1.1E-02	5.1E-05	5.2E-04	5.2E-04	7.4E-05	1.5E-04	1.7E-04
L14	243.121	4.5024	0.93623	1.5E-04	2.3E-04	1.2E-02	1.2E-02	8.3E-06	1.1E-03	1.1E-03	1.5E-06	1.5E-04	1.5E-04
L15	243.120	6.9963	0.87687	1.5E-04	3.2E-04	1.2E-02	1.2E-02	3.2E-06	1.1E-03	1.1E-03	1.7E-05	1.5E-04	1.5E-04
L16	243.120	9.0786	0.81941	1.6E-04	3.0E-04	1.2E-02	1.2E-02	3.4E-06	1.3E-03	1.3E-03	4.8E-05	1.5E-04	1.6E-04
L17	243.119	11.0281	0.75435	1.8E-04	1.5E-04	1.2E-02	1.2E-02	1.8E-05	2.7E-03	2.7E-03	6.6E-06	1.5E-04	1.5E-04
L18	243.120	12.5957	0.68575	2.0E-04	7.2E-05	1.3E-02	1.3E-02	6.6E-06	2.7E-03	2.7E-03	1.5E-05	1.5E-04	1.5E-04
L19 [e]	243.120	13.8663	0.59223	3.7E-04	3.7E-04	1.3E-02	1.3E-02	4.7E-06	2.7E-03	2.7E-03	9.7E-06	1.5E-04	1.5E-04
L20 [e]	243.121	14.0375	0.56416	6.4E-04	1.4E-04	1.3E-02	1.3E-02	1.1E-05	2.7E-03	2.7E-03	1.3E-06	1.5E-04	1.5E-04
L21 [e]	243.120	14.0753	0.55458	8.6E-04	2.0E-04	1.3E-02	1.3E-02	9.6E-06	2.7E-03	2.7E-03	3.7E-06	1.5E-04	1.5E-04
L22	263.133	3.1334	0.98995	1.8E-04	1.2E-04	8.9E-03	8.9E-03	7.4E-06	1.1E-03	1.1E-03	5.7E-06	1.5E-04	1.5E-04
L23	263.134	4.1668	0.96776	1.5E-04	1.1E-04	8.7E-03	8.7E-03	5.8E-04	1.3E-03	1.2E-03	1.8E-06	1.5E-04	1.5E-04
L24	263.134	5.1903	0.94463	1.6E-04	2.4E-04	9.1E-03	9.1E-03	8.8E-06	1.1E-03	1.1E-03	3.0E-06	1.5E-04	1.5E-04
L25	263.132	6.6151	0.91006	1.6E-04	2.5E-04	9.5E-03	9.5E-03	2.4E-06	1.1E-03	1.1E-03	3.2E-06	1.5E-04	1.5E-04
L26	263.132	8.0026	0.87315	1.5E-04	1.2E-06	9.8E-03	9.8E-03	1.4E-06	1.2E-03	1.2E-03	2.7E-06	1.5E-04	1.5E-04
L27	263.134	9.4181	0.83051	1.5E-04	1.9E-04	7.7E-03	7.7E-03	2.3E-06	1.4E-03	1.4E-03	2.7E-06	1.5E-04	1.5E-04
L28	263.134	11.1140	0.76717	1.7E-04	2.1E-04	8.6E-03	8.6E-03	5.9E-06	2.7E-03	2.7E-03	4.5E-06	1.5E-04	1.5E-04
L29 [e]	263.135	12.3209	0.69537	1.7E-04	2.2E-04	7.4E-03	7.4E-03	9.5E-06	2.7E-03	2.7E-03	5.3E-06	1.5E-04	1.5E-04
L30 [e]	263.135	12.5241	0.67129	1.6E-04	9.9E-05	7.2E-03	7.2E-03	1.0E-05	2.7E-03	2.7E-03	3.7E-06	1.5E-04	1.5E-04
L31 [e]	263.135	12.5867	0.65867	1.7E-04	2.2E-04	7.8E-03	7.8E-03	2.8E-06	2.7E-03	2.7E-03	5.0E-06	1.5E-04	1.5E-04
L32 [e]	263.134	12.6338	0.63983	2.6E-04	2.9E-04	7.8E-03	7.8E-03	5.1E-06	2.7E-03	2.7E-03	1.2E-05	1.5E-04	1.5E-04
L33 [c]	273.257	8.3970	0.87850	1.5E-04	1.9E-04	1.4E-03	1.4E-03	-	1.3E-03	1.3E-03	1.5E-05	1.5E-04	1.5E-04
L34 [c,e]	273.256	9.7371	0.83403	1.6E-04	1.2E-04	1.3E-03	1.3E-03	-	1.5E-03	1.5E-03	1.4E-05	1.5E-04	1.5E-04
L35 [c,e]	273.259	10.8119	0.78776	2.0E-04	2.0E-04	1.2E-03	1.2E-03	-	2.6E-03	2.6E-03	6.9E-06	1.5E-04	1.5E-04
L36 [c,e]	273.257	11.4475	0.74269	3.3E-04	9.2E-05	1.1E-03	1.1E-03	-	2.7E-03	2.7E-03	2.2E-05	1.5E-04	1.5E-04
L37 [c,e]	273.257	11.5889	0.71988	8.0E-04	6.0E-05	1.0E-03	1.0E-03	-	2.7E-03	2.7E-03	3.6E-05	1.5E-04	1.5E-04
L38	283.146	6.5205	0.95181	1.5E-04	2.4E-04	9.8E-04	1.0E-03	4.5E-06	1.1E-03	1.1E-03	2.4E-06	1.5E-04	1.5E-04
L39 [e]	283.145	8.5703	0.89281	1.5E-04	1.5E-04	1.4E-03	1.4E-03	8.5E-06	1.2E-03	1.2E-03	4.1E-06	1.5E-04	1.5E-04
L40 [e]	283.146	9.4405	0.86078	1.5E-04	1.9E-04	9.3E-04	9.5E-04	6.7E-06	1.4E-03	1.4E-03	6.3E-06	1.5E-04	1.5E-04
L41 [e]	283.144	9.7627	0.84627	1.5E-04	4.0E-04	1.0E-03	1.1E-03	1.0E-05	1.4E-03	1.4E-03	2.2E-06	1.5E-04	1.5E-04
L42 [e]	283.144	9.7627	0.84625	1.5E-04	7.3E-04	9.6E-04	1.2E-03	1.2E-05	1.4E-03	1.4E-03	3.2E-06	1.5E-04	1.5E-04
L43 [e]	283.144	10.1842	0.82121	1.5E-04	6.2E-04	1.0E-03	1.2E-03	1.2E-05	2.6E-03	2.6E-03	4.0E-06	1.5E-04	1.5E-04
L44	299.217	7.2436	0.98187	1.5E-04	4.5E-04	2.6E-03	2.6E-03	1.4E-04	1.1E-03	1.1E-03	2.4E-06	1.5E-04	1.5E-04
L45 [e]	299.218	7.8172	0.96284	1.5E-04	2.5E-04	2.5E-03	2.5E-03	7.5E-06	1.1E-03	1.1E-03	1.8E-06	1.5E-04	1.5E-04
L46 [e]	299.218	8.0370	0.95315	1.5E-04	1.6E-04	2.0E-03	2.1E-03	6.7E-06	1.1E-03	1.1E-03	1.8E-06	1.5E-04	1.5E-04
L47 [e]	299.218	8.0370	0.95314	1.5E-04	2.3E-04	2.1E-03	2.1E-03	1.3E-05	1.1E-03	1.1E-03	1.0E-06	1.5E-04	1.5E-04
L48 [e]	299.217	8.1205	0.94756	1.5E-04	6.3E-04	2.5E-03	2.6E-03	8.5E-06	1.2E-03	1.2E-03	1.3E-06	1.5E-04	1.5E-04
L49 [e]	299.218	8.1440	0.94468	1.5E-04	1.6E-04	2.7E-03	2.7E-03	6.6E-06	1.2E-03	1.2E-03	4.2E-06	1.5E-04	1.5E-04

[a] For the measurements performed without pressure stabilization, $\bar{p}_f$ and $\bar{x}_{CO_2}$ are interpreted as the estimated mean values before the first sample. See the main text for details.

[b] Estimated uncertainty terms listed in the table:

- $s(\bar{T}_f)$ Sample standard deviation of the mean of the temperatures
- $\bar{u}_c(\bar{T})$ Mean of the standard systematic uncertainty of the temperature measurements
- $u_c(\bar{T}_f)$ Combined standard uncertainty of the temperature data points
- $s(\bar{p}_f)$ Standard deviation of the mean of the sample pressures for the data points measured with pressure stabilization
- $\bar{u}_c(\bar{p})$ Mean of the standard systematic uncertainty of the pressure measurements
- $u_c(\bar{p}_f)$ Combined standard uncertainty of the pressure data point
- $s(\bar{x}_{CO_2})$ Sample standard deviation of the mean of the mole fractions for the data points measured with pressure stabilization during sampling, and the standard deviation of the regression line at $\bar{p}_f$ for data points measured without such pressure stabilization.
- $\bar{u}_c(x_{CO_2})$ Mean of the systematic standard uncertainty of the mole fractions
- $u_c(\bar{x}_{CO_2})$ Combined standard uncertainty of the mole fraction data point

[c] Sampling performed without pressure stabilization

[d] Solid phase present in cell (VLSE at three phase line). Identical data are provided in Table 3. All other data of Table 2 are from VLE measurements. The estimated standard deviation in pressure for this data point is estimated from the general fluctuations in pressure in the hours before and after sampling. See the main text for details.

[e] The fitted scaling law model presented in Section 200 is used to calculate the derivative $\left(\partial z_{CO_2}/\partial p\right)_T$ needed to estimate $u_{\mathrm{tot}}(\bar{y}_{\mathrm{CO_2}})$ from equation (5). For other data points, EOS-CG is used.

Table 3: Experimental liquid phase LSE and VLSE data for CO_2 + Ar at mean temperature $\overline{T}_f$, mean pressure $\overline{p}_f$, and mean liquid phase mole fraction $\overline{x}_{\mathrm{CO_2}}$, with estimated total compounded standard uncertainty of phase equilibrium measurements in terms of mole fraction, $u_{\mathrm{tot}}(\overline{x}_{\mathrm{CO_2}})$.[a]

	Data point				Temperature			Pressure			Composition		
ID	$\overline{T}_f$ / K	$\bar{p}_f$ / MPa	$\bar{x}_{\mathrm{CO_2}}$	$u_{\mathrm{tot}}(\bar{x}_{\mathrm{CO_2}})$	$s(\overline{T}_f)$ / K	$\bar{u}_c(\overline{T})$ / K	$u_c(\overline{T}_f)$ / K	$s(\bar{p}_f)$ / MPa	$\bar{u}_c(\bar{p})$ / MPa	$u_c(\bar{p}_f)$ / MPa	$s(\bar{x}_{\mathrm{CO_2}})$	$\bar{u}_c(x_{\mathrm{CO_2}})$	$u_c(\bar{x}_{\mathrm{CO_2}})$
L1 [b]	213.146	6.8455	0.86621	1.7E-04	5.0E-05	4.6E-03	4.6E-03	2.1E-03	1.2E-03	2.4E-03	7.7E-05	1.5E-04	1.7E-04
L7 [c]	213.137	13.9186	0.81524	2.9E-04	9.6E-05	5.1E-03	5.1E-03	4.4E-05	2.8E-03	2.8E-03	2.5E-04	1.4E-04	2.9E-04
L8 [c]	213.138	16.1441	0.78630	1.8E-04	1.6E-04	5.4E-03	5.4E-03	8.6E-06	2.8E-03	2.8E-03	1.1E-04	1.4E-04	1.8E-04

[a] Estimated $\bar{p}_f$ and $\bar{x}_{\mathrm{CO_2}}$ and uncertainty terms listed in the table are defined as in Table 2.

[b] Vapor phase present in cell (VLSE, three phase line). Identical data are provided in Table 2. All other data of Table 3 are from VSE measurements. The measurements are performed without pressure stabilization during sampling. The estimated standard deviation in pressure is estimated from the general fluctuations in pressure in the hours before and after sampling. See the main text for details

[c] The derivative $\left(\partial z_{CO_2}/\partial p\right)_T$ needed to estimate $u_{\mathrm{tot}}(\bar{y}_{\mathrm{CO_2}})$ from equation (5) is calculated by applying the two-point formula to the data. For L1 EOS-CG is used.

Table 4: Experimental vapor phase VLE and VLSE data for CO_2 + Ar at mean temperature $\overline{T}_f$, mean pressure $\overline{p}_f$, and mean vapor phase mole fraction $\overline{y}_{\mathrm{CO_2}}$, with estimated total compounded standard uncertainty of VLE measurement in terms of mole fraction, $u_{\mathrm{tot}}(\overline{y}_{\mathrm{CO_2}})$.[a]

	Data point				Temperature			Pressure			Composition		
ID	$\overline{T}_f$ / K	$\bar{p}_f$ / MPa	$\bar{y}_{\mathrm{CO_2}}$	$u_{\mathrm{tot}}(\bar{y}_{\mathrm{CO_2}})$	$s(\overline{T}_f)$ / K	$\bar{u}_c(\overline{T})$ / K)	$u_c(\overline{T}_f)$ / K	$s(\bar{p}_f)$ / MPa	$\bar{u}_c(\bar{p})$ / MPa	$u_c(\bar{p}_f)$ / MPa	$s(\bar{y}_{\mathrm{CO_2}})$	$\bar{u}_c(y_{\mathrm{CO_2}})$	$u_c(\bar{y}_{\mathrm{CO_2}})$
V5 [b,c]	213.146	6.8449	0.13132	2.7E-04	6.6E-05	4.8E-03	4.8E-03	4.0E-03	1.1E-03	4.1E-03	6.2E-05	1.4E-04	1.5E-04
V6	213.139	9.0302	0.13313	1.5E-04	1.1E-04	5.1E-03	5.1E-03	7.3E-05	1.4E-03	1.4E-03	6.8E-05	1.4E-04	1.6E-04
V7	213.137	9.0302	0.13349	1.4E-04	1.1E-04	4.8E-03	4.8E-03	1.5E-05	1.4E-03	1.4E-03	1.4E-05	1.4E-04	1.4E-04
V8 [b,d]	213.146	10.9217	0.14882	1.5E-04	1.3E-04	4.8E-03	4.8E-03	-	2.7E-03	2.7E-03	4.2E-05	1.4E-04	1.5E-04
V9 [b,d]	213.146	12.9793	0.19008	1.6E-04	1.3E-04	4.5E-03	4.5E-03	-	3.0E-03	3.0E-03	3.5E-05	1.4E-04	1.4E-04
V10 [b,d]	213.147	14.4762	0.25502	2.2E-04	7.7E-05	4.9E-03	4.9E-03	-	2.8E-03	2.8E-03	2.8E-05	1.4E-04	1.4E-04
V11 [b,d]	213.145	15.1040	0.31634	5.0E-04	9.4E-05	4.2E-03	4.2E-03	-	2.8E-03	2.8E-03	4.4E-05	1.4E-04	1.5E-04
V13 [b]	223.146	5.0632	0.21190	8.8E-04	7.2E-05	2.7E-03	2.7E-03	-	1.1E-03	1.1E-03	8.7E-04	1.4E-04	8.8E-04
V14 [b]	223.146	9.0512	0.18189	1.5E-04	8.9E-05	2.7E-03	2.7E-03	-	1.4E-03	1.4E-03	6.5E-05	1.4E-04	1.5E-04
V15 [b,d]	223.146	13.0196	0.23183	1.5E-04	1.3E-04	2.6E-03	2.6E-03	-	2.7E-03	2.7E-03	2.0E-05	1.4E-04	1.4E-04
V16 [b,d]	223.147	14.8924	0.36516	1.2E-03	1.4E-04	2.6E-03	2.6E-03	-	2.8E-03	2.8E-03	5.2E-05	1.4E-04	1.5E-04
V18	243.121	4.5024	0.41406	2.0E-04	8.5E-05	1.2E-02	1.2E-02	1.2E-06	1.1E-03	1.1E-03	1.7E-05	1.4E-04	1.4E-04
V19	243.120	6.9963	0.32878	1.7E-04	2.3E-04	1.2E-02	1.2E-02	8.3E-06	1.1E-03	1.1E-03	1.8E-05	1.4E-04	1.4E-04
V20	243.120	9.0787	0.30893	1.6E-04	2.4E-04	1.2E-02	1.2E-02	2.6E-06	1.3E-03	1.3E-03	6.2E-06	1.4E-04	1.4E-04
V21	243.120	11.0279	0.31569	1.6E-04	1.4E-04	1.2E-02	1.2E-02	8.1E-05	2.7E-03	2.7E-03	2.2E-05	1.4E-04	1.4E-04
V22	243.120	12.5957	0.34311	1.8E-04	6.7E-05	1.3E-02	1.3E-02	5.1E-06	2.7E-03	2.7E-03	6.5E-06	1.4E-04	1.4E-04
V23 [d]	243.120	13.8663	0.41171	3.4E-04	5.3E-05	1.2E-02	1.2E-02	2.0E-05	2.7E-03	2.7E-03	2.9E-05	1.4E-04	1.4E-04
V24 [d]	243.120	14.0375	0.43814	6.0E-04	1.6E-04	1.3E-02	1.3E-02	7.5E-06	2.7E-03	2.7E-03	6.6E-05	1.4E-04	1.5E-04
V25 [d]	243.120	14.0753	0.44809	8.1E-04	2.6E-04	1.3E-02	1.3E-02	1.0E-05	2.7E-03	2.7E-03	2.7E-05	1.4E-04	1.4E-04
V27	263.134	3.1334	0.88303	4.4E-04	1.8E-04	8.6E-03	8.6E-03	5.4E-06	1.1E-03	1.1E-03	2.2E-05	1.4E-04	1.4E-04
V28	263.134	4.1674	0.72201	2.0E-04	2.5E-04	8.8E-03	8.8E-03	1.5E-05	1.1E-03	1.1E-03	7.6E-06	1.4E-04	1.4E-04
V29	263.134	5.1903	0.62697	1.1E-03	1.2E-04	9.0E-03	9.0E-03	1.4E-05	1.1E-03	1.1E-03	5.9E-05	1.4E-04	1.5E-04
V30	263.133	6.6151	0.54864	1.9E-04	1.8E-04	9.6E-03	9.6E-03	5.8E-06	1.1E-03	1.1E-03	6.2E-06	1.4E-04	1.4E-04
V31	263.132	8.0026	0.50717	6.0E-04	3.1E-04	9.6E-03	9.6E-03	2.1E-06	1.2E-03	1.2E-03	3.5E-05	1.4E-04	1.4E-04
V32	263.134	9.4181	0.48823	2.9E-04	3.9E-04	8.2E-03	8.2E-03	5.9E-06	1.4E-03	1.4E-03	1.4E-05	1.4E-04	1.4E-04
V33	263.134	11.1140	0.49429	2.0E-04	2.5E-04	9.1E-03	9.1E-03	1.1E-05	2.7E-03	2.7E-03	7.0E-06	1.4E-04	1.4E-04
V34 [d]	263.134	12.3209	0.53774	1.9E-04	3.1E-04	7.6E-03	7.6E-03	7.5E-06	2.7E-03	2.7E-03	7.8E-06	1.4E-04	1.4E-04
V35 [d]	263.135	12.5240	0.56042	3.2E-04	5.3E-05	7.7E-03	7.7E-03	4.1E-06	2.7E-03	2.7E-03	1.9E-05	1.4E-04	1.4E-04
V36 [d]	263.134	12.5867	0.57349	1.8E-04	2.8E-04	7.4E-03	7.4E-03	7.1E-06	2.7E-03	2.7E-03	7.4E-06	1.4E-04	1.4E-04
V37 [d]	263.134	12.6338	0.59424	2.0E-04	2.5E-04	7.7E-03	7.7E-03	5.3E-06	2.7E-03	2.7E-03	8.3E-06	1.4E-04	1.4E-04
V39 [b]	273.258	6.8595	0.66489	1.6E-04	1.5E-04	1.4E-03	1.4E-03	-	1.1E-03	1.1E-03	7.0E-05	1.4E-04	1.6E-04
V40 [b,d]	273.256	8.3912	0.61313	1.4E-04	1.3E-04	1.5E-03	1.5E-03	-	1.3E-03	1.3E-03	1.2E-05	1.4E-04	1.4E-04
V41 [b,d]	273.257	9.7469	0.59654	1.4E-04	1.1E-04	1.3E-03	1.3E-03	-	1.5E-03	1.5E-03	2.1E-05	1.4E-04	1.4E-04
V42 [b,d]	273.257	10.8209	0.60553	1.5E-04	1.2E-04	1.1E-03	1.1E-03	-	2.6E-03	2.6E-03	1.3E-05	1.4E-04	1.4E-04
V43 [b,d]	273.257	11.4565	0.63721	2.9E-04	8.5E-05	1.0E-03	1.0E-03	-	2.7E-03	2.7E-03	1.5E-05	1.4E-04	1.4E-04
V44 [b,d]	273.257	11.5965	0.66165	9.0E-04	1.7E-04	1.0E-03	1.0E-03	-	2.7E-03	2.7E-03	4.1E-05	1.4E-04	1.5E-04

V46	283.145	6.5204	0.80919	1.4E-04	3.1E-04	9.4E-04	9.9E-04	9.4E-06	1.1E-03	1.1E-03	6.0E-06	1.4E-04	1.4E-04
V47 [d]	283.145	8.5703	0.72667	1.4E-04	1.2E-04	1.4E-03	1.4E-03	9.1E-06	1.2E-03	1.2E-03	5.2E-06	1.4E-04	1.4E-04
V48 [d]	283.144	9.4405	0.71655	1.4E-04	6.6E-04	1.1E-03	1.3E-03	1.4E-05	1.4E-03	1.4E-03	6.7E-06	1.4E-04	1.4E-04
V49 [d]	283.145	9.7626	0.71807	1.4E-04	4.7E-04	9.3E-04	1.0E-03	5.5E-06	1.4E-03	1.4E-03	4.1E-06	1.4E-04	1.4E-04
V50 [d]	283.143	10.1842	0.72944	1.4E-04	3.3E-04	8.9E-04	1.2E-03	1.2E-05	2.6E-03	2.6E-03	5.9E-06	1.4E-04	1.4E-04
V51 [d]	283.144	10.4050	0.75465	5.0E-04	4.4E-04	9.8E-04	1.1E-03	8.7E-06	2.6E-03	2.6E-03	9.7E-06	1.4E-04	1.4E-04
V53	299.218	7.2437	0.96083	1.4E-04	1.7E-04	2.5E-03	2.5E-03	1.4E-05	1.1E-03	1.1E-03	6.8E-07	1.4E-04	1.4E-04
V54 [d]	299.218	7.8173	0.93733	1.4E-04	3.0E-04	2.5E-03	2.6E-03	8.9E-06	1.1E-03	1.1E-03	3.5E-06	1.4E-04	1.4E-04
V55 [d]	299.218	8.0370	0.93312	1.4E-04	1.4E-04	2.0E-03	2.0E-03	1.1E-05	1.1E-03	1.1E-03	7.5E-06	1.4E-04	1.4E-04
V56 [d]	299.218	8.1205	0.93420	1.4E-04	3.2E-04	2.5E-03	2.6E-03	4.7E-06	1.2E-03	1.2E-03	1.6E-06	1.4E-04	1.4E-04
V57 [d]	299.218	8.1440	0.93613	1.4E-04	2.3E-04	2.6E-03	2.6E-03	3.4E-06	1.2E-03	1.2E-03	1.1E-06	1.4E-04	1.4E-04
V58 [d]	299.218	8.1440	0.93600	1.4E-04	1.5E-04	2.7E-03	2.7E-03	4.1E-06	1.2E-03	1.2E-03	8.8E-06	1.4E-04	1.4E-04

[a] Except that vapor mole fraction $\bar{y}_{CO_2}$ is used instead of liquid mole fraction $\bar{x}_{CO_2}$, estimated $\bar{p}_f$ and $\bar{y}_{CO_2}$ and uncertainty terms listed in the table are defined as in Table 2.

[b] Sampling performed without pressure stabilization

[c] Solid phase (dry ice) present in cell (VLSE, three phase line). Identical data are provided in Table 5. All other data of Table 4 are from VLE measurements. The estimated standard deviation in pressure of this data point is estimated from the general fluctuations in pressure in the hours before and after sampling. See the main text for details.

[d] The fitted scaling law model presented in Section 200 is used to calculate the derivative $\left(\partial z_{CO_2}/\partial p\right)_T$ needed to estimate $u_{\mathrm{tot}}(\bar{y}_{CO_2})$ from equation (5). For other data points, EOS-CG is used.

Table 5: Experimental vapor phase VSE and VSLE data for CO_2 + Ar at mean temperature $\bar{T}_f$, mean pressure $\bar{p}_f$, and mean liquid phase mole fraction $\bar{x}_{CO_2}$, with estimated total compounded standard uncertainty of VLE measurement in terms of mole fraction, $u_{\mathrm{tot}}(\bar{y}_{CO_2})$.[a]

	Data point				Temperature			Pressure			Composition		
ID	$\bar{T}_f$ / K	$\bar{p}_f$ /MPa	$\bar{y}_{CO_2}$	$u_{\mathrm{tot}}(\bar{y}_{CO_2})$	$s(\bar{T}_f)$ / K	$\bar{u}_c(\bar{T})$ / K	$u_c(\bar{T}_f)$ / K	$s(\bar{p}_f)$ /MPa	$\bar{u}_c(\bar{p})$ /MPa	$u_c(\bar{p}_f)$ /MPa	$s(\bar{y}_{CO_2})$	$\bar{u}_c(y_{CO_2})$	$u_c(\bar{y}_{CO_2})$
V2	213.146	1.0495	0.42357	2.6E-04	1.2E-04	5.1E-03	5.1E-03	-	5.1E-04	5.1E-04	1.0E-04	1.4E-04	1.7E-04
V3	213.146	2.5952	0.20333	1.6E-04	5.4E-05	5.1E-03	5.1E-03	-	5.2E-04	5.2E-04	6.4E-05	1.4E-04	1.5E-04
V4	213.146	5.4909	0.13572	1.5E-04	1.4E-04	5.2E-03	5.2E-03	-	1.1E-03	1.1E-03	6.2E-05	1.4E-04	1.5E-04
V5	213.146	6.8449	0.13132	2.7E-04	6.6E-05	4.8E-03	4.8E-03	4.0E-03	1.1E-03	4.1E-03	6.2E-05	1.4E-04	1.5E-04

[a] Estimated uncertainty terms listed in the table defined as in Table 4. All data points are collected without pressure stabilization during sampling. EOS-CG is used to calculate the derivative $\left(\partial z_{CO_2}/\partial p\right)_T$ needed to estimate $u_{\mathrm{tot}}(\bar{y}_{CO_2})$ from equation (5).

[b] Liquid phase present in cell (VLSE, three-phase line). Identical data are provided in Table 4. All other data of Table 5 are from VSE measurements. The estimated standard deviation in pressure of this data point is estimated from the general fluctuations in pressure in the hours before and after sampling. See the main text for details.

Table 6: CO_2 vapor pressure measurements, with estimated total compounded standard uncertainty in terms of pressure, $u_{\mathrm{tot}}(\bar{p}_f)$, compared with reference model results[a].

	Data point				Estimated uncertainties			Analysis			
ID	$\bar{T}_f$ / K	$\bar{p}_f$ / MPa	$\bar{y}_{CO_2}$	$u_{\mathrm{tot}}(\bar{p}_f)$ / MPa	$u_c(\bar{T}_f)$ / K	$u_c(\bar{p}_f)$ / MPa	$u_c(\bar{y}_{CO_2})$	p_{ex} / MPa	p_{mod} / MPa	Δp_{ex} / MPa	$\Delta\bar{p}_f$ / MPa
V1 [b]	213.220	0.4104	0.99999	1.0E-03	5.1E-03	5.2E-04	1.0E-05	0.4104	0.4106	-2.2E-04	-1.7E-04
V12	223.146	0.6818	0.999993	1.3E-03	2.7E-03	1.1E-03	1.5E-06	0.6817	0.6822	-4.8E-04	-4.2E-04
V17 [b]	243.129	1.4263	0.99999	5.1E-03	1.1E-02	5.2E-04	1.0E-05	1.4261	1.4268	-7.1E-04	-5.4E-04
V26 [b]	263.134	2.6467	0.99999	6.5E-03	8.9E-03	5.2E-04	1.0E-05	2.6463	2.6475	-1.2E-03	-8.4E-04
V38	273.220	3.4913	0.999998	1.7E-03	1.4E-03	1.1E-03	1.0E-06	3.4912	3.4916	-4.4E-04	-3.3E-04
V45	283.146	4.5023	0.999997	1.6E-03	1.0E-03	1.1E-03	1.0E-06	4.5021	4.5017	3.6E-04	5.7E-04
V52	299.219	6.5950	0.999985	4.1E-03	2.6E-03	1.1E-03	3.0E-06	6.5929	6.5940	-1.1E-03	1.0E-03

[a] Estimated uncertainty terms listed in the table defined as in Table 2, except that the total compounded uncertainty is provided in terms of pressure. In addition, the following parameters are provided:

- p_{ex}: Measured vapor pressure $\bar{p}_f$ extrapolated to pure CO_2 using the gradients of EOS-CG [12]
- p_{mod}: Vapor pressure from Span-Wagner [31] / Jäger-Span [24]
- $\Delta p_{\mathrm{ex}} = p_{\mathrm{ex}} - p_{\mathrm{mod}}$
- $\Delta\bar{p}_f = \bar{p}_f - p_{\mathrm{mod}}$

[b] Composition of the cell content was not measured, and values and uncertainties of $\bar{y}_{CO_2}$ are set to 1- 10 ppm and 10 ppm, respectively. Hence all measured cases (with impurities up to 15 ppm) are included within one standard uncertainty.

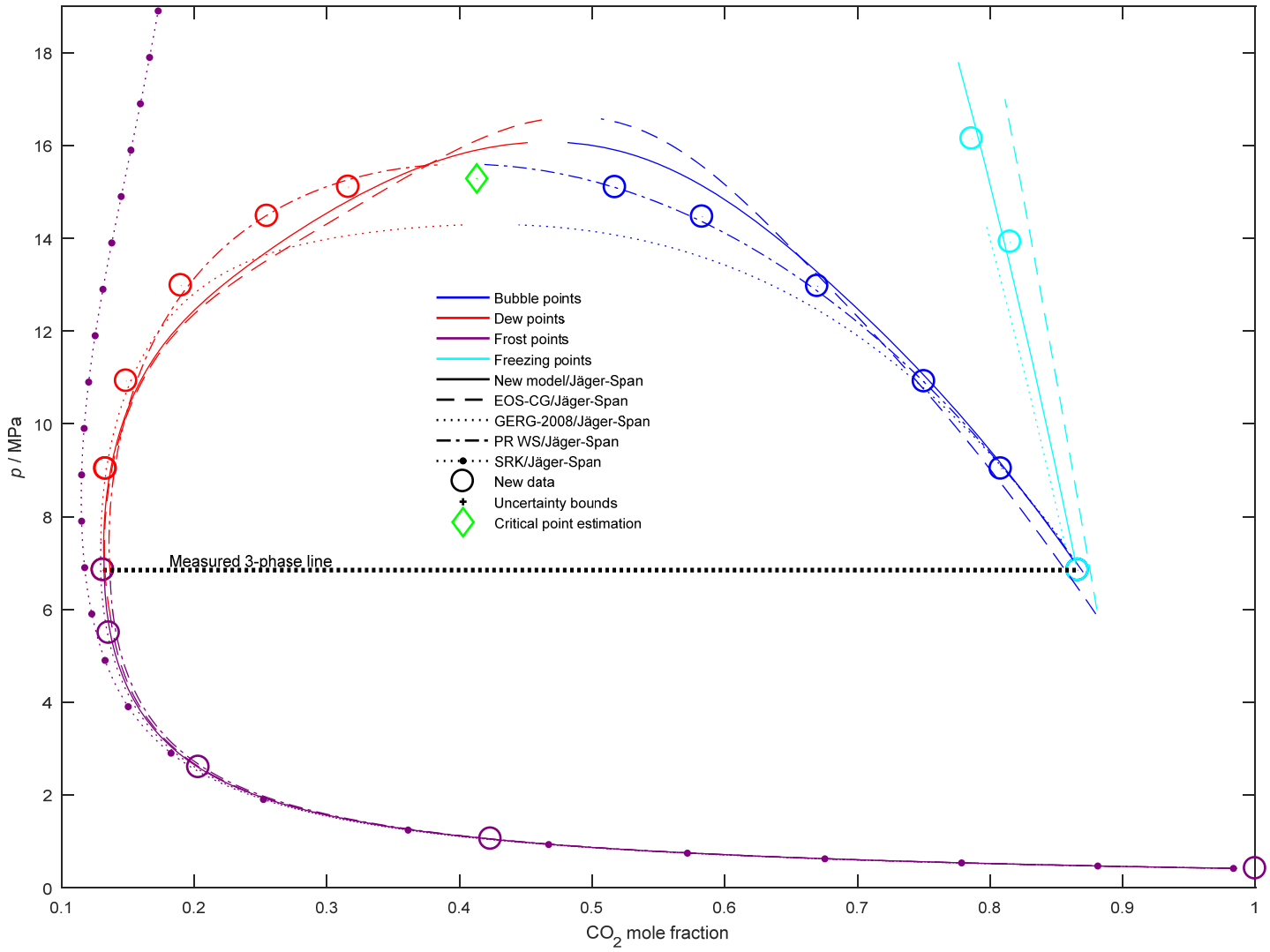

Fig. 2: Isothermal VLE, VLSE, VSE, and LSE measurements of the current work at 213.146 K for the binary system CO_2 + Ar. Measurement uncertainties in pressure and mole fraction is indicated by the cross within each marker. Model predictions for VLE are shown for the new model presented in Section 5, the original EOS-CG [12], GERG-2008 [32, 33], SRK with binary interaction coefficient k_{CO2+Ar} = 0.180 from [34], and PR-WS fitted to the phase equilibrium measurements of the current work. More details on the latter is provided in Section 4.4. Freezing (LSE) equilibria were calculated using the solid model of Jäger-Span [24] combined with fluid models, as discussed in more detail in Section 4.3.

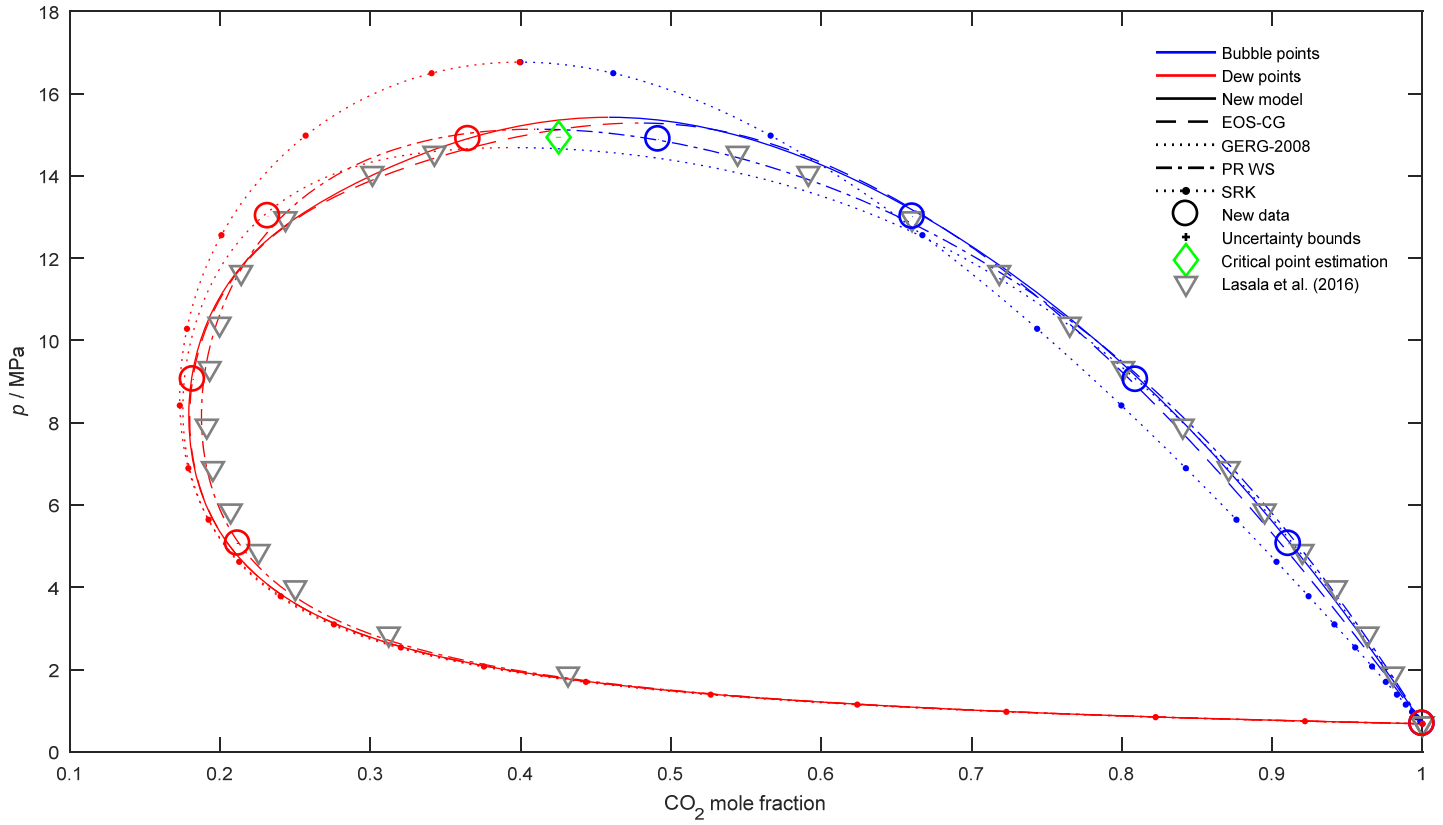

Fig. 3: As Fig. 2, but at a temperature of 223.146 K. No solids are present at this temperature. In addition, literature data of Lasala et al. [35] at 223.07 K are included.

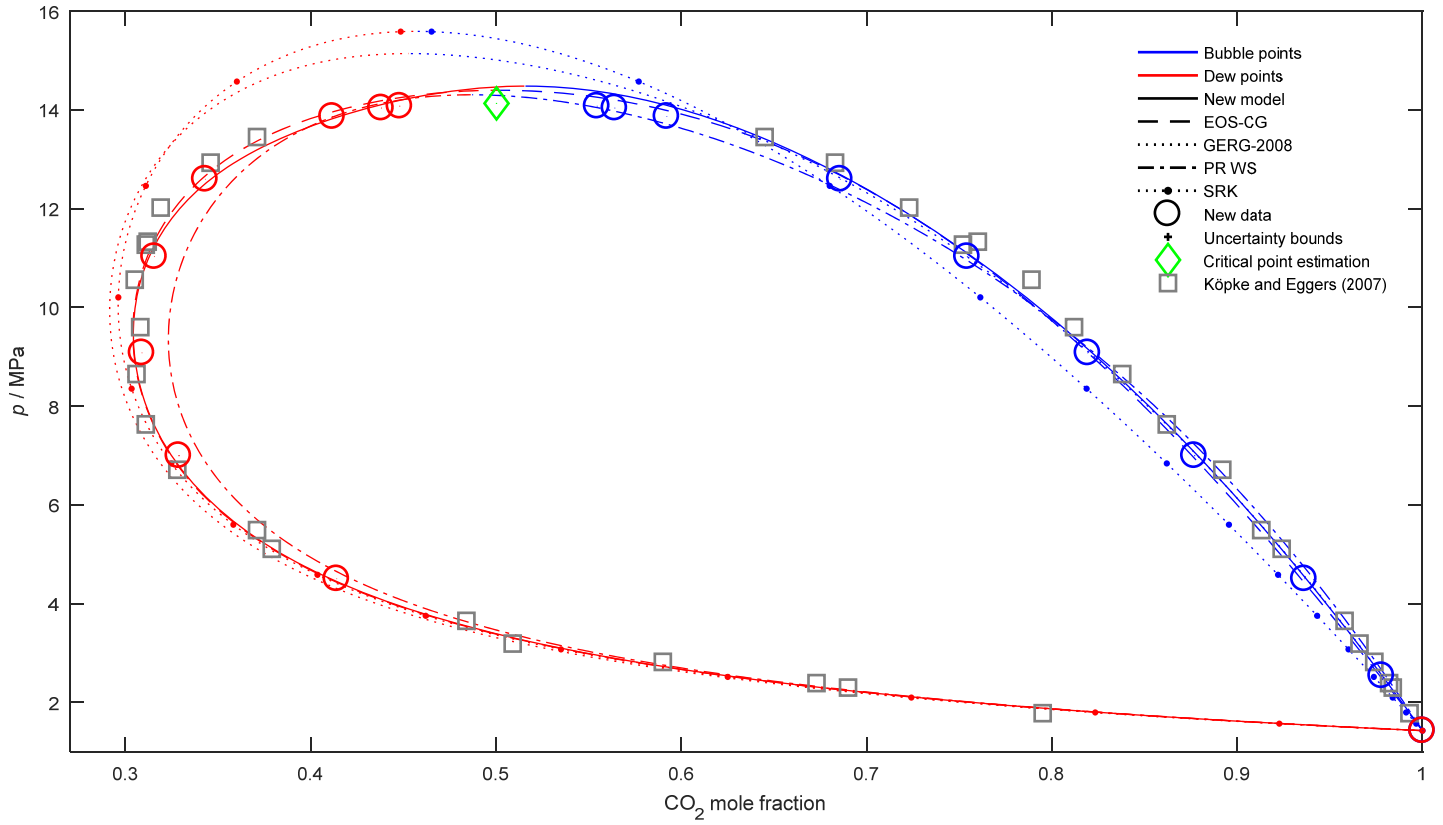

Fig. 4: As Fig. 3, but at a temperature of 243.120 K and with literature data of Köpke and Eggers [36, 37] at 244.5 K.

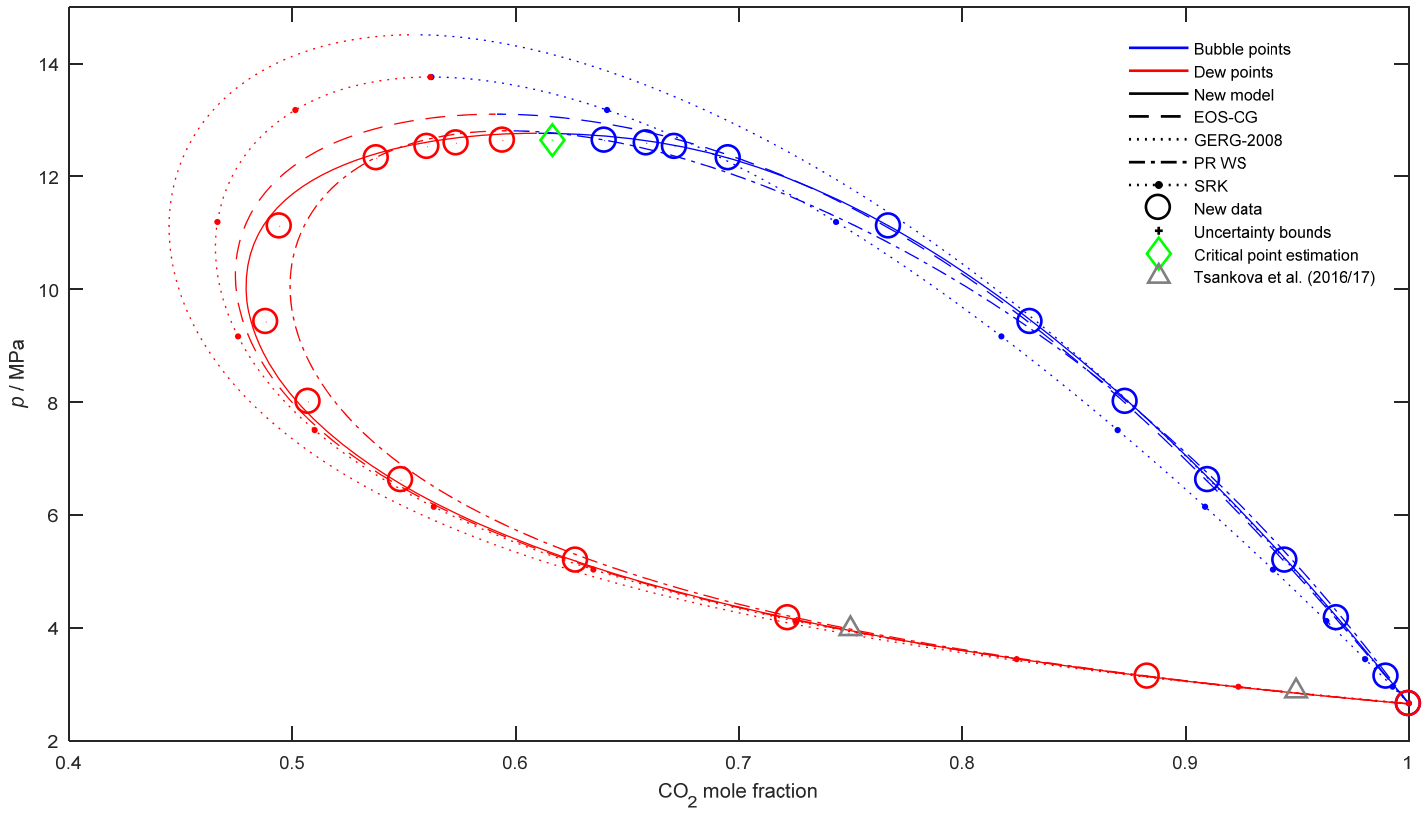

Fig. 5: As Fig. 3, but at a temperature of 263.134 K and with dew point data of Tsankova et al at temperatures 263.418 [26] and 263.577 K [27] for CO_2 mole fractions of 0.7499 and 0.9495, respectively.

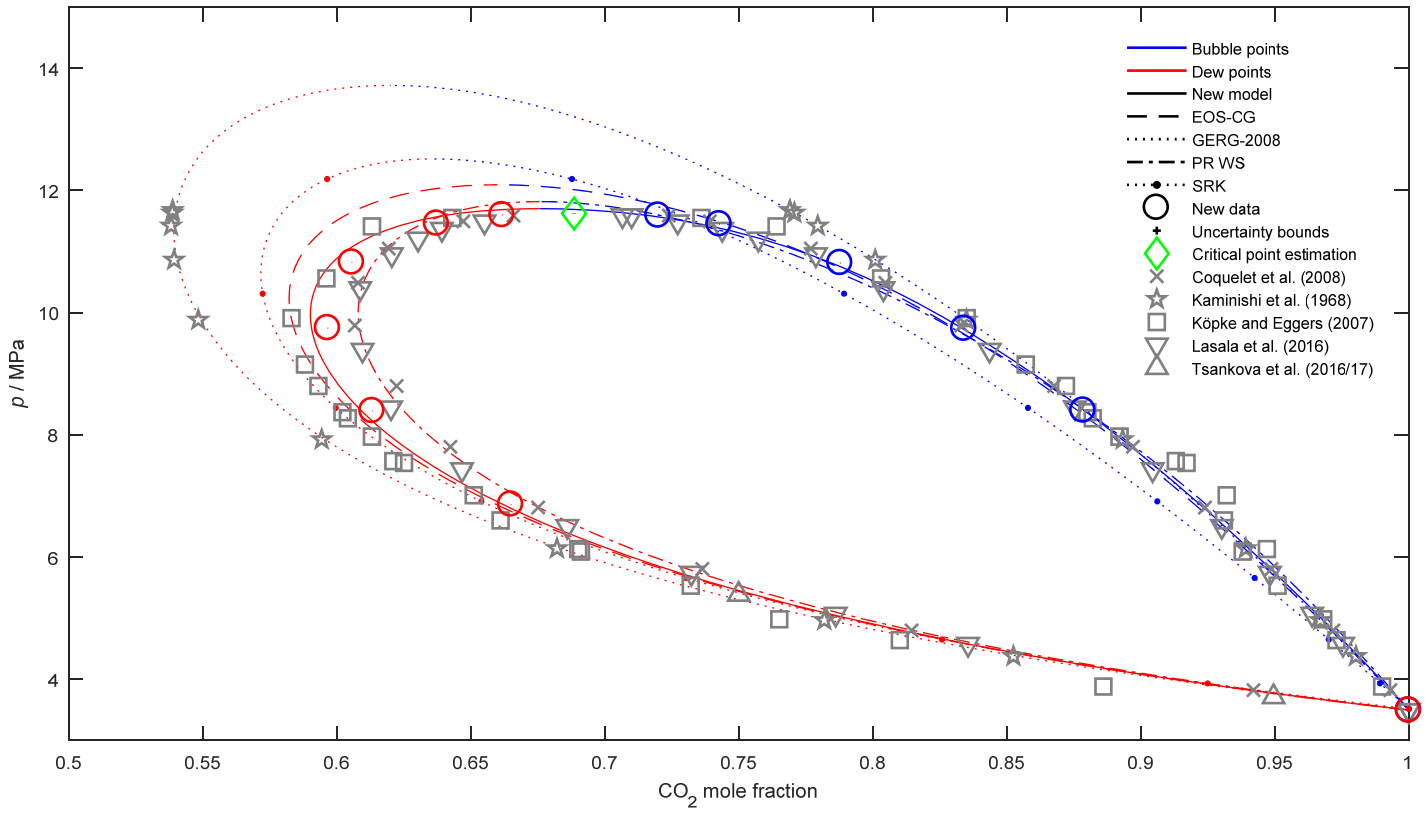

Fig. 6: As Fig. 3, but at a temperature of 273.257 K and with literature data of Coquelet et. al. at [38] 273.26 K, Kaminishi et al. at 273.15 [39], Köpke and Eggers [36, 37] at 273.1 K, Lasala et al. [35] and Tsankova et al. at temperatures 272.895 [26] and 272.696 K [27] for CO_2 mole fractions of 0.7499 and 0.9495, respectively.

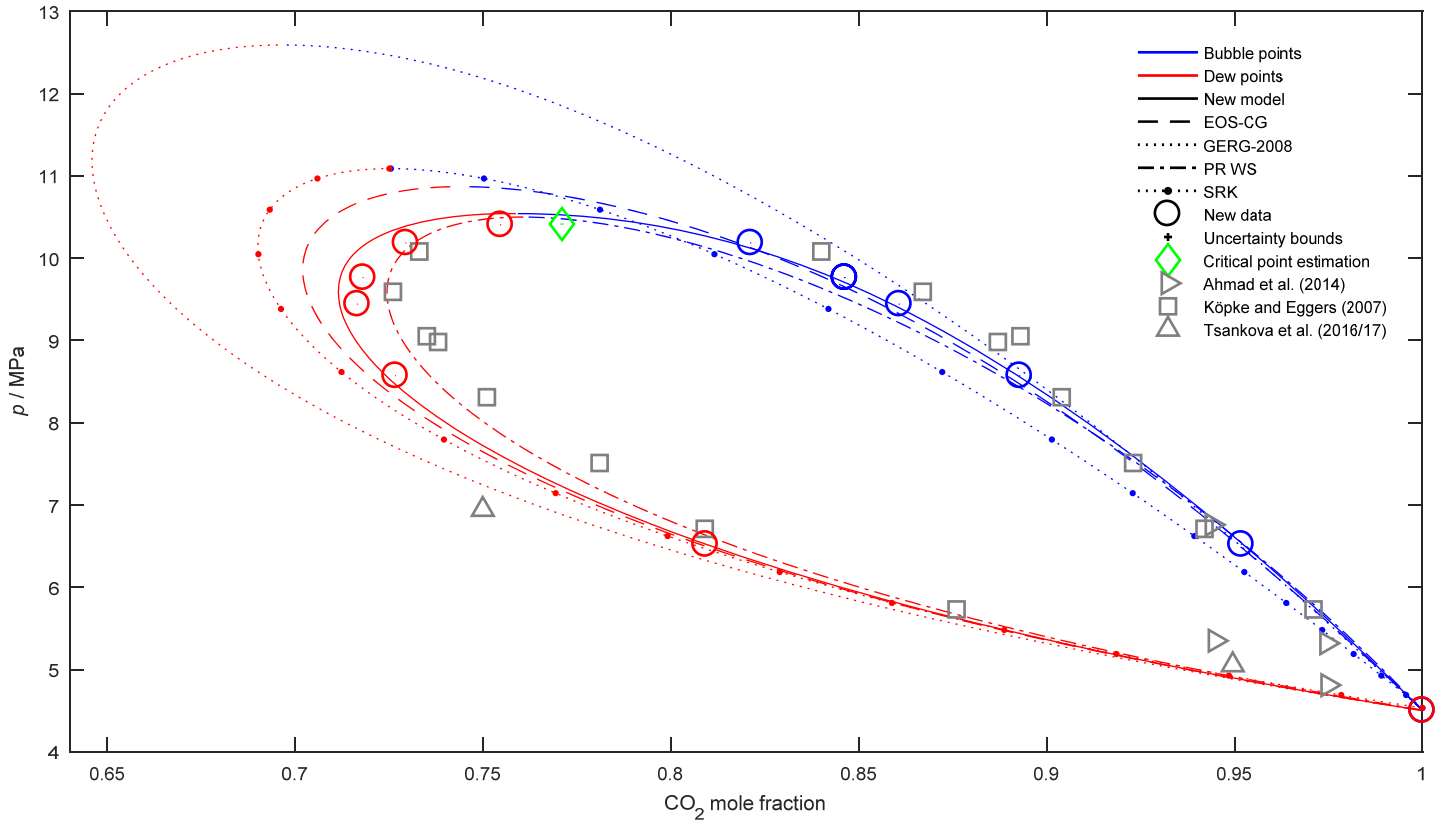

Fig. 7: As Fig. 3, but at a temperature of 283.144 K and with literature data of Ahmad et al. [40] at 283.4 K and Köpke and Eggers [36, 37] at 283.3 K and Tsankova et al. at temperatures 280.444 [26] and 284.395 K [27] for CO_2 mole fractions of 0.7499 and 0.9495, respectively.

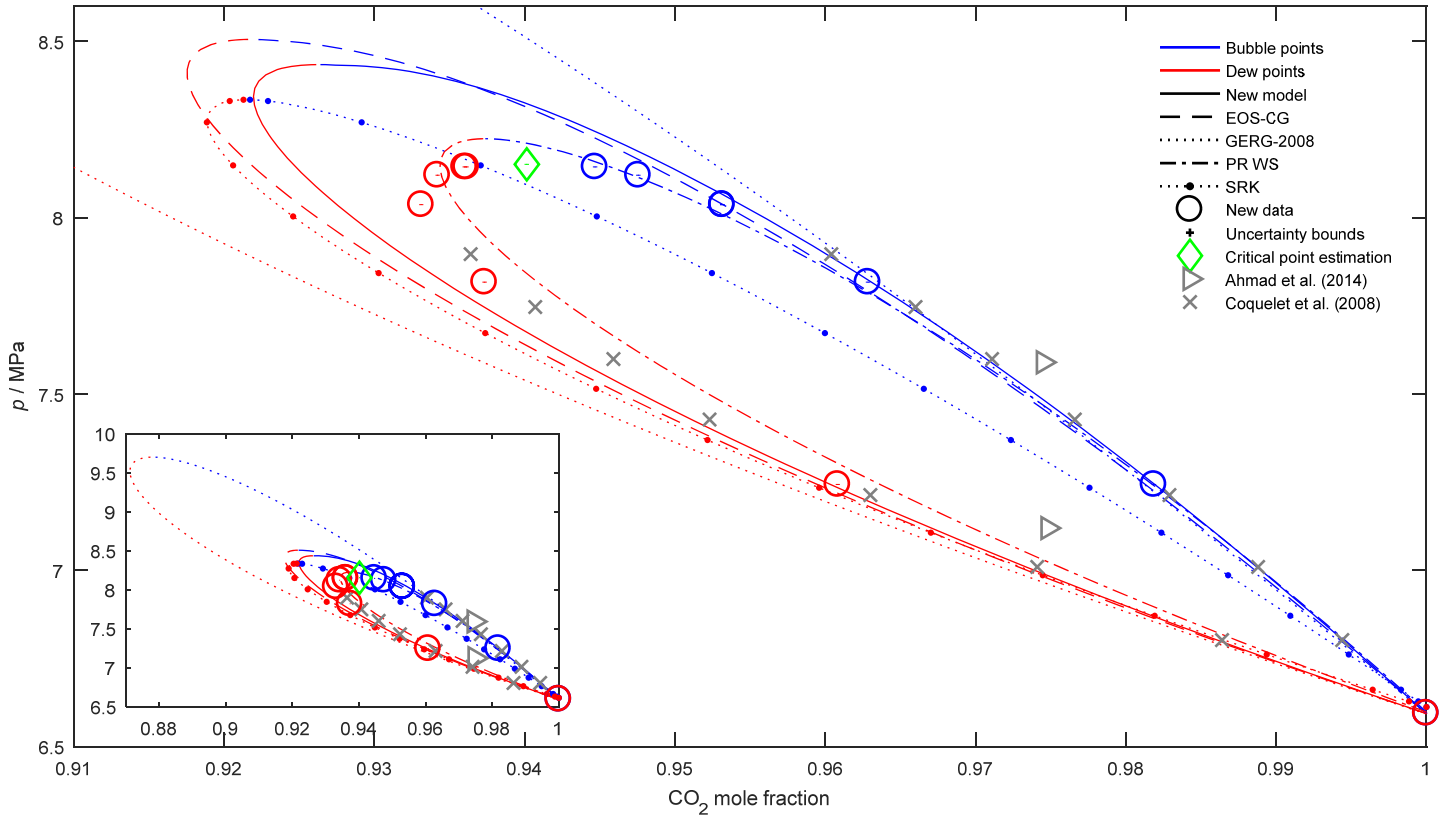

Fig. 8: As Fig. 3, but at a temperature of 299.218 K. In addition, literature data of Ahmad et al. [40] at 299.8 K and Coquelet et al. [38] at 299.21 K are included. The insert shows the same information with wider axis ranges.

The combined composition uncertainty of the calibration mixtures in the cell, $u_c(y_{\mathrm{CO_2,cal}})$ are calculated as a root sum squared of these contributions, i.e. assuming they are independent of each other. As seen in Table 7, , $u(y_{\mathrm{CO_2,cal}}, M_{\mathrm{eff}})$ is highest when the two components have similar concentration, $u(y_{\mathrm{CO_2,cal}}, \mathrm{ads.})$ is increasing with decreasing $y_{\mathrm{CO_2,cal}}$, whereas there is no clear trend regarding $u(y_{\mathrm{CO_2,cal}}, m)$. The combined uncertainty in $y_{\mathrm{CO_2,cal}}$ is for all calibration mixtures below 40 ppm, which will be seen is not of significance for the composition measurements of the phase equilibrium data. Further details regarding the preparation of the calibration mixtures and their uncertainty estimates can be found in Ref. [18]

Table 7: Estimated composition and uncertainty contributions and combined uncertainty of the composition for the 6 reference mixtures used to calibrate composition measurements of this work.

$y_{\mathrm{CO_2,cal}}$	$u(y_{\mathrm{CO_2,cal}}, m)$	$u(y_{\mathrm{CO_2,cal}}, M_{\mathrm{eff}})$	$u(y_{\mathrm{CO_2,cal}}, \mathrm{ads.})$	$u_c(y_{\mathrm{CO_2,cal}})$
0.1368765	$3.8\cdot10^{-6}$	$3.1\cdot10^{-6}$	$3.8\cdot10^{-5}$	$3.8\cdot10^{-5}$
0.3031530	$1.1\cdot10^{-6}$	$5.6\cdot10^{-6}$	$1.4\cdot10^{-5}$	$1.5\cdot10^{-5}$
0.5148980	$9.3\cdot10^{-7}$	$6.6\cdot10^{-6}$	$5.6\cdot10^{-6}$	$8.7\cdot10^{-6}$
0.7016058	$1.8\cdot10^{-6}$	$5.6\cdot10^{-6}$	$2.5\cdot10^{-6}$	$6.4\cdot10^{-6}$
0.9002078	$2.7\cdot10^{-6}$	$2.4\cdot10^{-6}$	$6.6\cdot10^{-7}$	$3.7\cdot10^{-6}$
0.9494091	$2.1\cdot10^{-6}$	$1.3\cdot10^{-6}$	$3.2\cdot10^{-7}$	$2.5\cdot10^{-6}$

3.2.2. Fitting of calibration function

The results of the fitting of equation (1) to the calibration measurement as discussed in Section 2.4 are provided in Table 8. Deviations between the fit and calibration measurements are plotted in Fig. 9. As seen, these deviations are at least a factor four higher than the uncertainty of the calibration mixtures. Since these uncertainty terms can be considered independent of each other, the estimated total systematic uncertainty in composition measurements is hence indistinguishable from the standard error of regression of the mole fraction, $S_E(z_{CO_2})$, where z_{CO_2} is substituted with x_{CO_2} and y_{CO_2} for samples from the liquid and vapor samplers, respectively. In other words, the systematic uncertainty in mole fraction is given by $\bar{u}_c(x_{\mathrm{CO_2}}) = 1.5 \cdot 10^{-4}$ and $\bar{u}_c(y_{\mathrm{CO_2}}) = 1.4 \cdot 10^{-4}$.

Table 8: Fitting results of the parameters of equations (1) to sampling of the calibration mixtures.

Variable	Liquid sampler	Vapor sampler
c_1	0.130432	0.093257
c_2	1.748033	1.776062
c_3	1.079110	1.079383
c_4	1.430834	0.811486
c_5	1.423961	1.504501
$S_E(z_{CO_2})$	1.5×10^{-4}	1.4×10^{-4}
N	20	28

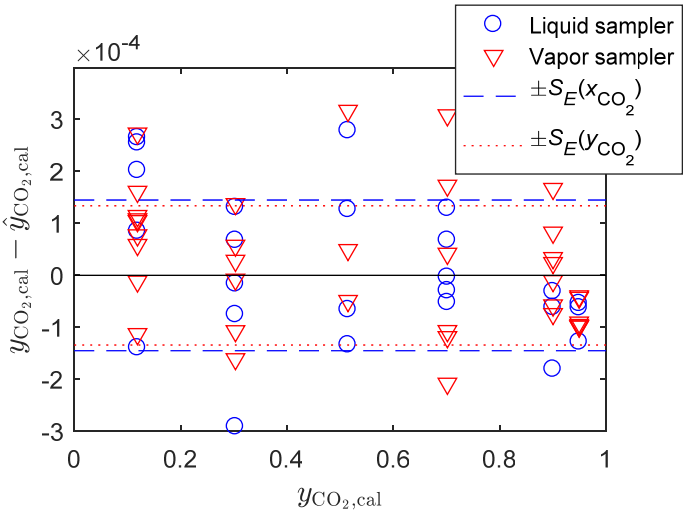

Fig. 9: Difference between nominal calibration mixture composition $y_{\mathrm{CO_2,cal}}$ from gravimetric preparation and estimated compositions $\hat{y}_{\mathrm{CO_2,cal}}$ equation (1) of GC calibration samples extracted by the liquid and vapor samplers. Standard error of regression for the liquid, $S_E(x_{CO_2})$, and vapor, $S_E(y_{CO_2})$ sampler

3.3. Data and uncertainty estimation

In Tables 2 - 5, the sample standard deviations, the systematic standard uncertainties, and the combined uncertainties of the mean temperature, pressure, and composition measurements of the data points are provided. In addition, the total standard uncertainties of the phase equilibrium data are provided in terms of composition. The nomenclature for these properties are provided in Tables 2 and 4. In general, the sources and estimation of systematic uncertainty was identical to what was described in Refs. [18, 19], and will not be further described here. Estimation of standard deviations and measurement points

For the phase equilibrium measurements with pressure compensation employed bellows, the estimation of standard deviations and measurement points in temperature, pressure, and composition was also performed in an identical manner as described in Section 3 of Ref. [19].

3.3.1. Data and standard deviation estimation when pressure compensation was not employed

Without pressure compensation, the temperature measurement point and its standard deviation have been estimated the same way as for the other data points. However, each sampling drives the system to a slightly lower pressure. Because the time period between each sample is limited and without stirring, the system will not necessarily return to an equilibrium state (at lower pressure) within measurement accuracy. Nevertheless, after the two flushing samples of these

phase equilibrium measurements, a clear linear trend is seen in the measured pressure as a function of measured composition for the subsequent data samples, as illustrated in Fig. 10. Hence, the pressure of these data points, $\bar{p}_f$, was set equal to pressure prior to the first flushing sample, whereas data point composition ($\bar{x}_{CO_2}$ or $\bar{y}_{CO_2}$) was found by linear regression from the data samples. The estimator of the variance of the mole fraction of the regressed line at $\bar{p}_f$ was used as standard deviation of the mean composition [41]:

$$s(\bar{z}_{CO_2}) = S_E(z_{CO_2})\sqrt{\frac{1}{n_s} + \frac{(\bar{p}_f - \bar{p})^2}{s_{pp}}}, \qquad (3a)$$

where

$$s_{pp} = \sum_{i=1}^{n_s} (p_i - \bar{p})^2, \qquad (3b)$$

and z should be substituted with x or y for liquid or vapor sample, respectively, n_s is he number of measurement samples, p_i are the pressures of each measurement sample, $\bar{p}$ is the mean measured pressure of these samples, and $S_E(z_{CO_2})$ is the standard error of regression of the measurement samples' composition as a function of pressure.

Since the pressure standard deviation $s(\bar{p}_f)$ is implicitly included in $s(\bar{z}_{CO_2})$ from equation (3), $s(\bar{p}_f)$ is for these data points in most cases not provided in the tables. For the two data points L1 and V5 at the three-phase line at 213 K, however, the pressure standard deviations were estimated from the fluctuations during a prolonged period prior to the first flushing sample, as these fluctuations were higher than the systematic pressure uncertainty. This exception will be further discussed in Section 3.3.3.

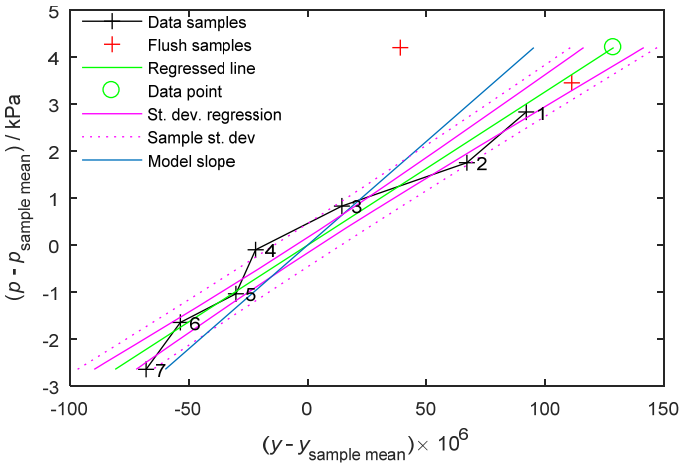

Fig. 10: Example of estimation of data point and composition uncertainty when pressure stabilization was not employed during sampling.

3.3.2. *Systematic and combined uncertainty*

The systematic standard uncertainties in temperature, $\bar{u}_c(\bar{T})$, pressure, $\bar{u}_c(\bar{p})$, and composition, $\bar{u}_c(x_{CO_2})$ or $\bar{u}_c(y_{CO_2})$ for each data point were estimated using the same methodology as was presented in Refs. [18, 19]. As discussed in Section 3.2, the uncertainty in composition is dominated by deviations between the calibration function and the composition calibration measurements.

As in previous work, the combined uncertainties in the three measurands pressure, temperature, and composition is found by a root mean sum of the estimated standard deviation and systematic uncertainty, since these uncertainty contributions can be assumed independent of each other. In order to get the total uncertainty of a phase equilibrium measurement, the uncertainties of all three measurands must be propagated and combined into a single uncertainty [42]. The estimation of total uncertainty will be further discussed in Section 3.3.4.

The combined estimated uncertainty in pressure ranges from 0.5 kPa (V2) to 4.1 kPa (V5). It should be noted though, that the former is attained without any estimate for standard deviation, for reasons discussed in Section 3.3.1. However, except for the three-phase line, where the pressure uncertainty will be further discussed in Section 3.3.3, all pressure standard deviations $s(\bar{p}_f)$ of data points that actually have been calculated are significantly smaller than the systematic uncertainty. Excluding the three-phase line measurements, the maximum estimated pressure measurement uncertainty is 3.2 kPa (L4 and L6). In relative terms, the combined uncertainty in pressure varies between $1.4 \cdot 10^{-4}$ (several points) and $6.1 \cdot 10^{-4}$ (again V5). Except the vapor point at the three-phase line, the maximum relative uncertainty is at V2 with $4.9 \cdot 10^{-4}$, i.e. the data point with *smallest* estimated absolute pressure uncertainty.

The estimated uncertainty in temperature ranges from around 1 mK to 13 mK, the latter attained at 243 K.

The estimated composition measurement uncertainty ranges between $1.4 \cdot 10^{-4}$ (several points) and $8.8 \cdot 10^{-4}$ (V13). The latter is an outlier in terms of uncertainty due to high estimated standard deviation. For this data point, there was no pressure compensation, so the estimated standard deviation in composition also implicitly includes scatter in pressure measurements, as explained in Section 3.3.1. Except the freezing point L7, all other data points have estimated uncertainty in the composition measurement at or lower than $1.8 \cdot 10^{-4}$, and an estimated standard deviation smaller than the systematic uncertainty. Hence, even if there is a tendency that the standard deviation estimates for composition data are somewhat lower with pressure compensation than without,

the composite uncertainty is in most cases not affected to a large degree. However, even with the careful procedures followed in this work, described in Sections 2.2 and 3.3.1, data point V13 illustrates that pressure compensation could reduce uncertainty at certain conditions, and certainly for other binary mixtures.

3.3.3. Measurement of the three-phase line at 213.146 K

With solid, liquid and vapor simultaneously present in the cell at 213.146 K, the system was significantly slower to reach equilibrium than the other investigated systems. Further, the instability in pressure was higher than the systematic uncertainty in the pressure measurements. Hence, in this case, the uncertainty in pressure data is expected to be mainly due to deviations from equilibrium state rather than the uncertainty in the pressure measurements.

In order to verify and get a better estimate of the three-phase line pressure, it was measured twice, separated by a period of about 8 days, during which ordinary VLE states were measured at the same temperature. The first investigation of the three-phase line pressure was ended by a composition measurement of the vapor phase, data point V5 in Tables 4-5. The second investigation was ended by a composition measurement of the liquid phase, data point L1 in Tables 2-3. A more detailed description of the two three-phase line measurements and the estimation of their unsystematic uncertainties is provided in Appendix A.

Our best estimate of the three-phase line pressure is found by calculating an average of the two measurements weighted with their inverse uncertainties:

$$\bar{p}_{3p} = \frac{\bar{p}_f(\mathrm{L1})u_c^2(\bar{p}_f,\mathrm{L2}) + \bar{p}_f(\mathrm{L2})u_c^2(\bar{p}_f,\mathrm{L1})}{u_c^2(\bar{p}_f,\mathrm{L1}) + u_c^2(\bar{p}_f,\mathrm{L2})}, \quad (4a)$$

$$u_c(\bar{p}_{3p}) \approx \sqrt{\bar{u}_c^2(\bar{p}_{3p}) + \frac{\left[s(\bar{p}_f,\mathrm{L1})s(\bar{p}_f,\mathrm{L2})\right]^2}{s^2(\bar{p}_f,\mathrm{L1}) + s^2(\bar{p}_f,\mathrm{L2})}}. \quad (4b)$$

Here $\bar{p}_{3p}$ is the best estimate of the three-phase pressure at 213.146 K, whereas the nomenclature defined in Table 2 is used otherwise. The value and uncertainty of the two measurements of the three-phase line pressure measurements as well as the best total estimate are shown in Table 9. It should be noted, that the total uncertainty for both the vapor and liquid point is dominated by the composition measurement, not the pressure measurements.

Table 9: Estimation of the three-phase pressure at 213.146 K

	$\bar{p}_f$ or $\bar{p}_{3p}$ / MPa	u_c / MPa	Bounds of $\bar{p}_f$ or $\bar{p}_{3p}$ / MPa		$\bar{T}_f$ / K
			Min	Max	
Liquid (L1)	6.8455	2.4E-03	6.8431	6.8479	213.146
Vapor (V5)	6.8449	4.1E-03	6.8408	6.8490	213.146
Weighed mean	**6.8453**	2.2E-03	6.8431	6.8476	213.146

3.3.4. Total uncertainty

Like in Refs. [18, 19], total standard uncertainty of the phase equilibrium data, $u_{\mathrm{tot}}(\bar{x}_{\mathrm{CO_2}})$ or $u_{\mathrm{tot}}(\bar{y}_{\mathrm{CO_2}})$, are provided in terms of mole fractions, assuming that the combined uncertainty in temperature, pressure, and composition measurements are independent of each other. From basic theory of uncertainty propagation [42], it follows that:

$$u_{\mathrm{tot}}(\bar{z}_{\mathrm{CO_2}}) = \sqrt{\left(\frac{\partial z_{CO_2}}{\partial T}\right)_p^2 u_c^2(\bar{T}_f) + \left(\frac{\partial z_{CO_2}}{\partial p}\right)_T^2 u_c^2(\bar{p}_f) + u_c^2(\bar{z}_{\mathrm{CO_2}})}, \quad (5)$$

where z should be substituted with x or y for liquid or vapor samples, respectively. The partial derivatives are estimated in different ways. The temperature derivatives $\left(\partial z_{CO_2}/\partial T\right)_p$ and pressure derivatives $\left(\partial z_{CO_2}/\partial p\right)_T$ at lower pressures are estimated using EOS-CG [12]. For the VLE data points closer to the critical point, the scaling model to be discussed in Section 4.1 is used to estimate $\left(\partial z_{CO_2}/\partial p\right)_T$ as all equation of state (EOS) models deviate somewhat from the data. For the freezing point data above the three-phase line, a simple two-point estimation based on the data is used. The selected method to estimate $\left(\partial z_{CO_2}/\partial p\right)_T$ is indicated for each data point.

For most data points the combined uncertainty in composition, $u_c^2(\bar{y}_{\mathrm{CO_2}})$, is the dominating term on the right-hand side of equation (5). Hence, the estimate for total uncertainties of majority of the data points are indistinguishable from the measurement uncertainty in composition, or $u_{\mathrm{tot}}(\bar{z}_{\mathrm{CO_2}}) \approx u_c(\bar{z}_{\mathrm{CO_2}})$, with the minimum value of the systematic uncertainties of $\bar{u}_c(x_{\mathrm{CO_2}}) = 1.5 \cdot 10^{-4}$ and $\bar{u}_c(y_{\mathrm{CO_2}}) = 1.4 \cdot 10^{-4}$ attained for many of them. Around the critical points, minor changes in pressure lead to major changes in composition, and the dominating systematic uncertainty source are due to the pressure measurements, mainly the uncertainty of the calibration of these sensors. The maximum standard measurement uncertainty of the data points is $u_{\mathrm{tot}}(\bar{y}_{\mathrm{CO_2}}) = 1.2 \cdot 10^{-3}$ for V16. According to the estimate to be presented in Section 0, this data point is 42 kPa, or 0.3 %, below the critical pressure of this isotherm. At no data point is

temperature uncertainty $u_c\ (\bar{T}_f)$ a significant contributor to the total estimated uncertainty $u_{\mathrm{tot}}(\bar{z}_{\mathrm{CO_2}})$.

3.4. CO_2 vapor pressure measurements

In Table 6 the vapor pressure measurement of this work is presented. Unlike Refs. [18, 19], impurities of the second component, in this case Ar, have been taken into account. For most of the data points, the content of the cell was analyzed, and a crude estimate of the impurity level was estimated from the gas chromatograms where a small peak occurred at the retention time of Ar, which indicate that the flushing of the cell was not complete within detection limits. For V1, V17 and V26, the cell content was not sampled, and the impurity level and composition uncertainty was set to 10 ppm, which for these data points ensures inclusion of all measured impurity levels within the standard uncertainty limits. The total uncertainties of the vapor pressure measurements have been calculated similarly to the total uncertainty in terms of composition for the other data points:

$$u_{\mathrm{tot}}(\bar{p}_f) = \sqrt{\left(\frac{\partial p}{\partial T}\right)^2_{y_{\mathrm{CO_2}}} u_c^2(\bar{T}_f) + u_c^2(\bar{p}_f) + \left(\frac{\partial p}{\partial y_{\mathrm{CO_2}}}\right)^2_{T} u_c^2(\bar{y}_{\mathrm{CO_2}})}. \quad (6)$$

Based on the estimated impurity, the vapor pressure was extrapolated down to pure CO_2 using the gradient of EOS-CG [12], p_{ex}. Further, the model vapor pressure, p_{mod}, of Jäger-Span at 213 K [24] and Span-Wagner [31] at other temperatures were calculated. In all cases, the deviation between the model vapor pressure and both the measured and extrapolated values are well within the estimated measurement standard uncertainty $\pm u_{\mathrm{tot}}(\bar{p}_f)$.

4. Analysis of data

4.1. Comparison with literature data

Nine previous experimental works on the phase equilibria of this binary system have been identified and are summarized in Table 17. Only Preston et al. [25] have reported freezing point data (LSE), but at temperatures about 100 K lower than the present work and ambient pressure where the liquid phase has a very low CO_2 content. The other previous work all reports VLE data. Except for Refs. [26, 27, 40, 43], all authors report analytical measurements where the compositions of the fluid phases present are measured at a given equilibrium condition to identify the phase borders.

No comparable previous data have been found for the isotherms at 213 of the current work, but for the other isotherms plotted in Figs. 4-8 literature data has been included where relevant. Of the previous works, the data by Coquelet et al. [38], Tsankova et al. [27] , and Lasala et al. [35] appear most self-consistent. The data of Ref. [27] seems consistent with the current data where comparable at 263, 273 and 283 K, noting that the measurements of Ref. [27] shown in Fig. 7 are at slightly different temperatures. The data set of Ref. [38] has a match in temperature with the current measurements at 273 and 299 K, whereas the data set of Ref. [35] matches the current work in temperature at 223 and 273 K. The facilities used in Refs. [35, 38] are similar, both being designed and constructed by the same group. For the data at 273 K shown in Fig. 6, there is a deviation between the current work and Refs. [35, 38] of about 1 % for the dew points around 10 MPa, where the CO_2 concentration is at its lowest. These deviations are larger than the experimental uncertainties reported by those two works. Ref. [35] reports a standard uncertainty in composition of about 0.5 %. Ref. [38] provides an estimated uncertainty in mole measurements of 1.6 and 0.8 % for pure Ar and CO_2, respectively. At a vapor mole fraction of $y_{\mathrm{CO_2}} \approx 0.6$, this corresponds to an uncertainty in mole fraction between 0 and 0.6 % dependent on if and how the deviations in mole measurements are correlated. Hence, the deviation between the current measurements and those of Ref. [38] in this specific region seems outside their mutual estimated uncertainty bounds. Similarly, there is a deviation of about 0.8 % in composition between the present data and that of Ref. [35] in the same region of the 223 K isotherm shown in Fig. 3, compared with the 0.4 % standard uncertainty reported by Ref. [35] for those data points. It is beyond the scope of this work to speculate about the reasons for these discrepancies, but in our experience, multipoint rather than pure component GC calibration, the use of a GC integration technique that takes into account overlap between peaks in the spectrographs, and sufficiently long test cell stabilization periods prior to sampling are all important factors needed to obtain accurate composition measurements.

In other regions of the 223 and 273 K isotherms, as well as at 299 K shown in Fig. 8, Refs. [35, 38] are consistent with each other within measurement uncertainty. This is probably also true regarding the deviations between the current work and the data of Köpke and Eggers [36, 37] at 243 K in Fig. 4 and perhaps 273 K in Fig. 6, judging by the scatter of the latter's data. Finally, the data of Kaminishi et al. [39] at 273 K shown in Fig. 6 and Ahmad et al. at 283 K shown in Fig. 7 cannot be said to be in agreement with the current work or any other sources. None of the isotherms of the current work are close in

temperature to the single isotherm of Sarashina et al. [43] at 288 K or the two data points at cryogenic temperatures of Preston et al. [25].

The temperature, pressure, and type of phase equilibria investigated by all VLE works listed in Table 17 are shown in Fig. 11. The VLE regions of $CO_2 + Ar$ in terms of pressure and temperature estimated by EOS-CG and the new equations of state to be presented in Section 5 are also indicated in the figure, as well as the pure CO_2 freezing curve. The current data spans most of the VLE region, and measures VLE at lower temperatures, and at slightly higher pressures, and hence closer to the critical locus, than previous works. With the assumption that Refs. [26, 27, 35, 38] and possibly Ref. [43] have reported the most accurate data until now, the new data also fills rather wide gaps in data around 263 K and 243 K. Finally, with regards to the binary phase equilibria measurements involving dry ice of the current work, the only related measurement for any binary system with CO_2 that has been identified is the three-phase line measurements of $CO_2 + N_2$ and $CO_2 + H_2$ by Fandiño et al. [44].

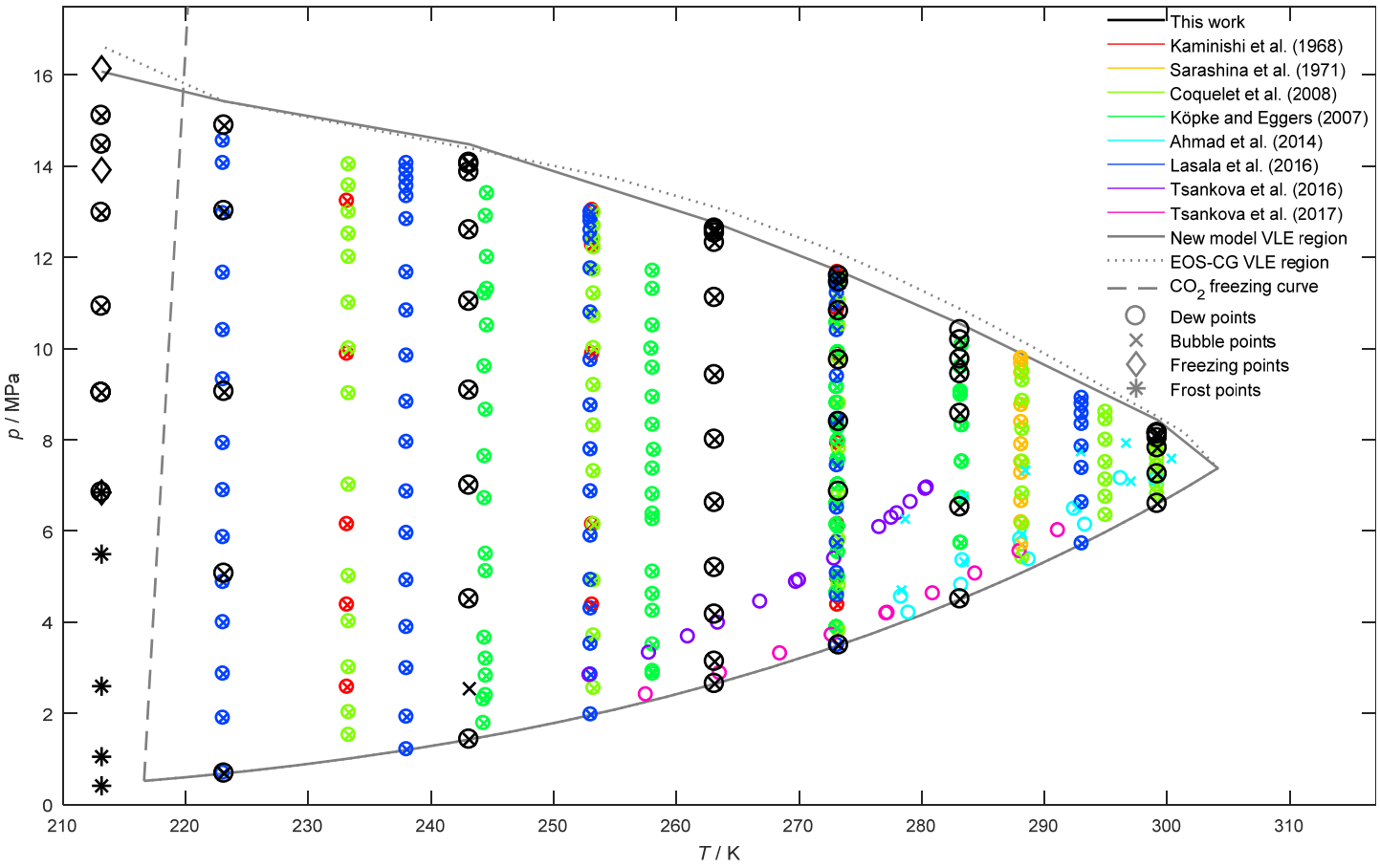

Fig. 11: Summary of phase equilibrium data of current and previously published work [26, 27, 35-40, 43]. For illustration, the critical loci of the original EOS-CG [12] and the new model and the pure CO_2 vapor pressure curve from Span Wagner [31] are included, as well as the pure CO_2 freezing curve from Jäger and Span [45]. The freezing point data of Preston et al. [25] at 109 and 116 K are far off the temperature scale and hence not included.

4.2. Comparison of VLE data with SRK, GERG-2008, and EOS-CG

In Figs. 2–8 of the isotherms, the isothermal VLE phase envelopes of five EOS are included:

- Soave-Redlich-Kwong (SRK) cubic EOS [46] with the binary interaction coefficient $k_{CO2+Ar} = 0.180$ of Li and Yan [34].
- Peng-Robinson cubic EOS with mixing rule by Wong-Sandler (PR-WS), fitted to the present data and to be further discussed in Section 4.4.
- GERG-2008 multiparameter EOS [32, 33]
- Original EOS-CG multiparameter EOS [12]
- A new model to be presented in Section 5 based on EOS-CG with revised mixing rule

These modeling curves have been produced by the internal thermodynamic tool of SINTEF Energy Research [47].

The SRK EOS with $k_{12} = 0.180$ generally fits the dew point data at higher CO_2 fractions fairly well, but estimates bubble points with too low pressure at high CO_2 fractions and critical points with too high pressure and too low CO_2 fraction. In preparation for this work, VLE curves have been produced with a range of different binary interaction coefficients. However, with only one fitting parameter available, it is in fact not possible to fit the SRK EOS satisfactory to the experimental data even for a single temperature. It is possible to obtain better fits in selected regions, though, say at high CO_2 mole fraction or for the critical region at a given temperature, but it would come at cost of higher deviations in other temperature/pressure/composition domains. As will be further discussed in Section 4.3, SRK with $k_{12} = 0.180$ do not predict liquid phase at any pressure at 213 K.

GERG-2008 [32, 33] is an advanced multiparameter EOS designed mainly for accurate prediction of natural gas properties, and not for high CO_2-content mixtures relevant for CCS. One consequence is that GERG-2008 uses a simplified model for pure CO_2 compared with the Span-Wagner EOS [31] used by EOS-CG. In general, GERG-2008 agrees fairly well with the data at high CO_2 mole fractions. However, compared with the data, the model predicts a lower critical point pressure at 213 K, and a significantly higher critical point pressure and lower CO_2 mole fraction for temperatures at and above 243 K. At 283 K, the mismatch in pressure is about 2.2 MPa. At 299 K, the critical argon mole fraction of GERG-2008 is more than twice as high as the data supports. One problem with GERG might be that the CO_2 + Ar model seems to have been developed for GERG-2004, at which time only the VLE data of Kaminishi et al. [39] and Sarashina et al. [43] were available. As seen in Fig. 6 on the 273 K isotherm, GERG-2008 seems to fit the data of Ref. [39] almost perfectly, but these data differ systematically from all the three more recent sources.

As expected for a multiparameter EOS targeting CO_2-rich mixtures, EOS-CG [12] has significantly better agreement with both the current data and literature data than the SRK EOS used in this work and GERG-2008. The largest absolute deviations are seen at 213 K displayed in Fig. 2, which is natural, since the previous literature at lowest temperature until now were at 233 K [38, 39]. Compared with the data, the dew point line of EOS-CG above the three-phase line generally is too low in pressure, but the critical point comes at a too high pressure and CO_2 fraction. The overall shape of the VLE curve is more pointed than the data. For the isotherms at 263 K and higher temperatures, EOS-CG estimates a higher critical pressure and lower critical CO_2 mole fraction than the data. Hence, in relative terms, the largest deviations between the experimental data and EOS-CG occur at 299 K, as seen in Fig. 8. At high CO_2 fractions, EOS-CG in general conforms well with the data at all investigated temperatures

The performance of the new multiparameter model of this work will be analyzed in detail in Section 5. However, from Figs. 2–8, it is clear that the new mixing rule significantly improves the model's agreement with the measurements at the investigated temperatures.

4.3. Models for phase equilibria with solid state

In Fig. 2, the measurements of frost points (VSE), freezing points (LSE) and three-phase line (VLSE) is accompanied by model predictions using the dry ice model of Jäger-Span [24] combined with fluid models in a way also prescribed by Ref. [24]:

$$g^{\mathrm{sol}}_{\mathrm{CO_2}}(T,p) = \mu^{\mathrm{liq}}_{\mathrm{CO_2}}\left(T,p,x_{\mathrm{CO_2}}\right) \quad \text{(LSE)}, \tag{7a}$$

$$g^{\mathrm{sol}}_{\mathrm{CO_2}}(T,p) = \mu^{\mathrm{vap}}_{\mathrm{CO_2}}\left(T,p,y_{\mathrm{CO_2}}\right) \quad \text{(VSE)}. \tag{7b}$$

Here $g^{\mathrm{sol}}_{\mathrm{CO_2}}$ is the molar Gibbs free energy of solid CO_2 from Ref. [24] and $\mu^{\mathrm{liq}}_{\mathrm{CO_2}}$ and $\mu^{\mathrm{vap}}_{\mathrm{CO_2}}$ are the chemical potentials of CO_2 in the liquid and vapor phase, respectively, calculated from the fluid model. The underlying assumptions is that the solid phase is pure CO_2.

The fluid models used are listed in Section 4.2, but regarding the freezing point curve (SLE), only the predictions of the multiparameter equations of state are shown. The calculations are performed using the thermodynamic tool of SINTEF Energy Research [47].

At the three-phase line pressure (VLSE), a further constraint compared with equations (7) is that the chemical potentials $\mu^{\mathrm{liq}}_{\mathrm{CO_2}}$ and $\mu^{\mathrm{vap}}_{\mathrm{CO_2}}$ must be equal. Compared with the data, the fitted PR-WS and the new model to be presented in Section 5 in combination with Jäger-Span estimate a three-phase line pressure about 50 kPa below and 0.13 MPa above the measured value, respectively. The other models have higher deviations. In fact, for SRK with a binary interaction coefficient of $k_{12} = 0.180$ combined with Jäger-Span, no second fluid phase is apparent, and hence no VLE envelope, three-phase line, or freezing curve. Further studies revealed that k_{12} must be reduced to 0.16 before the liquid phase appears.

The main differences between the freezing point curves (SLE) produced using GERG-2008 versus EOS-CG and the new model

seem to be the starting point which is determined by the three-phase line pressure and liquid composition. As such, the new model curve provides the clearly best fit, although it does not appear to include the full curvature suggested by the two measured freezing points.

The frost points of all models at lower pressure agree reasonably well with each other and the experimental data. The convergence of the different models at lower pressure is expected since the vapor is approaching an ideal gas.

It should be noted that unlike Wong-Sandler, the new model to be further discussed in Section 5 has not been fitted to the measured frost point or freezing point data. Hence, the great improvement in the description of the fluid - solid phase equilibria seen from the original to the revised EOS-CG is due to improvements in the fluid model only. As discussed in Section 3.4, the Jäger and Span method for EOS vapor pressure prediction of solid state CO_2 [24] agree with the current experimental results within measurement uncertainty.

4.4. Peng-Robinson EOS with Wong-Sandler mixing rule

As in previous works [18, 19], Peng-Robinson EOS with Wong Sandler mixing rules [48, 49], the formulation of Mathias and Copeman [50] for the alpha correction, and the NRTL formulation [51] for the Gibbs free energy were fitted to the experimental data. The model has been denoted the acronym PR-WS in the current work. Three parameters have been fitted: the binary interaction parameter k_{12} of the Wong-Sandler mixing rule, and the two parameters τ_{12} and τ_{21} of the NRTL model. Further details and nomenclature of the models, nomenclature, and fitting technique can be found in Ref. [18].

Although PR-WS has relatively few fitting parameters, it has shown to describe VLE data with CO_2 fairly well. It is also of interest to compare the fitting results of the new recent data on CO_2 + Ar to the results of Coquelet et al. [38], who employed the same model.

The pure component critical and Mathias-Copeman coefficients are provided in Table 10.

Table 10: Critical and pure component critical data and Mathias-Copeman used in the PR-WS model fitted in this work.

i	$T_{c,i}$ / K	$P_{c,i}$ / MPA	$c_{1,i}$	$c_{2,i}$	$c_{3,i}$
Ar	150.8	4.8737	0.397483	-0.28239	0.796288
CO_2	304.2	7.3765	0.704606	-0.31486	1.89083

The results of the temperature dependent fit of the three parameters k_{12}, τ_{12}, and τ_{21} to the seven measured isotherms of this work are provided in shown in Fig. 12, labeled "Case 1" in line with [18, 19]. In the same figure, also the similar results of Coquelet et al. [38] are indicated. The binary interaction coefficients of the two works are fairly similar except for the isotherm at 299 K, but the NRTL parameters differ significantly at all temperatures. It should be noted though, that in Ref. [38] the objective function is very different from the one used here. In the current work, as defined in Refs. [18, 19], both composition and pressure are minimized using orthogonal distance regression (ODR) [52]. In Ref. [38] the relative composition is fitted. In addition, the parameters of Table 10 is somewhat different, so exact match in the model parameters are not to be expected.

As in Refs. [18, 19], a temperature dependent model was made ("Case 2") for the three fitted parameters k_{12}, τ_{12}, and τ_{21} of the PR-WS model. Unlike previous work, no strong nonlinear trend at the higher temperatures could be identified, and a simple linear model was assumed:

$$k_{12} = a_{k_{12}} + b_{k_{12}} T, \quad (8a)$$

$$\tau_{12} = a_{\tau_{12}} + b_{\tau_{12}} T, \quad (8b)$$

$$\tau_{21} = a_{\tau_{21}} + b_{\tau_{21}} T. \quad (8c)$$

The fitted coefficients a_i and b_i are provided in Table 12, the resulting values of k_{12}, τ_{12}, and τ_{21} are provided in Table 11, and the resulting VLE curves are shown in Figs. 2-8 together with the measured isotherms and the other models. In Fig. 2 also the frost curve is provided for 213 K, which already is commented on in Section 4.3. Overall, the model provides one of the best fit to the VLE data of the investigated models. It behaves particularly well at higher temperatures and close to the critical point. However, it tends to overestimate the

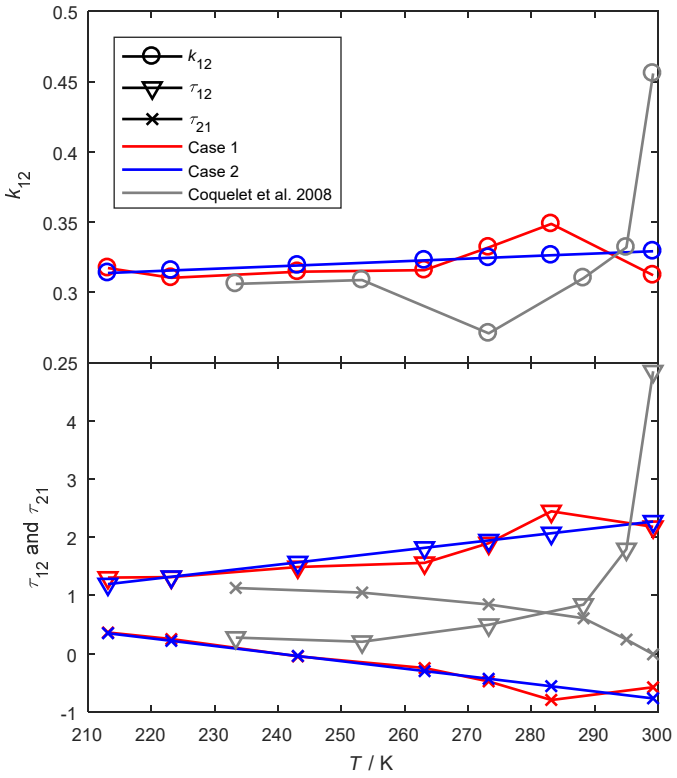

Fig. 12: PR-WS parameters k_{12} (top) and τ_{12}, and τ_{21} (bottom) fitted to each measured isotherm of this work ("Case 1") and linearly regressed values of these values as a function of temperature ("Case 2"), as well as the results of Coquelet et al. [38]

Table 11: Fitted parameters of the PR-WS model in this work, as well as a characterization of the quality of the fit in terms of objective function value (S), absolute average deviation in terms of composition, and bias in terms of composition.

T / K	Case 1						Case 2					
	k_{12}	τ_{12}	τ_{21}	S	AAD / %	Bias / %	k_{12}	τ_{12}	τ_{21}	S	AAD / %	Bias / %
213.146	0.317	1.306	0.362	28.1	0.56	0.19	0.314	1.193	0.349	62.9	1.25	-0.71
223.146	0.310	1.314	0.250	37.2	0.77	-0.06	0.316	1.318	0.219	40.2	0.87	-0.29
243.120	0.315	1.487	-0.047	59.6	1.19	-0.35	0.319	1.568	-0.040	66.3	1.22	0.06
263.134	0.316	1.558	-0.249	52.7	0.92	-0.19	0.323	1.818	-0.300	62.7	0.91	0.40
273.257	0.332	1.897	-0.477	49.0	0.79	-0.14	0.325	1.945	-0.432	59.0	0.80	0.32
283.144	0.349	2.445	-0.796	49.2	0.94	0.15	0.326	2.068	-0.561	53.0	0.94	0.37
299.218	0.312	2.177	-0.577	12.7	0.15	0.01	0.329	2.269	-0.769	18.0	0.21	-0.15

minimum CO_2 concentration of all phase envelopes, in particular at higher temperatures. It should further be noted that this model is only fitted to phase equilibrium data, and due to inherent properties of the cubic model it will probably not provide estimates of other thermodynamic properties that will be as accurate as those of eg. the new model.

Table 12: Fitting results for the coefficients of a_i and b_i of the simple linear model defined in equations (8) for the three fitted coefficients k_{12}, τ_{12}, and τ_{21} of PR-WS

i:	k_{12}	τ_{12}	τ_{21}
a_i	0.32452	1.9435	-0.4306
b_i	0.00018	0.0125	-0.013

4.5. *Critical point estimation*

Like in Refs. [18, 19], a scaling law model was fitted to the data in order to estimate the critical CO_2 mole fraction, $z_{CO_2,C}$, and pressure, p_c of each isotherm [53, 54]:

$$z_{CO_2,C} = \hat{z}_{CO_2,C} + \left(\lambda_1 + \varepsilon\frac{\lambda_2}{2}\right)(\hat{p}_c - p) + \varepsilon\frac{\mu}{2}(\hat{p}_c - p)^{\beta}, \quad (9)$$

where

$$\varepsilon = \begin{cases} 1 \text{ for bubble points} \\ -1 \text{ for dew points} \end{cases},$$

and z_{CO_2} was the bubble or dew point CO_2 mole fraction at pressure p. β was kept at 0.325 while the other 5 parameters were fitted to the data specified in Table 13. The model is most suitable close to the critical point, and hence only the data points with highest pressures were considered. The number of data point selected was for 6 of the isotherms such that the standard error of the regression in pressure and in most cases mole fraction, $z_{CO_2,C}$, was minimized. With 5 parameters to fit, the smallest number of data points needed in order to estimate the standard error of regression is $n = 6$. For 283 K, the smallest error of regression was achieved with this least possible value of n, and two of the data points were very close to each other and with overlapping standard uncertainty bounds. Hence, in this case, two additional data points were included in the fit.

The fitted parameters of the scaling model (9) are provided in Table 13 together with the standard errors of regression of pressure, $S_E(\hat{p})$ and composition, $S_E(\hat{z}_{CO_2})$, for the seven isotherms, as well as standard uncertainties of the critical point estimates in pressure, $u(\hat{p}_c)$, and composition $u(\hat{z}_{CO_2,c})$. The standard uncertainties include experimental uncertainty in addition to regression errors. These terms are defined and discussed in more detail in Ref. [18]. The estimated uncertainty of the critical points varies between 1 and 7 kPa in pressure and 0.02 and 0.07 % in mole fraction.

The scaling law curves are plotted together with the data points used in the fit, the estimated critical points, and the two versions of PR-WS presented in Section 4.4. The estimated critical points are also included in the plots of the different isotherms provided in Figs. 2–8. As discussed in Section 4.4, the fit of PR-WS is fairly good even in the critical region, but neither this EOS nor EOS-CG adequately reproduces the flatness of the phase envelope around the critical point, and hence, as discussed in Section 3.3.4, should not be used to calculate total uncertainty from equation (5).

In Fig. 14, the critical point estimation presented in the current section is compared with the results of the new model for CO_2 + Ar to be presented in Section 5 and the results of the critical point estimation provided by Coquelet et al. [38]. Compared with the scaling law estimates, it appears as if the new model provides a better estimate of critical pressure and composition at the highest temperatures than Ref. [38]. This is not surprising, given that this model has included the current measurements in its data basis. However, the critical point estimations of the new model seem to drift off somewhat compared with the scaling law estimates at the lower temperatures.

Table 13: Data selection and result of fitting of scaling law model (9) applied around the critical point of the 7 isotherms experimentally investigated in this work.

Mean T / K	Used data points	n	λ_1 / (MPa^{-1})	λ_2 /(MPa^{-1})	μ /(MPa$^{-\beta}$)	$\hat{z}_{CO_2,c}$	$\hat{p}_c$ /MPa	$S_E(\hat{z}_{CO_2})$	$u(\hat{z}_{CO_2,c})$	$S_E(\hat{p})$ /MPa	$u(\hat{p}_c)$ /MPa
213.146	L4-6, V9-11	6	$7.1620\cdot10^{-3}$	$1.7231\cdot10^{-2}$	0.33441	0.41301	15.2911	$4.3\cdot10^{-4}$	$5.3\cdot10^{-4}$	$6.3\cdot10^{-3}$	$6.6\cdot10^{-3}$
223.146	L10-12, V14-16	6	$1.1671\cdot10^{-2}$	$3.9390\cdot10^{-3}$	0.34070	0.4252	14.9350	$1.7\cdot10^{-3}$	$1.8\cdot10^{-3}$	$5.8\cdot10^{-3}$	$6.2\cdot10^{-3}$
243.120	L19-21, V23-25	8	$9.1690\cdot10^{-3}$	$2.1801\cdot10^{-2}$	0.26899	0.50026	14.1307	$3.5\cdot10^{-4}$	$3.8\cdot10^{-4}$	$3.0\cdot10^{-3}$	$3.6\cdot10^{-3}$
263.134	L29-32, V34-37	8	$-3.1000\cdot10^{-4}$	$2.8957\cdot10^{-2}$	0.21461	0.61642	12.6422	$3.9\cdot10^{-4}$	$4.1\cdot10^{-4}$	$8.4\cdot10^{-4}$	$2.0\cdot10^{-3}$
273.257	L35-37, V42-44	6	$9.8370\cdot10^{-3}$	$1.2721\cdot10^{-2}$	0.18455	0.68845	11.6204	$7.2\cdot10^{-4}$	$7.4\cdot10^{-4}$	$4.8\cdot10^{-3}$	$5.2\cdot10^{-3}$
283.144	L40-43, V48-51	8	$1.7855\cdot10^{-2}$	$-4.1910\cdot10^{-3}$	0.14981	0.77098	10.4145	$4.9\cdot10^{-4}$	$5.2\cdot10^{-4}$	$1.5\cdot10^{-3}$	$2.2\cdot10^{-3}$
299.218	L46-49, V55-58	8	$2.6054\cdot10^{-2}$	$-5.7110\cdot10^{-3}$	0.041886	0.94014	8.1514	$4.6\cdot10^{-5}$	$1.5\cdot10^{-4}$	$6.3\cdot10^{-4}$	$1.3\cdot10^{-3}$

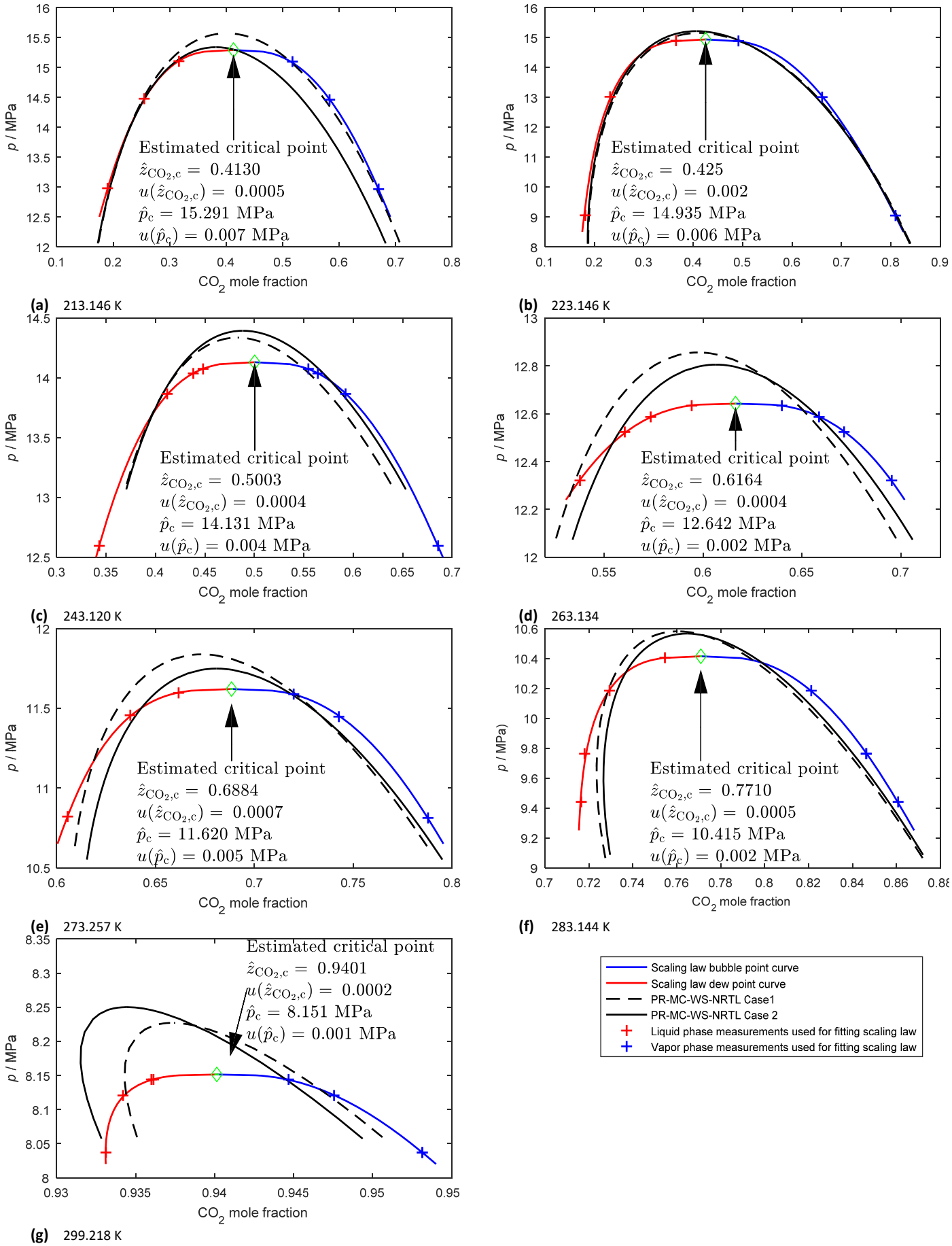

Fig. 13: Critical point estimation using the scaling law model (9) compared with the fitted PR-MC-WS-NRTL Case 1 and 2 fitted models

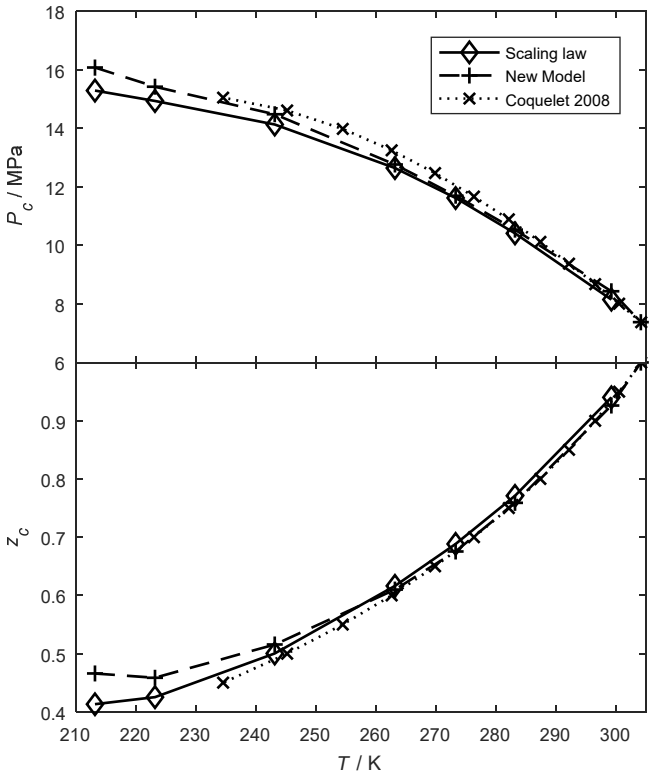

Fig. 14: Critical locus in terms of pressure (top) and composition (bottom) of the CO_2 + Ar binary system predicted by the scaling law model at the measured temperatures and the new model of this work, compared with the model of Coquelet et al. [38].

5. New Model

5.1. Fundamental Equation of State

Thermodynamic properties of the system CO_2 + Ar can be calculated by means of various equations of state. Two of these equations are based on the state-of-the-art approach of thermodynamic mixture modelling, namely the GERG-2008 of Kunz and Wagner [33] and the EOS-CG of Gernert and Span [12]. This approach enables the description of multicomponent mixtures by modelling each binary combination of the involved components. Since the GERG-2008 was developed for the description of natural-gas mixtures, CO_2 + Ar was a binary system of minor relevance during the development of the mixture model. Thus, the GERG-2008 model for this binary mixture is significantly less accurate than the one included in the EOS-CG, which was explicitly developed for an accurate description of CO_2-rich mixtures as relevant for CCS applications. However, within this article, results calculated from the GERG-2008 are compared to values obtained from the new mixture model, since the GERG-2008 is widely used within the CCS-community, although it was not developed for this application. Furthermore, such comparisons are meaningful, since the new model is based on the mathematical structure introduced with the GERG-2008. The EOS-CG mixture model was published in 2016, but its development had already been completed in 2013. Since then, additional accurate data for CO_2 + Ar became available that allowed for a refit of the existing binary model. The new data sets include accurate density, speed of sound, and dew point measurements carried out at Ruhr-Universität Bochum, as well as the vapor-liquid equilibrium data measured at SINTEF Energy Research and presented within this article. The refit of the binary model for CO_2 + Ar , is part of the ongoing work on extending and updating the EOS-CG mixture model.

5.2. Mathematical Structure

The thermodynamic correlation presented here is a fundamental equation of state. This type of equation provides a mathematical connection between thermal and caloric state properties. The result is a functional form that allows for the calculation of all thermodynamic properties by combining its derivatives. The most commonly used type of these correlations is explicitly formulated in the Helmholtz energy a with temperature T, density ρ, and molar composition $\vec{z}$ as independent variables. These input variables enable a clear description of all state points including phase-equilibria. In practical applications, it is more convenient to work with dimensionless correlations. Therefore, the present equation of state follows the reduced functional form, which was also applied for the GERG-2008 of Kunz and Wagner [33] and the EOS-CG of Gernert and Span [12]. The general structure of the mixture model reads

$$\frac{a(\rho,T,\vec{z})}{RT} = \alpha(\delta,\tau,\vec{z}) = \alpha^{\mathrm{o}}(\rho,T,\vec{z}) + \alpha^{\mathrm{r}}(\delta,\tau,\vec{z}), \qquad (10)$$

where α is the reduced Helmholtz free energy, R is the molar gas constant, δ is the reduced density and τ is the reciprocal reduced temperature according to

$$\delta = \frac{\rho}{\rho_{\mathrm{r}}(\vec{z})} \text{ and } \tau = \frac{T_{\mathrm{r}}(\vec{z})}{T}. \qquad (11)$$

As apparent from equation (10), the functional form is separated in two parts. The first part α^{o} considers the behavior of a hypothetical mixture of ideal gases, whereas α^{r} represents the residual Helmholtz energy that results from molecular interactions in the real mixture. The ideal-gas part of the equation is given as

$$\alpha^{\mathrm{o}}(\rho,T,\vec{z}) = \sum_{i=1}^{N} z_i\left[\alpha_{0,i}^{\mathrm{o}}\left(\delta_{0,i},\tau_{0,i}\right) + \ln z_i\right], \qquad (12)$$

where N is the number of components in the mixture and $\alpha^{0}_{0,i}$ is the dimensionless ideal-gas part of the Helmholtz free energy of the pure component i with the mole fraction z_i in the mixture. The ideal-gas Helmholtz energy of each component is calculated from the corresponding equation of state for the pure component at the reduced density $\delta_{0,i}$ and the reciprocal reduced temperature $\tau_{0,i}$. For the pure fluids, density and temperature are reduced by their critical parameters. Consequently, the reduced input variables are defined as

$$\delta_{0,i} = \frac{\rho}{\rho_{\mathrm{c},i}} \text{ and } \tau_{0,i} = \frac{T_{\mathrm{c},i}}{T}. \tag{13}$$

The residual part of the Helmholtz free energy of the mixture reads

$$\alpha^{\mathrm{r}}(\rho, T, \vec{z}) = \sum_{i=1}^{N} z_i \alpha^{\mathrm{r}}_{0,i}(\delta, \tau) + \Delta\,\alpha^{\mathrm{r}}(\delta, \tau, \vec{z}), \tag{14}$$

where $\alpha^{\mathrm{r}}_{0,i}$ is the residual, reduced Helmholtz free energy of the pure component i which is here evaluated at δ and τ according to equation (11). For real mixture calculations, temperature and density are not reduced by their critical parameters, since these are different for each pure component. Besides, the overall critical point of the mixture is, if existing, composition dependent and therefore complex to determine [55]. Instead, Kunz and Wagner [33] formulated the so-called "reducing functions" $T_{\mathrm{r}}(\vec{z})$ and $\rho_{\mathrm{r}}(\vec{z})$ spanning a composition-dependent surface between the critical parameters for density and temperature of each pure component in the mixture. These functions are given by

$$\begin{aligned} T_r(\vec{z}) &= \sum_{i=1}^{N} z_i^2\, T_{\mathrm{c},i} \\ &+ \sum_{i=1}^{N-1} \sum_{j=i+1}^{N} 2 z_i z_j \beta_{T,ij}\, \gamma_{T,ij} \frac{z_i + z_j}{\beta_{T,ij}^2 z_i + z_j} \left(T_{\mathrm{c},i} T_{\mathrm{c},j}\right)^{0.5} \end{aligned} \tag{15}$$

and

$$\begin{aligned} \frac{1}{\rho_{\mathrm{r}}(\vec{z})} &= \sum_{i=1}^{N} z_i^2 \frac{1}{\rho_{\mathrm{c},i}} \\ &+ \sum_{i=1}^{N-1} \sum_{j=j+1}^{N} 2 z_i z_j \beta_{v,ij} \frac{z_i + z_j}{\beta_{v,ij}^2 z_i + z_j} \frac{1}{8} \left(\frac{1}{\rho_{\mathrm{c},i}^{1/3}} + \frac{1}{\rho_{\mathrm{c},j}^{1/3}} \right)^3 . \end{aligned} \tag{16}$$

These two reducing functions contain the binary parameters β and γ, which are adjustable parameters fitted to experimental data. They obey the following symmetry rules

$$\begin{aligned} &\beta_{T,ij} = \frac{1}{\beta_{T,ji}}, \beta_{v,ij} = \frac{1}{\beta_{v,ji}}, \text{and} \\ &\gamma_{T,ij} = \gamma_{T,ji}, \gamma_{v,ij} = \gamma_{v,ji}. \end{aligned} \tag{17}$$

For every binary system within a multicomponent mixture one to all four of these parameters can be fitted to experimental data. If no or no reliable data are available, they can be adjusted by means of a simple linear or quadratic combination rule. For the system CO_2 + Ar, the experimental database is comprehensive enough to fit all four parameters. The corresponding values are given in Table 14.

Equation (14) additionally contains the function $\Delta\alpha^{\mathrm{r}}(\delta, \tau, \vec{z})$, which models the deviation of the real mixing behavior from the simple linear combination of the residual equations of the pure components evaluated at corresponding states. This so-called "departure function" is defined as

$$\Delta\alpha^{\mathrm{r}}(\delta, \tau, \vec{z}) = \sum_{i=1}^{N} \sum_{j=i+1}^{N} z_i z_j F_{ij}\, \alpha^{\mathrm{r}}_{ij}(\delta, \tau). \tag{18}$$

The departure function includes the binary specific departure function $\alpha^{\mathrm{r}}_{ij}(\delta, \tau)$ for the binary mixture of the components i and j as well as the weighting factor F_{ij}, which enables the use of generalized binary departure functions for a group of binary systems [56]. Since the database for the system CO_2 + Ar allowed for the development of a binary specific departure function, F_{ij} was not adjusted but set to unity. The binary specific departure function is an empirical model that is only loosely tied to physical information. Its mathematical structure can contain different types of terms such as simple polynomials, exponential terms or so-called "special exponential terms". The number of terms is chosen by the correlator while fitting the equation to experimental thermodynamic properties of a specific binary mixture. For the system CO_2 + Ar, the functional form contains two polynomials and four "special exponential terms". It reads:

$$\begin{aligned} \alpha^{r}_{ij}(\delta, \tau) &= \sum_{k=1}^{2} n_{ij,k} \delta^{d_{ij,k}} \tau^{t_{ij,k}} + \sum_{k=3}^{6} n_{ij,k} \delta^{d_{ij,k}} \tau^{t_{ij,k}} \\ &\cdot \exp\left[-\eta_{ij,k} \left(\delta - \varepsilon_{ij,k}\right)^2 - \beta_{ij,k} \left(\delta - \gamma_{ij,k}\right) \right]. \end{aligned} \tag{19}$$

The coefficients n_{ij} and the exponents d_{ij}, t_{ij}, l_{ij}, η_{ij}, ε_{ij}, β_{ij}, and γ_{ij} are adjustable parameters varied by the fitting algorithm to obtain the best agreement between the experimental data and

the respective properties calculated from the equation of state. The final set of parameters for CO_2 + Ar is given in Table 14.With regards to equations (10) to (19) it becomes apparent that the mixture model contains not only mixture-related terms ($\rho_r(\vec{z})$, $T_r(\vec{z})$, and $\Delta\alpha^r(\delta,\tau,\vec{z})$) but also the functions $\alpha^o_{0,i}$ and $\alpha^r_{0,i}$ describing the pure components in the mixture. For each component considered in the mixture model, an equation of state describing the pure fluid states is mandatory. These equations have to be structured analogously to equation (10) consisting of an ideal and residual part, which are then contributing to equations (12) and (14). The parameters of the reducing functions as well as the binary specific departure function for CO_2 + Ar were developed by applying the reference equations of state for pure carbon dioxide and argon of Span and Wagner [31] and Tegeler et al. [57], respectively. The structure of these reference equations will not be discussed in here, but can be seen in the corresponding publications. The mixture specific functions presented here could also be used in combination with different equations of state for the pure fluids. However, the results of such calculations might significantly deviate from the ones shown in this work.

As initially mentioned, all mixture properties can be calculated by combining derivatives of the mixture model. These derivatives will not be presented within this article, but can be taken from Span [58] or Kunz and Wagner [33]. Nevertheless, to assist users in computer-program verification, test values for various state properties are given in Table 15 and Table 16.

Table 14: Parameters of the new equation of state.

Parameters of the reducing functions							
	$\beta_{T,12}$	$\gamma_{T,12}$	$\beta_{v,12}$	$\gamma_{v,12}$	F_{12}		
	0.998705	1.0396748	1.0037659	1.0138330	1		
Parameters of the binary specific departure function							
k	$n_{12,k}$	$t_{12,k}$	$d_{12,k}$	$\eta_{12,k}$	$\varepsilon_{12,k}$	$\beta_{12,k}$	$\gamma_{12,k}$
1	–0.0656	3.22	2	-	-	-	-
2	0.0237	2.9	3	-	-	-	-
3	3.5217	1.9	1	1.243	0.65	1.208	0.5
4	–2.831	1.57	1	1.072	0.727	0.82	0.5
5	–1.406	2.73	1	1.465	0.648	1.527	0.5
6	0.864	1.08	2	0.946	0.706	0.86	0.5

Table 15: Thermodynamic property values in the single-phase region for selected values of temperature *T*, density ρ, and composition z_{CO2} as calculated with the new equation of state.

T / K	ρ / (mol m^{-3})	z_{CO2}	p / MPa	c_v / (J mol^{-1} K^{-1})	w / (m s^{-1})
273.15	915	0.25	2.00274	16.7461	286.969
	4000	0.50	6.98643	24.6084	255.285
	18400	0.70	18.0108	33.3998	415.969
323.15	1175	0.50	2.99922	22.0310	293.881
	40	0.75	0.107170	25.6280	287.368
	24000	0.95	89.4303	39.5474	922.065

Table 16: Thermodynamic property values in the two-phase region for selected values of temperature *T* and composition z_{CO2} as calculated with the new equation of state. The specified vapor and liquid phases are not in equilibrium, but at the same composition.

T / K	z_{CO2}	p_{vap} / MPa	p_{liq} / MPa	ρ_{vap} / (mol m^{-3})	ρ_{liq} / (mol m^{-3})
223.15	0.60	1.20861	14.2684	716.791	23240.3
	0.95	0.722354	3.27724	430.586	25974.9
273.15	0.70	6.13145	11.6669	4038.89	14337.0
	0.99	3.53628	3.95956	2250.97	20957.3

5.3. Fitting Procedure

The adjustable parameters of the new mixture model for the system CO_2 + Ar were fitted to experimental data by means of a nonlinear fitting algorithm developed by Dr. Eric W. Lemmon at the National Institute of Standards and Technology (NIST) in Boulder, Colorado. The algorithm allows to adjust all coefficients and exponents at the same time. A selection of the reliable experimental data is individually weighted corresponding to the data type, state region, and experimental uncertainty. During the fitting process, all types of thermodynamic data can be simultaneously used as input data. These weighted data contribute to an overall sum of squares, which is minimized by varying the adjustable parameters of the model. In addition to the experimental values, various thermodynamic constraints can be included in the fit. These constraints shape the representation of the physical behavior of the fluid in between and beyond the experimentally investigated state points. This possibility is especially important for mixtures, since the experimental data are not only dependent on temperature and density or pressure, but also on composition. Thus, in most cases the available experimental data just partly cover the entire composition range. During the fitting process, the model was continuously evaluated by means of the software packages REFPROP [59] and TREND [60]. A more detailed description of the fitting procedure and the employed nonlinear algorithm was given by Lemmon and Jacobsen [61].

5.4. Comparisons to the Data

Compared to many other binary mixtures, the experimental database used for developing the new equation of state for CO_2 + Ar is quite comprehensive. It includes homogeneous density data over a wide range of composition for pressures up to 101 MPa and within a temperature range of 253 K to 573 K. In addition, experimentally obtained dew and bubble points are available covering temperatures from 213 K to about 300 K. Reliable speed of sound data at equimolar composition and at 75 mol% CO_2 were also used to fit the new mixture model. These speed of sound values range from 275 K to 500 K in temperature and cover pressures up to 8 MPa. Additionally, some data on the second virial coefficient and the Joule-Thomson coefficient can be found in the literature. However, these data were of less importance during the fitting process and will not be discussed here.

Within this section, comparisons between the relevant experimental data and calculated values from the equation of state are discussed. Therefore, the percentage deviations of measured data points to values obtained from the equation of state are calculated. Relative deviations in any thermodynamic property *X* can be written as

$$\Delta X/X = \left(\frac{X_{\mathrm{exp}} - X_{\mathrm{calc}}}{X_{\mathrm{exp}}}\right). \tag{5.1}$$

Comparisons of the equation to complete data sets are based on the average absolute relative deviation (AAD). This property is defined as the arithmetic average of all absolute relative deviations of a data set and reads

$$\mathrm{AAD} = \frac{1}{n}\sum_{i=1}^{n} |100\ \Delta X_i/X_i|, \tag{5.2}$$

where *n* is the number of data points given in the corresponding reference. The AAD for all collected data sets are given in Table 17. It has to be noted that calculating an overall AAD for one data set might lead to false conclusions. For example, the AAD of a data set including many excellent measurements at one given composition can be deteriorated completely by some less accurate data points for a mixture with different mole fractions. Thus, for all references presenting data in the homogeneous state regions not only an overall AAD, but also AAD for every investigated composition were calculated. For vapor-liquid equilibrium (VLE) data, it is not reasonable to combine deviations of dew and bubble points within one data set. The shapes of the saturation lines are often quite different and thus the accuracy of their descriptions. Therefore, the AAD are separately given for both phases. With regards to the AAD for VLE data sets, some further comments on the calculation of deviations are important. Within the literature, different ways of presenting such deviations are common, namely with regard to saturation pressure, saturation temperature, or composition along the phase boundary. Since the order of magnitude of these deviations varies significantly, it can be challenging to provide meaningful information. The values given in Table 17 were calculated according to the experimental method employed by the presenting authors. For dew-point or bubble-point experiments at given composition, the AAD was calculated with regards to the saturation pressure. When the data was obtained by taking samples from the separated phases in a vapor-liquid-equilibrium cell and analyzing their compositions, the AAD is the average absolute deviation with regards to composition and given in mol%.

Table 17: Overview of the available experimental thermodynamic property data and the representation of fluid state points with the new equation of state. For solid-phase-equilibrium data no average absolute relative deviation (AAD) is given, since the Helmholtz-energy-explicit model is limited to the description of fluid phases.

VLSE data										
Authors	Year	N	N_x	N_y	T / K	p / MPa	x	y		
This work	2017	7	3	4	213.14	1.05 - 16.14	0.786 - 0.866	0.131 - 0424		
Preston et al. [25]	1971	2	2	0	109.00 - 115.90	0.10	<0.0002			
VLE data										
Authors	Year	N	N_x	N_y	T / K	p / MPa	x	y	AAD_x	AAD_y
This work*	2017	100	46	54	213.14 - 299.22	2.54 - 15.01	0.492 - 0.990	0.131 - 1.000	1.035[a]	0.688[a,b]
Ahmad et al. [40]	2013	21	10	10	278.35 - 300.35	4.20 - 7.93	0.944 - 0.975	0.945 - 0.975	2.942[c]	2.739[c]
Coquelet et al. [38]	2008	62	62	62	233.32 - 299.21	1.52 - 14.03	0.423 - 0.993	0.292 - 0.986	1.068[a]	1.680[a]
Kaminishi et al. [39]	1968	19	13	19	233.18 - 273.15	2.57 - 13.20	0.650 - 0.967	0.246 - 0.851	0.509[a]	1.250[a]
Köpke and Eggers [36, 37]	2007	63	63	63	244.30 - 283.30	1.78 - 13.45	0.645 - 0.990	0.305 - 0.886	0.602[a]	1.458[a]
Lasala et al. [35]	2016	137	66	71	223.07 - 293.07	0.70 - 14.55	0.544 - 0.989	0.012 - 1.000	1.820[a]	3.270[a,b]
Sarashina et al. [43]	1971	12	4	8	288.15	5.69 - 9.78	0.833 - 0.940	0.793 - 0.940	0.768[c]	0.755[c]
Tsankova et al. [26]*	2016	14	0	14	252.95 - 280.44	2.83 - 6.94		0.750		0.075[c]
Tsankova et al. [27]	2017	10	0	10	257.54 - 291.13	2.41 - 6.01		0.950		0.042[c]
***w* data**										
Authors		N			T / K	p / MPa	z		AAD	
Al-Siyabi [62]	2013	59			268.15 - 301.15	9.31 - 41.75	0.955		0.906	
Wegge et al. [30]	2016	67			274.99 - 500.50	0.45 - 8.22	0.501		0.065	
		82			276.09 - 500.49	0.49 - 8.20	0.750		0.140	
Overall*		149			274.99 - 500.50	0.45 - 8.22	0.501 - 0.750		0.106[d]	
***pρT* data**										
Authors		N			T / K	p / MPa	z		AAD	
Abraham and Bennett [63]	1960	13			323.13	5.07 - 101.33	0.831		0.255	
		13			323.13	5.07 - 101.33	0.751		0.276	
		13			323.13	5.07 - 101.33	0.642		0.295	
		13			323.13	5.07 - 101.33	0.464		0.12	
		13			323.13	5.07 - 101.33	0.371		0.162	
		13			323.13	5.07 - 101.33	0.238		0.135	
		13			323.13	5.07 - 101.33	0.129		0.046	
Overall*		91			323.13	5.07 - 101.33	0.129 - 0.831		0.184[d]	
Al-Siyabi [62]	2013	47			283.15 - 301.15	7.80 - 48.23	0.95		1.052	
Altunin and Koposhilov [64]	1976	15			313.14	0.32 - 15.33	0.351		0.182	
		15			313.14	0.66 - 18.71	0.811		0.221	
		14			313.14	0.66 - 20.91	0.501		0.234	
		16			313.14	0.30 - 14.81	0.661		0.216	
Overall		60			313.14	0.30 - 20.91	0.351 - 0.811		0.213[d]	
Altunin and Koposhilov [65]	1977	14			303.14	0.30 - 10.76	0.362		0.212	
		12			303.14	0.51 - 10.98	0.481		0.104	
		14			303.14	0.31 - 10.30	0.534		0.052	
		10			303.14	1.01 - 9.29	0.647		0.208	
		12			303.14	0.31 - 10.30	0.665		0.134	
		13			313.14	0.56 - 14.83	0.351		0.29	
		14			313.14	0.66 - 20.91	0.501		0.233	
		15			313.14	0.32 - 13.24	0.575		0.172	
		16			313.14	0.30 - 14.81	0.661		0.235	
		15			313.14	0.66 - 18.71	0.811		0.224	
		16			323.14	0.36 - 23.07	0.37		0.104	
		13			323.14	0.88 - 21.95	0.486		0.094	
		17			323.14	0.32 - 24.72	0.528		0.073	
		16			323.14	0.42 - 23.71	0.559		0.172	
		17			323.14	0.37 - 20.80	0.801		0.091	
		14			343.14	0.53 - 20.07	0.435		0.054	
		15			343.14	0.38 - 18.21	0.483		0.277	
		15			343.14	0.48 - 18.63	0.608		0.268	
		15			343.14	0.56 - 22.20	0.754		0.340	
		14			373.14	0.53 - 20.40	0.526		0.128	
		15			373.14	0.43 - 20.23	0.673		0.223	
Overall		302			303.14 - 373.14	0.30 - 24.72	0.351 - 0.811		0.175[d]	
Ben Souissi et al. [28]	2016	15			273.15 - 298.15	0.51 - 8.01	0.500		0.005	
		6			323.15	0.52 - 9.02	0.500		0.008	
		35			273.15 - 323.15	0.50 - 9.05	0.751		0.022	
Overall*		56			273.15 - 323.15	0.50 - 9.05	0.500 - 0.751		0.016[d]	

Kestin et al. [66]	1966	48	293.14 – 303.14	0.10 - 2.60	0.268 - 0.918	0.877
Kosov and Brovanov [67]	1979	31	313.03 - 353.12	6.46 - 58.80	0.714	3.297
		30	313.03 - 353.12	5.96 - 58.80	0.479	1.07
		30	313.03 - 353.12	5.87 - 58.81	0.204	0.533
Overall		91	313.03 - 353.12	5.87 - 58.81	0.204 - 0.714	1.652[d]
Mantovani et al. [68]	2012	100	303.22 - 383.14	1.00 - 20.01	0.969	0.570
		94	303.22 - 383.14	1.00 - 20.00	0.831	1.676
Overall		194	303.22 - 383.14	1.00 - 20.01	0.831 - 0.969	1.106[d]
Sarashina et al. [43]	1971	88	288.15	2.43 - 14.53	0.700 - 0.940	1.332
Schönmann [69]	1971	28	373.01	0.50 - 59.02	0.188	0.103
		54	473.14 - 573.05	0.50 - 58.32	0.200	0.065
		29	373.01	0.42 - 59.23	0.398	0.094
		55	473.14 - 573.05	0.41 - 58.92	0.411	0.060
		30	373.01	0.39 - 59.27	0.598	0.090
		55	473.15 - 573.05	0.43 - 58.86	0.609	0.071
		29	373.00	0.47 - 58.88	0.802	0.086
		55	473.15 - 573.05	0.45 - 59.38	0.804	0.093
Overall*		355	373.00 - 573.05	0.39 - 59.38	0.188 - 0.804	0.079[d]
Tsankova et al. [26]	2016	30	273.20 - 293.28	0.45 - 6.50	0.751	0.170
		29	255.10 - 313.30	0.97 - 7.08	0.950	0.185
Overall		59	255.10 - 313.30	0.45 - 7.08	0.751 - 0.950	0.177[d]
Wang et al. [70]	2015	18	308.15 - 358.15	7.00 - 23.00	0.858	12.538
Wegge [71]	2016	121	253.15 - 453.15	2.39 - 18.79	0.500	0.947
		13	253.15	1.02 - 4.50	0.500	0.076
		58	253.15 - 453.15	2.30 - 20.01	0.750	0.213
		53	253.15 - 283.15	1.00 - 5.99	0.751	0.069
Overall*		245	253.15 - 453.15	1.00 - 20.01	0.500 - 0.751	0.537[d]
Yang et al. [72]	2015	66	298.17 - 423.36	10.97 - 30.96	0.010	0.274
		66	298.12 - 423.34	10.98 - 30.96	0.050	0.490
Overall		132	298.12 - 423.34	10.97 - 30.96	0.010 - 0.050	0.382[d]
Yang et al. [29] *	2016	38	273.15 - 323.36	0.49 - 8.99	0.950	0.037

Joule Thomson coefficient data

Authors		*N*	*T* / K	*p* / MPa	*z*	AAD
Strakey et al. [73]	1974	41	233.16 - 383.12	1.01 - 20.27	0.464	1.818
		32	233.16 - 383.12	1.01 - 20.27	0.754	5.185
Overall*		73	233.16 - 383.12	1.01 - 20.27	0.464 - 0.754	3.294[d]

2nd virial coefficient data

Authors		*N*	*T* / K	*p* / MPa	*z*	AAD
Bose and Cole [74]	1970	5	320.84 - 322.84		0[e]	62.19[f]
Cottrell et al. [75]	1956	3	303.13 - 363.12		0[e]	6.308[f]
Martin et al. [76]*	1982	3	290.00 - 319.99		0[e]	0.359[f]
Schmiedel et al. [77]	1980	12	213.01 - 474.96		0[e]	6.615[f]
Schönmann [69]*	1971	22	373.12 - 573.11		0.050 - 0.950	0.578[f]
Schramm and Müller [78]	1982	1	296.14		0[e]	1.418[f]

[a] Composition of phases measured by means of an analytical measurement technique. AAD given with respect to composition in mol%.

[b] AAD without deviations for pure vapor pressures, since these are not defined by the mixture model but by the pure-fluid reference equation of state.

[c] Dew or bubble point of a prepared mixture was identified by means of a synthetic measurement technique. AAD given with respect to saturation pressure.

[d] Calculated deviation between the equation of state and the complete data set.

[e] The 2nd cross virial coefficient is independent on composition.

[f] The deviation is given in $cm^3 \cdot mol^{-1}$.

* Data set included in the fitting process.

5.4.1. Comparisons to Vapor-Liquid Equilibrium Data

An overview of the available vapor-liquid equilibrium (VLE) data is given in Fig. 15. Within this figure, deviations between calculated saturation pressures at given temperature and composition and the experimental values are presented.

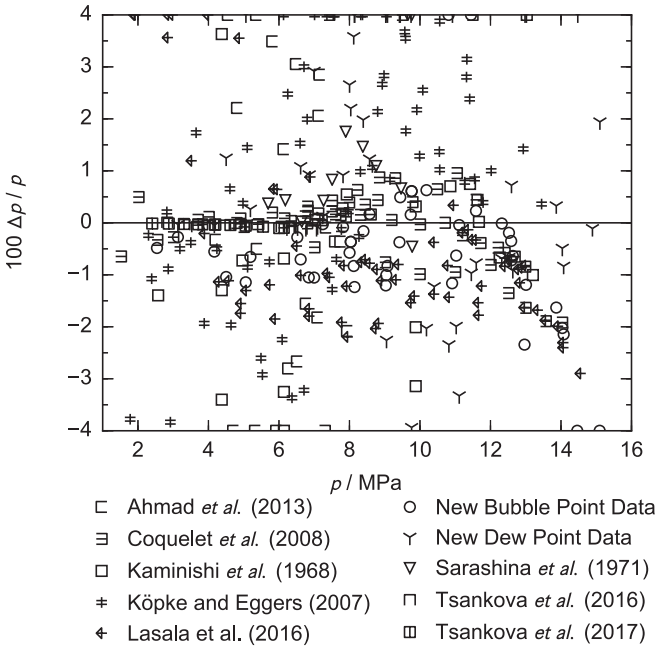

Fig. 15: Percentage deviations $\Delta p / p = (p_{exp} - p_{calc}) / p_{exp}$ between various experimental VLE data [26, 27, 36-40, 43] and values calculated with the new equation of state. Data points that are outside the VLE region predicted by the model are not included.

It can be seen that the mixture model represents most of the reliable data within deviations of about 2 % in pressure. However, based on deviations in saturation pressure it is apparently quite challenging to make a clear statement on the accuracy of the mixture model. Even the new and most accurate data measured at SINTEF Energy Research and presented within this article exhibit a wide spread of deviations, although the model was intensively and almost exclusively fitted to these VLE measurements. The reason for this becomes more evident with regard to the pressure versus composition diagrams given in Figs. 2–8. Since argon is a super-critical fluid at all investigated conditions, the vapor-liquid equilibrium region of the mixture does not cover the entire composition range. The shape of the dew line at "lower" CO_2-fractions is consequently defined by retrograde-condensation effects. At these conditions, small changes in composition lead to comparably large differences in saturation pressure (large value of dp / dy). Thus, the discussion of deviations in pressure is not meaningful over the entire range of the vapor-liquid-equilibrium region. Nevertheless, the accuracy with regards to this property is of special interest during the development of the mixture model, since the standard method of fitting its parameters to VLE information is a minimization of deviations between calculated saturation pressures (at given T and $\vec{z}$) and the experimental data. In order to provide a more meaningful impression of the modelling accuracy, deviations in composition (at given T and p) should be considered too.

As above-mentioned, the description of phase boundaries by means of the new model was defined by fitting its adjustable parameters to the new VLE data. Deviations between the data and calculated values are shown in Fig. 16. Following the considerations discussed in the previous paragraph, deviations in saturation pressure as well as in composition are presented. The data points are plotted over temperature and pressure to get a clearer impression of their location along the phase boundary.

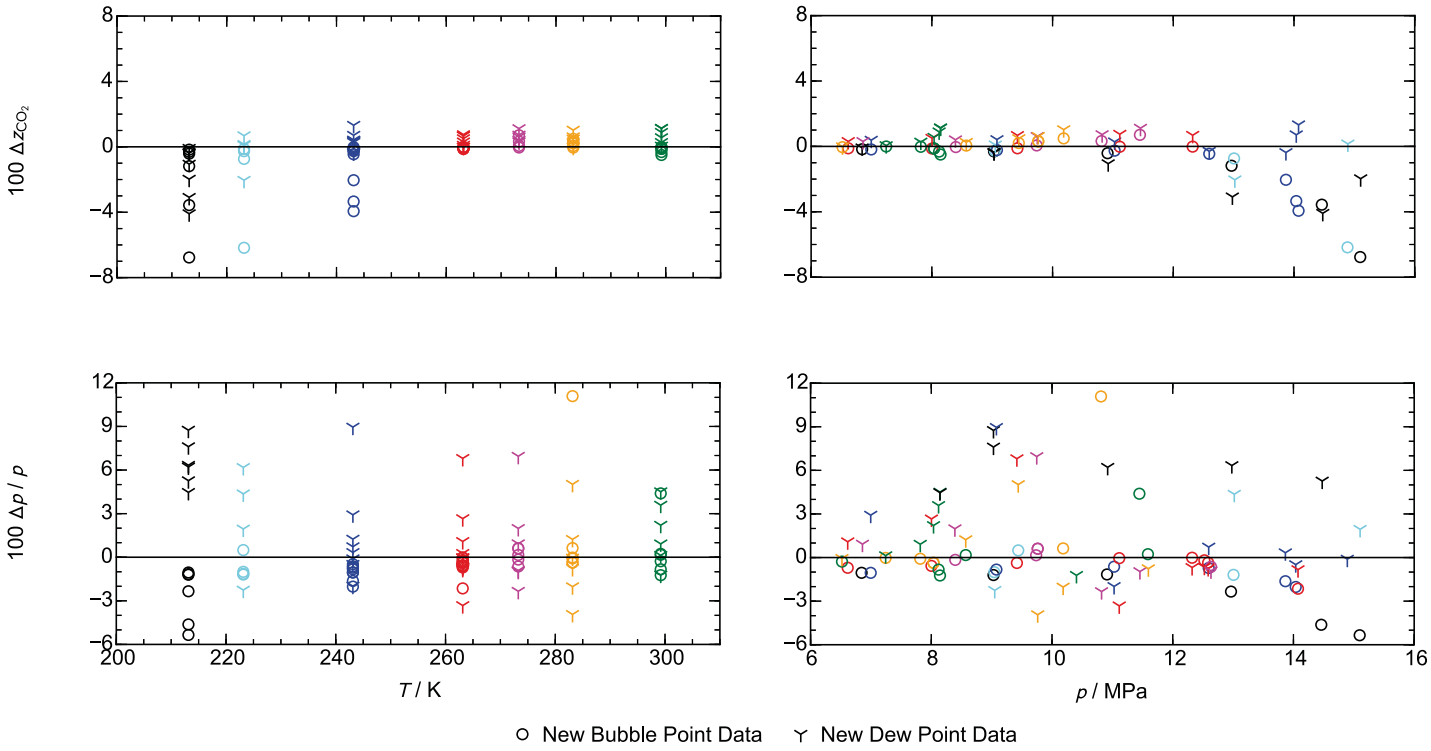

Fig. 16: Deviations between the new experimental VLE data and values calculated with the new equation of state. Depending on the location of a state point along the dew or bubble line, the deviation in composition might be more meaningful then in saturation pressure or vice versa. Deviations in pressure are given as $\Delta p / p = (p_{exp} - p_{calc}) / p_{exp}$ and deviations in composition as $\Delta z_{CO2} = (z_{CO2,exp} - z_{CO2,calc})$. Data points that are outside the VLE region predicted by the model are not included.

The mixture model represents the majority of the data within deviations of 1 mol% in composition. Higher deviations occur along the 213 K isotherm and in the critical region at 223 K and 243 K. During the fitting process, the representation of the data at 213 K could not be improved without deteriorating the description of accurate data on homogeneous density and speed of sound. This behavior is probably not caused by a contradiction between these different data sets, but by numerical problems that occur when evaluating the reference equation for pure CO_2 below the triple-point temperature ($T_{t,CO2}$ = 216.59 K). With regards to the critical region data, it has to be noted that a quantitatively accurate description of this region is always particularly challenging not only for mixtures but even for pure fluids. For quite asymmetric mixtures, it requires strong and thus mathematically complex departure terms, which are in most cases not compatible with a reasonable extrapolation behavior beyond the experimentally covered region. In addition, deviations in terms of composition are less meaningful in the critical region due to the flat shape of the phase boundaries. In this region, relatively small uncertainties in pressure lead to large deviations in composition (large dy / dp). The deviations in saturation pressure are relatively smooth along the bubble line - with higher deviations in the critical region of each isotherm - but exhibit significant scatter along the dew line. The reason for this is the introductorily explained change of dp / dy along the dew line. The highest deviations occur at medium pressures for each isotherm, hence in the region defined by retrograde-condensation effects.

The pressure versus composition diagrams given in Figs. 2-8 also enable some qualitative comparisons of the VLE description provided by other mixture models with the new equation of state. The diagrams include the original EOS-CG model of Gernert and Span [12], the GERG-2008 of Kunz and Wagner [33] and the cubic equations of Soave [46] (SRK, Soave-Redlich-Kwong) and Wong and Sandler [49] (PR WS, Peng-Robinson equation with Wong-Sandler mixing rule). As mentioned in Section 4.2, within the SRK the binary interaction coefficient of Li and Yan [34] (k_{CO2+Ar} = 0.180) was employed, whereas the parameters of the PR WS were fitted to the new VLE data and are given in Section 4.4. In general, the new model provides significantly more accurate results than the GERG-2008 or the SRK. Especially for temperatures above 243 K, it also enables a much better description of the experimental data than the original EOS-CG model. VLE calculations with the PR WS yield excellent results along the bubble line and for the lowest two isotherms (213 K and 223 K) even more accurate

results than the Helmholtz-energy model presented within this section. However, as already noted the parameters of the PR WS were exclusively fitted to the new VLE data and do not enable an accurate description of the available data on homogeneous state properties.

Prior to the measurements presented in this article, the work of Coquelet and co-workers [38] had provided the most comprehensive and reliable VLE database including 62 data points on five different isotherms. Thus, these data were an important input for the description of this binary mixture within the EOS-CG model of Gernert and Span [12]. Within the corresponding publication Coquelet et al. [38] explain that they obtained the data by a so-called "static-analytic" method, which is based on sampling the liquid and vapor phase from a fully established equilibrium. The uncertainty of the pressure measurement is claimed to be within 0.0003 MPa. This value seems too optimistic, since the manufacturer specifies the full-scale stability with 0.02 MPa. The purity of the carbon dioxide and argon samples is 99.999 vol% and 99.995 vol%, respectively. For the gas chromatograph estimated uncertainties of 1.6 % and 0.8 % for the mole fractions of argon and carbon dioxide in both phases are given. Since the authors did not estimate a total combined uncertainty in terms of pressure, it was calculated according to the propagation of error. The estimation for an average total combined expanded (k = 2) uncertainty is 4.5 % for the liquid phase and 2.5 % for the gas phase. As can be seen from Fig. 15, most of the data are represented within this experimental uncertainty except for very few points, for which deviations in saturation pressure are as discussed not meaningful. The overall good description of the data highlights the quality of the mixture model, since none of the data points was included in the final fit.

As already described in section 4.1, Lasala et al. [35] used a similar apparatus to measure 137 VLE data points along three isotherms. The data deviates from the ones by Coquelet et al. [38]. Thus, they also exhibit higher deviations to the EOS that lead to an AAD of 1.820 mol% for the vapor phase and 3.270 mol% for the liquid phase. The data were not included in the fitting process, since the model was fitted to the VLE data presented within this article.

Accurate dew point measurements were performed by Tsankova and co-workers at Ruhr-Universität Bochum. The results are published in Tsankova et al. [26] and recently in Tsankova et al. [27]. Two mixtures containing 75 mol% and 95 mol% carbon dioxide were investigated in a microwave re-entrant cavity resonator. This apparatus is designed for the experimental determination of dielectric permittivity values. In order to obtain dew points, the investigated sample is cooled at isochoric conditions while the permittivity is continuously detected. A sudden change in the derivative of this property with respect to temperature occurs when the dew line is crossed. Thoroughly analyzing the thereby collected data leads to quite accurate dew point data. The total combined uncertainty in terms of pressure are between 0.146 % and 0.303 % for the mixture containing 75 mol% carbon dioxide and between 0.237 % and 0.391 % for 95 mol% carbon dioxide. Deviations between these data and calculated values from the new mixture model and the original EOS-CG model are shown in Fig. 17. Since all data points are given with the corresponding uncertainty, these are indicated as error bars.

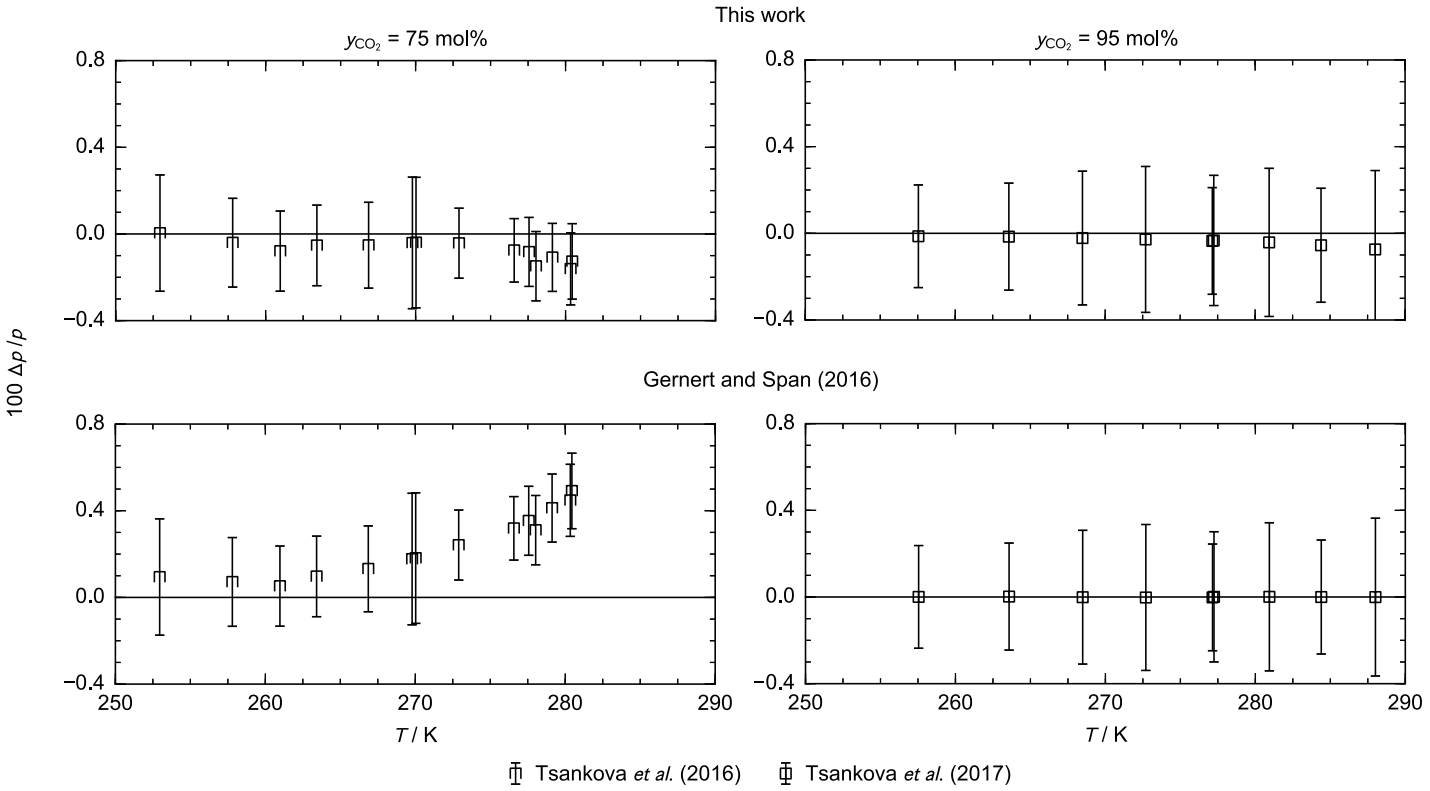

Fig. 17: Percentage deviations $\Delta p / p = (p_{exp} - p_{calc}) / p_{exp}$ between experimental VLE data measured by Tsankova et al. [26, 27] and values calculated with the new equation of state (top) as well as calculated with the original EOS-CG model of Gernert and Span [12] (bottom).

Although these data were not available for the development of the original EOS-CG model, the binary function represents all dew points of the 95 mol% mixture within their uncertainty. Thus, only the representation of the 75 mol% mixture needed to be improved in the refit. As apparent in the deviation plots, the new model enables a description of all data points within their experimental uncertainty. This aspect is particularly important, since it allows for a reliable statement on the uncertainty of calculated VLE properties with respect to saturation pressure. Conservatively estimated, this uncertainty is below 0.4 % for the experimentally investigated compositions.

In addition to the data discussed above, dew and bubble point measurements of Ahmad et al. [40]and Sarashina et al. [43] as well as complete VLE data sets of Kaminishi et al. [39] and Köpke and Eggers [36, 37] are available. However, comparisons with the model and the reliable VLE data presented here and by Coquelet et al. [38] show that these data are of lower accuracy or simply obsolete. Thus, none of these data sets was included in the fitting process.

5.4.2. Comparison to Homogeneous Density Data

Highly accurate density data in the homogeneous gas phase were published by Ben Souissi et al. [28] in a temperature range of 273.15 K to 323.15 K and for pressures up to 9.1 MPa. The authors investigated two different mixtures at 50 mol% and 75 mol% carbon dioxide. The measurements were performed by means of a two-sinker magnetic suspension densimeter. The combined expanded (k = 2) uncertainty was calculated according to GUM and is stated to be within 0.033 %. The same apparatus was used to obtain the data of Yang et al. [29]. These data cover the same temperature and pressure range for a CO_2-rich mixture containing 95 mol% carbon dioxide. The total expanded combined uncertainty of the data for this mixture is 0.043 %. Comparisons between both data sets and the mixture model are given in Fig. 18 for all three compositions along selected isotherms.

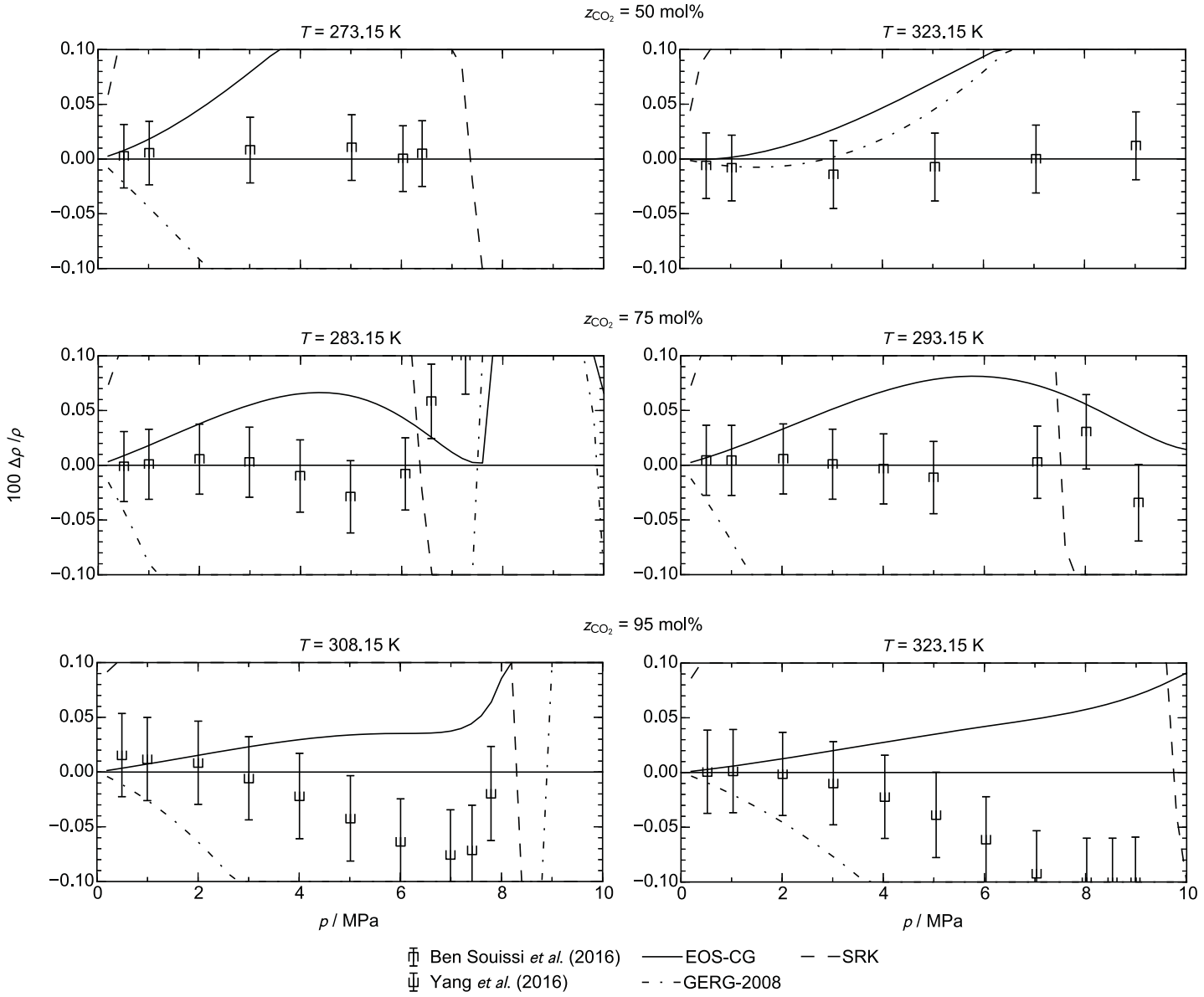

Fig. 18: Percentage deviations $\Delta\rho / \rho = (\rho_{exp} - \rho_{calc}) / \rho_{exp}$ between highly accurate experimental density data measured by Ben Souissi et al. [28] and Yang et al. [29] and values calculated with the new equation of state at selected isotherms. For further comparisons, deviations to values calculated with the original EOS-CG model of Gernert and Span [12], the GERG-2008 by Kunz and Wagner [33], and the SRK by Soave [46] (k_{CO2+Ar} = 0.180 from [34]) are presented as well.

The new model represents most of these data within their experimental uncertainty. However, for some points the deviations are somewhat higher, especially at elevated pressures. Further fitting of these data reduced these deviations, but always led to a less accurate description of other properties. Thus, minor concessions had to be made in order to enable a description that represents the best compromise along all types of data. Still the AAD between the new model and the data of Ben Souissi et al. [28] is 0.016 % and thus exceptionally small. The data of Yang et al. [29] are represented with an AAD of 0.037 %. The new mixture model provides for both data sets a significantly more accurate description than the original EOS-CG model. Thus, it can be noted that the accuracy of the model presented here was significantly enhanced by the experimental work carried out after the development of the EOS-CG model.

Prior to the initially discussed measurements with a two-sinker densimeter Yang et al. [72] measured the gas density of two CO_2-rich mixtures with a single-sinker densimeter. The authors calculated a combined expanded (k = 2) uncertainty of 0.12 %. Within this uncertainty analysis the composition was found to be the main contributor. During the fitting process it was not

possible to set up a functional form that would reproduce the data within their experimental uncertainty. As apparent in Fig. 19, all isotherms exhibit a systematic offset. Since the corresponding publication contains density measurements in pure carbon dioxide, which are in good agreement with the reference equation of state, it seems unlikely that the offset is caused by an error in the apparatus. Discussions with the authors lead to the result that the reported composition does not agree with the one of the investigated sample, because of adsorption effects in the measuring cell or insufficient purging of the system. In order to prove this, the composition was adjusted to the equation of state during the fitting process. Thereby, the compositions were corrected from 95 mol% to 93.25 mol% and from 99 mol% to 97.873 mol%. As a result, the offset vanished. None of these or the original data points was included in the final fit, but the corrected data set was used for comparisons.

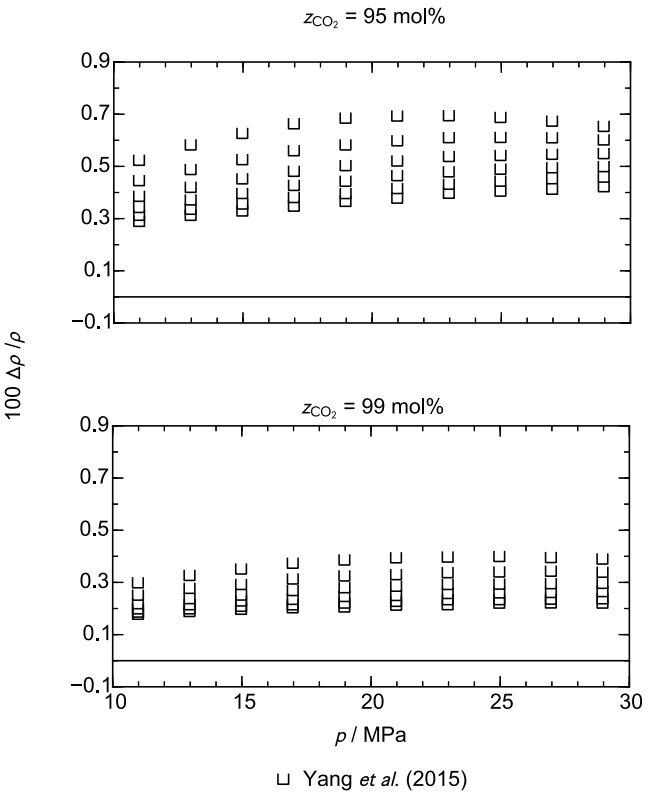

Fig. 19: Percentage deviations $\Delta\rho / \rho = (\rho_{exp} - \rho_{calc}) / \rho_{exp}$ between experimental density data measured by Yang et al. [72] and values calculated with the new equation of state at selected isotherms. Compositions are as given in the corresponding reference without any corrections.

The single-sinker densimeter technique was also employed by Wegge [71]. The author carried out measurements in two gaseous mixtures containing 50 mol% and 75 mol% CO_2. The data cover temperature from 253.15 K to 453.15 K and pressures up to 20 MPa. Exemplary comparisons to the results are shown in Fig. 20.

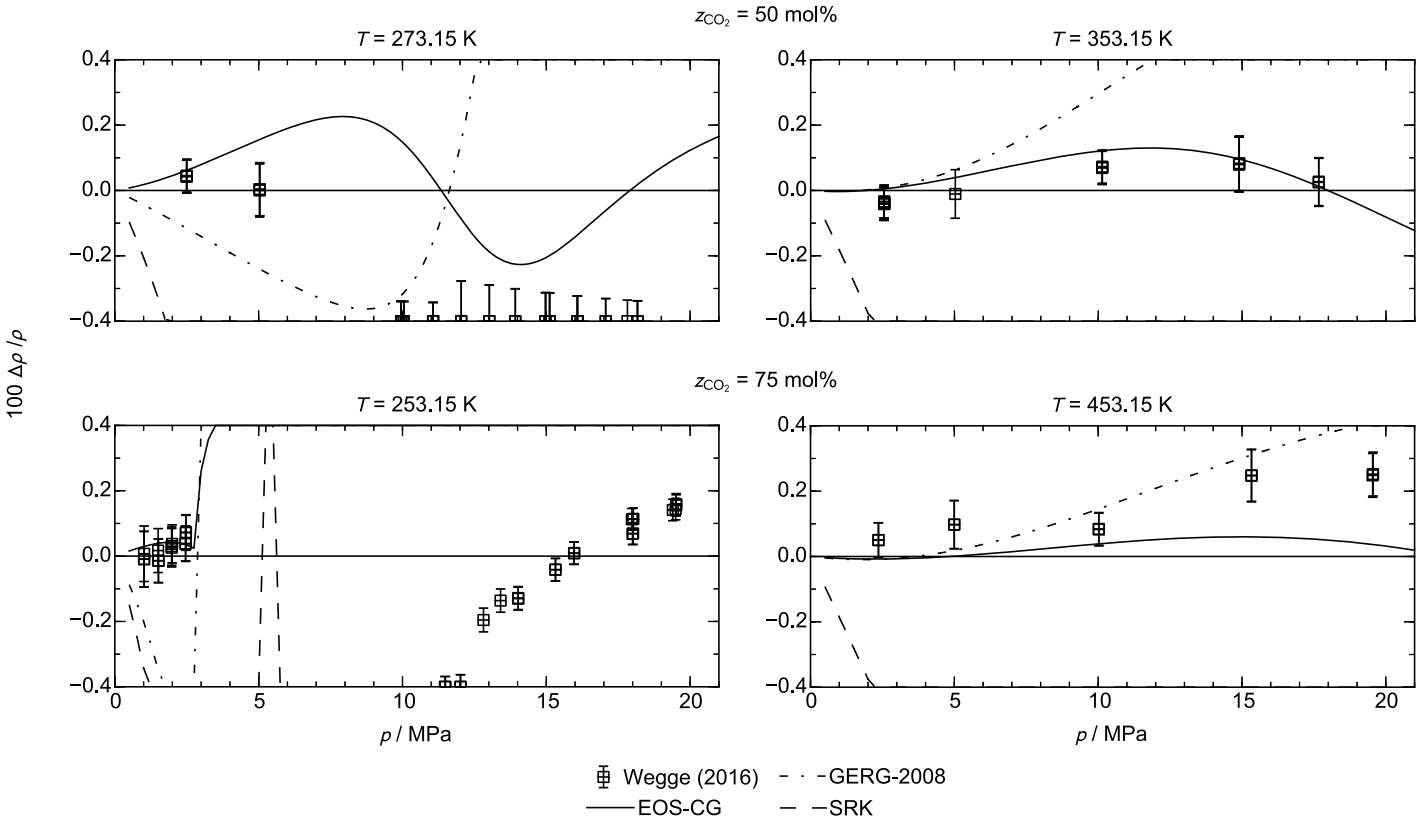

Fig. 20: Percentage deviations $\Delta\rho / \rho = (\rho_{exp} - \rho_{calc}) / \rho_{exp}$ between experimental density data measured by Wegge [71] and values calculated with the new equation of state at selected isotherms. For further comparisons, deviations to values calculated with the original EOS-CG model of Gernert and Span [12], the GERG-2008 by Kunz and Wagner [33], and the SRK by Soave [46] (k_{CO2+Ar} = 0.180 from [34]) are presented as well.

The author provides total expanded (k = 2) uncertainties for every state point that range from 0.047 % to 0.123 % for the equimolar mixture and from 0.032 % to 0.130 % for the sample containing 75 mol% CO_2. As apparent from the deviation plots in Fig. 20, neither the new model nor the original EOS-CG model represents the data within their experimental uncertainty. Especially at low temperatures and elevated pressures both models deviate considerably from the data. Personal communication with the author revealed that filling the utilized densimeter at these conditions is challenging and that the mixture might have decomposed during this process. However, while the resulting shift in composition would be a satisfying explanation for high deviations of a single isotherm, it contradicts with the good reproducibility of the results of the different, independent measurement runs performed at low temperatures and elevated pressures. Since the data are currently being further evaluated by the author and no other experimental data were available to prove the trend of the data, they were not included in the final fit of the present mixture model. Nevertheless, it should be noted that a more intensive fitting of the data at supercritical temperatures probably would have led to a description that matches the experimental uncertainty at these conditions.

The two initially discussed references by Ben Souissi et al. [28] and Yang et al. [29] provide by far the most accurate density data for the system CO_2 + Ar. Nevertheless, some other sources of data were used to fit the mixture model or were at least of interest for the validation of the model. A rough overview of the data situation is given in Fig. 21, which shows deviations between the new equation of state and the available data at various compositions along four different isotherms. In one of the deviation plots included in Fig. 21 the data situation at about 300 K is presented. With regards to this isotherm it becomes evident that the overlapping data of Kestin et al. [66], Mantovani et al. [68], and Al-Siyabi [62] are of low accuracy. Thus, these data were not included in the fitting process and will not be discussed here. The work of Altunin and Koposhilov [65] is one of the most comprehensive experimental studies of the thermophysical properties of CO_2 + Ar. A detailed analysis of their data revealed inconsistencies at pressures higher than about 5 MPa and other references were found to be more reliable; their data were consequently not used to fit the mixture model.

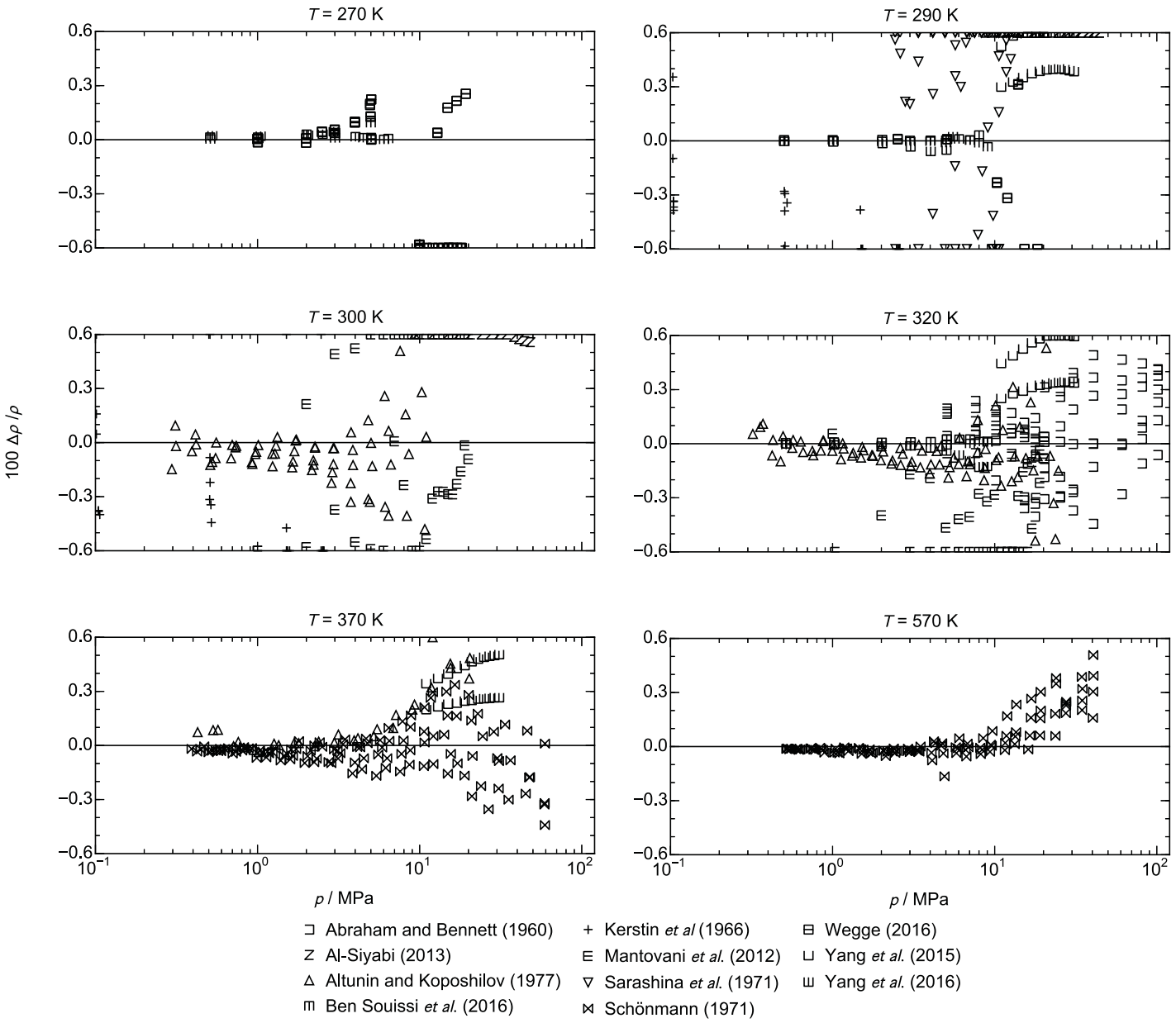

Fig. 21: Percentage deviations $\Delta\rho / \rho = (\rho_{exp} - \rho_{calc}) / \rho_{exp}$ between various experimental density data [28, 29, 43, 62, 63, 65, 66, 68, 69, 71, 72] and values calculated with the new equation of state at selected isotherms.

Abraham and Bennett [63] published compressibility factors over a wide range of compositions and for pressures up to 100 MPa. These values were converted into gas densities and partly included in the fitting process to shape the functional form at elevated pressures. Within the corresponding publication no details about the experimental apparatus are provided, but some information regarding uncertainties is given. The temperature and pressure measurements are accurate within 0.01°K and 0.01 %, respectively. The investigated samples contained impurities of up to 0.1 mass%, which means a relatively high level of contamination. The compressibility factors are given as smoothed values with four digits resulting in a rounding error of 0.1 % to 0.3 %. Thus, the given uncertainty of 0.14 % is quite questionable. An estimation of a combined expanded uncertainty as calculated in this work lead to a more realistic average value of 0.24 % and a maximum uncertainty of 0.65 %. These results are in line with the minimum deviations obtained during the fitting process and are shown for some isotherms in Fig. 21. The AAD between the data and the mixture model is 0.184 %. Thus, the model agrees with the data within their experimental uncertainty.

A comprehensive experimental data set was published by Schönmann [69]. This study includes gaseous mixtures with

eight different compositions at temperatures up to 573 K and pressures up to 60 MPa. The data was obtained by means of the Burnett method. The author estimates the overall uncertainty for the compressibility factor to be within a range of 0.04 % to 0.3 %. Since the corresponding publication provides relatively detailed information on the accuracy of the employed experimental set-up this total combined uncertainty was recalculated in order to avoid "overfitting" the data. The uncertainty with regards to pressure is given with 0.0002 bar, whereas the uncertainty in temperature is stated to be 0.06 K for temperatures up to 100 °C and 0.16 K up to 300 °C. The estimated uncertainty in composition is 0.5 mol%. Considering all given uncertainties, the recalculated total combined expanded (k = 2) uncertainties range from 0.06 % to 0.72 %. As shown in Fig. 21 the mixture model represents the data with a deviation of 0.08 % for pressures up to 3 MPa and 0.3 % for pressure up to 30 MPa. At higher pressures, the offset increases to 0.5 %. The AAD between this data set and the mixture model is 0.079 % and thus clearly within the experimental uncertainty range.

The experimental work of Tsankova and co-workers [26] was mentioned above within the discussion of the VLE database. The microwave re-entrant cavity resonator employed to obtain the presented dew point measurements also allows for the determination of homogenous gas densities. In fact, these densities are not directly measured but calculated from dielectric permittivity values. For these data, no exact uncertainty analyses were carried out, but the accuracy was estimated by means of the overlapping and highly accurate measurements of Ben Souissi et al. [28]. The total combined expanded (k = 1.73) uncertainty was thereby estimated to be within 0.3 %. With regard to the deviations shown in Fig. 22, this estimation seems to be reasonable. The new mixture model agrees with these data with an AAD of 0.177 %. Unsurprisingly this AAD agrees with the estimated uncertainty, since the model was fitted to the experimental data of Ben Souissi et al. [28]. Although the data of Tsankova and co-workers consequently are not the most accurate values, they are mentioned here for completeness. In addition, their work demonstrates that the technique leads to reliable mixture densities, that can be obtained comparably quickly, namely within one day per isotherm.

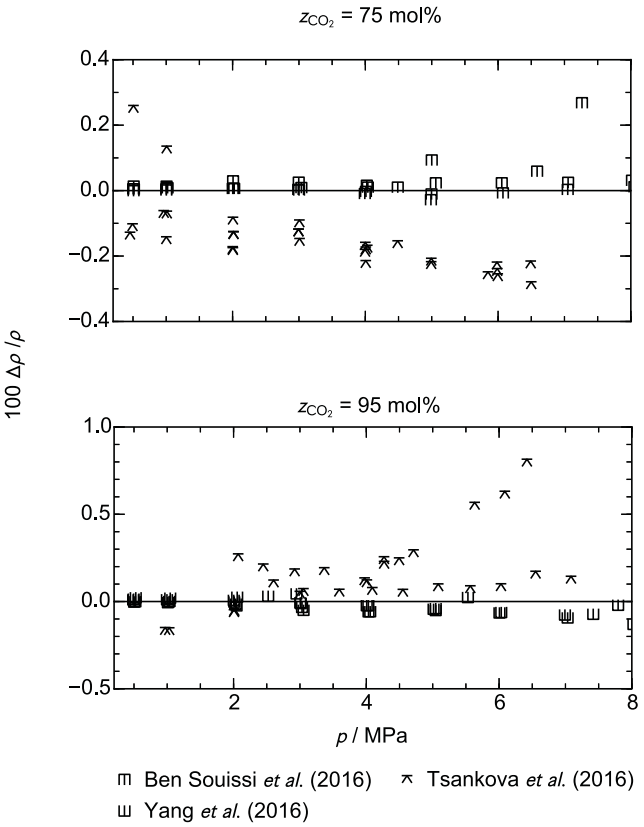

Fig. 22: Percentage deviations $\Delta\rho / \rho = (\rho_{exp} - \rho_{calc}) / \rho_{exp}$ between experimental density data measured by Tsankova et al. [26] and values calculated with the new equation of state. For further comparisons, deviations to overlapping data points from the most accurate density measurements by Ben Souissi et al. [28] and Yang et al. [29] are presented as well.

5.4.3. Comparisons to Speed of Sound Data

Speed of sound data are always of high interest during the fitting process of mixture models or pure-fluid equations of state, since calculating this property requires the combination of multiple different derivatives of the functional form. Consequently, fitting such data has a strong impact on the final equation of state. In addition, by thorough experimental work quite low uncertainties can be achieved, which makes this type of data very valuable for fitting. The database for the speed of sound in CO_2 + Ar is unfortunately very limited. Two sources of experimental results are available, namely the dissertation of Al-Siyabi [62] and the work of Wegge et al. [30]. During the fitting process, the data of Al-Siyabi [62] were found to be of low accuracy, which is most likely caused by their means of filling the apparatus with the sample. During the filling process, the author had no technical capability to heat the mixture above its critical temperature. Consequently, the almost isenthalpic expansion when filling the mixture from the cylinder into the measuring cell results in crossing the two-phase region, which leads to a shift in the composition of the investigated sample. With regard to the systematic offset of the data, as evident in Fig. 23, this explanation seems plausible. The

measurements of Al-Siyabi [62] were therefore not used to fit the present mixture model.

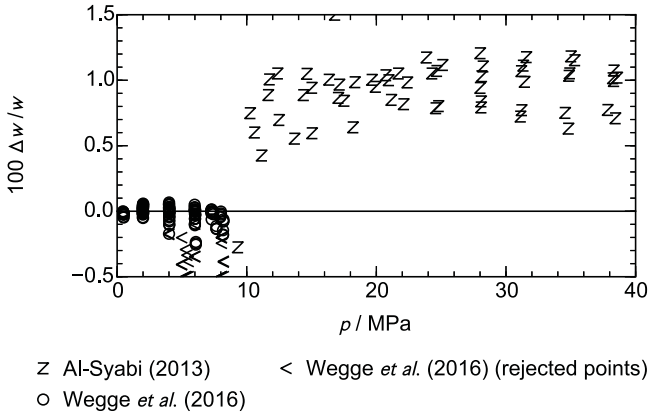

Fig. 23: Percentage deviations $\Delta w / w = (w_{exp} - w_{calc}) / w_{exp}$ between experimental speed of sound data [30, 62] and values calculated with the new equation of state.

In their publication Wegge et al. [30] describe a supercritical filling procedure. Due to the use of this method and the overall thoroughness of their experimental work, the presented data are deemed to be of quite high quality. The measurements were carried out with a spherical acoustic resonator for temperatures between 275 K and 500 K and pressures up to 8 MPa. The fluid was investigated at two different compositions with mole fractions of 50 % and 75 % carbon dioxide. The authors calculated total combined expanded (k = 2) uncertainties ranging from 0.042 % to 0.056 %.

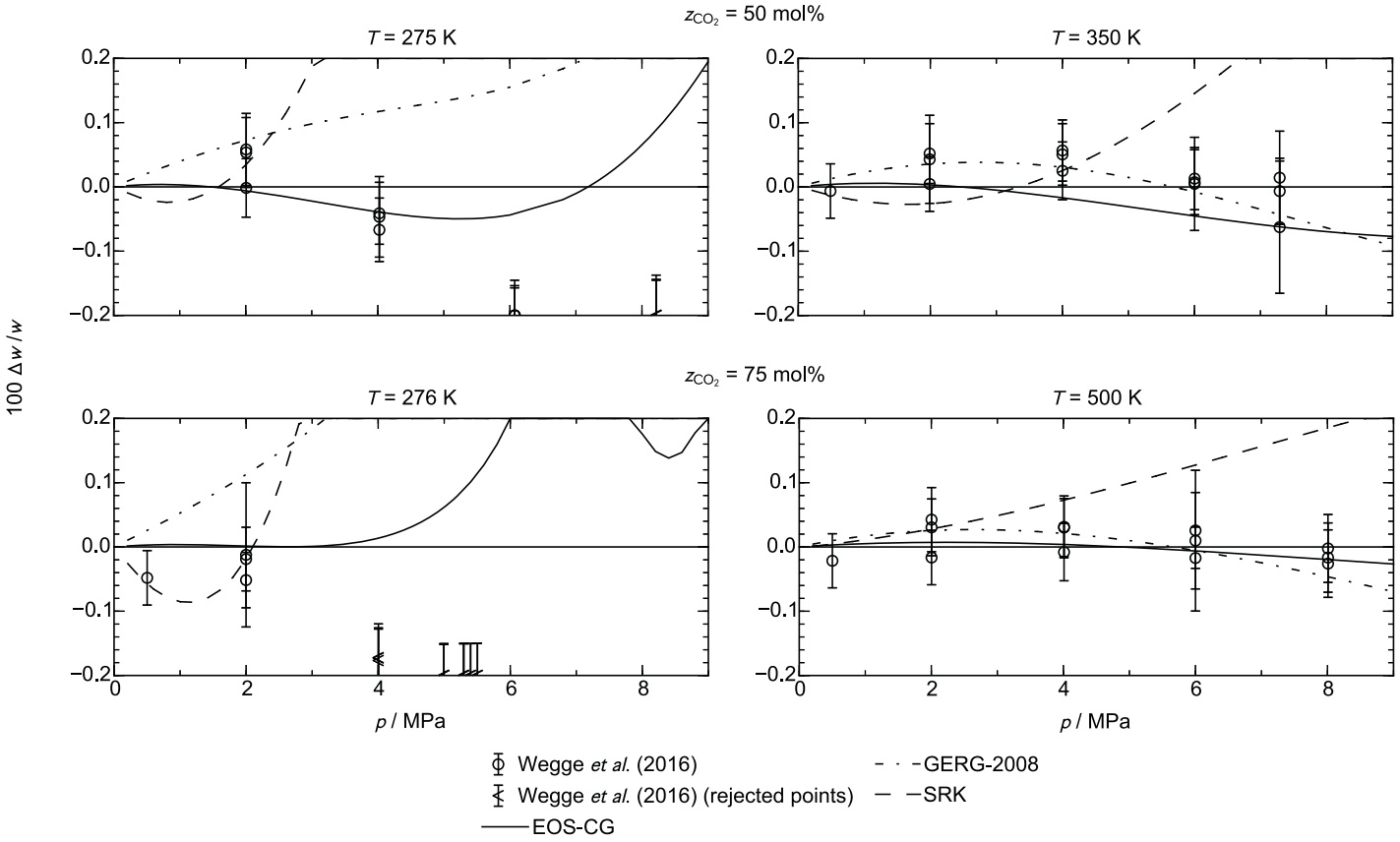

Fig. 24: Percentage deviations $\Delta w / w = (w_{exp} - w_{calc}) / w_{exp}$ between experimental speed of sound data measured by Wegge et al. [30] and values calculated with the new equation of state. The data labelled as "rejected points" may be influenced by pre-condensation effects in the vicinity of the phase boundary. For further comparisons, deviations to values calculated with the original EOS-CG model of Gernert and Span [12], the GERG-2008 by Kunz and Wagner [33], and the SRK by [46] (k_{CO2+Ar} = 0.180 from [34]) are presented as well.

The mixture model represents most of the data within their experimental uncertainty, except for some points at low temperatures and higher pressures. The original EOS-CG model of Gernert and Span [12] was developed prior to the publication of these experimental results and is thus in surprisingly good agreement with the data. In fact, the points that cannot be reproduced within their experimental uncertainty by means of the new model, also significantly deviate from the EOS-CG. Since Wegge and co-workers carried out comparisons between the data and the EOS-CG, these higher deviations are discussed within the corresponding publication. Finally, the authors identified some data points for which they assume pre-condensation effects caused by sound-indicated pressure waves. In Fig. 23 to Fig. 25 these points are depicted with different symbols and indicated as "rejected points". Pre-condensation effects seem to be possible in the vicinity of the phase boundary. With regards to Fig. 25, only some of the measurements for the CO_2-rich mixture were carried out that close to the saturation line.

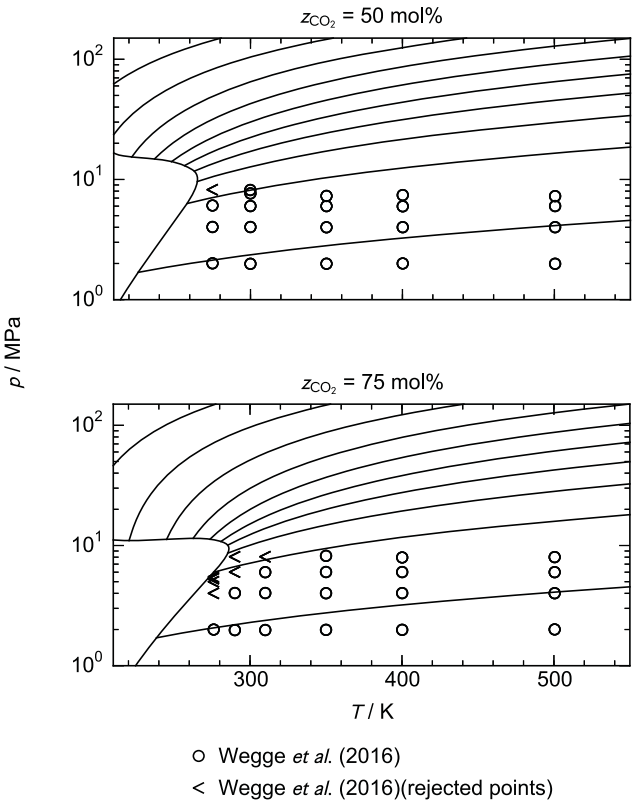

Fig. 25: *p*,*T*-diagrams along isochors calculated with the new equation of state for the two compositions covered by the experimental speed of sound data of Wegge et al. [30]. The location of the data is presented with regard to the phase boundary.

For the other state points, other factors contributed to higher uncertainties and thus larger deviations from the mixture models. Including all data points, the AAD to the new model is 0.106 %, whereas rejecting the less reliable points leads to an AAD of 0.04 %.

5.5. Extrapolation Behavior

As briefly discussed before, the development of empirical mixture models based on experimental data is particularly challenging, since the Helmholtz-energy function has to be shaped within a multidimensional surface defined by temperature, density, and composition. Thus, only parts of this large surface are defined by experimental data. In order to ensure that the final model also yields reasonable results in state regions where it was not fitted to experimental data, diagrams of various state properties are consistently calculated from preliminary models during the fitting process. The validation of these diagrams is of special interest in state regions defined by extreme values of temperature, pressure, or density. A smooth extrapolation behavior of the model is crucial not only to ensure reasonable results at extreme conditions, but also in technically relevant state regions that are not sufficiently covered by the experimental database. In Fig. 26, the pressure is plotted over enthalpy, density, and temperature. Within these property plots the mixing behavior is shown for pressures up to 1 GPa and temperatures up to 3000 K in the *p*,*h*-diagram and 10000 K in the *p*,ρ-diagram. Even at high temperatures and pressures the isolines are smoothly shaped and no bumps or crossings are found. In addition to these plots, a variety of other diagrams were calculated and validated including a selection of derivatives of the Helmholtz energy function. Based on these validations, the overall extrapolation behavior of the mixture model was found to be excellent. However, it has to be noted that especially at very high pressures or temperatures below the triple point of pure CO_2 ($T_{t,CO2}$ = 216.59 K), the formation of solid structures has to be considered. Since the present model enables only the description of fluid phases, additional models and algorithms (as implemented within the software package TREND) are required to predict solidification (see, e.g., Jäger and Span [24] and Jäger et al. [79]) .

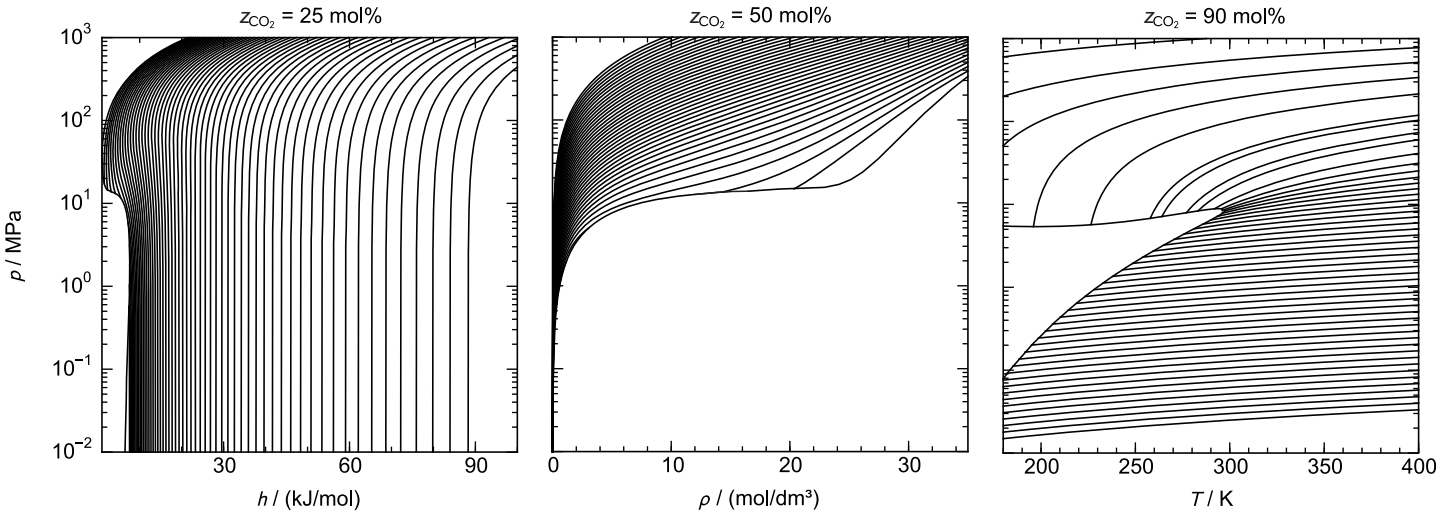

Fig. 26: Left to right: *p*,*h*-, *p*,*ρ*-, and *p*,*T*-diagrams calculated with the new equation of state for three different compositions (25 mol%, 50 mol%, and 90 mol% CO_2) at extreme conditions. The mixing behavior is shown for pressures up to 1 GPa and along isotherms up to 3000 K in the *p*,*h*-diagram and 10000 K in the *p*,*ρ*-diagram. The *p*,*T*-diagram includes isochors up to 33000 mol m^{-3}.

5.6. Estimated Uncertainties of Calculated Properties

Based on comparisons to the most recent and accurate VLE measurements presented within this article, the uncertainty of VLE data calculated from the new mixture model for CO_2 + Ar is within 1 mol% except for temperatures below the triple point of pure CO_2 ($T_{t,CO2}$ = 216.59 K) and in the critical region at low temperatures ($T \leq$ 243 K). For the uncertainty in saturation pressure, reliable estimations are only possible for dew points of the experimentally investigated mixtures containing 75 mol% and 95 mol% CO_2. Within a temperature range from 253 K to 291 K this uncertainty is below 0.4 %. Over most of the composition range and for temperatures up to 573 K, homogenous densities in the gas phase and in supercritical states can be calculated with an uncertainty of 0.3 % for pressures up to 30 MPa and 0.6 % for pressures up to 100 MPa. For the molar composition of 50 mol%, 75 mol%, and 95 mol% CO_2, highly accurate homogeneous gas densities were used to fit the mixture model within a temperature range from 273 K to 323 K and for pressures up to 9 MPa. Thus, the maximum uncertainty of calculated gas densities in this temperature and pressure region is within 0.035 % for the 50 mol% and 75 mol% CO_2 mixture and within 0.045 % for the mixture containing 95 mol% CO_2. The uncertainty of calculated liquid densities cannot be estimated, since no reliable $p\rho T$ data are available in this state region. Comparisons to the reliable speed of sound data in the gas phase at 50 mol% and 75 mol% CO_2 for temperatures up to 500 K and pressures up to 8 MPa yield an estimated uncertainty of the model below 0.06 %.

In general, the present mixture model is valid over the entire fluid state region. However, estimating uncertainties of calculated properties is only possible in state regions that are covered by reliable experimental data or at least by data of known accuracy. Since the extrapolation behavior of the model was carefully constrained even at extreme values of temperature and pressure, calculated properties at other conditions than above-discussed are in most cases within the same order of accuracy. Nevertheless, for more detailed information about the quality of calculated data in a state region of interest, the experimental database as presented in Table 17 should be evaluated thoroughly.

6. Conclusions

A thorough investigation of the CO_2 + Ar mixture system has been reported. The investigation has produced both new and accurate phase equilibrium data and a new multiparameter fundamental equation of state based on explicit expression of the Helmholtz free energy. In addition, the accurate new phase equilibrium data has been used to fit a scaling-law model to predict the critical point as well as a Peng-Robinson equation of state with Wong-Sandler mixing rule.

The new phase equilibrium data cover a large part of the VLE region of the system, spanning from 213 K to 299 K in temperature, and from 0.4 to 16 MPa in pressure. 7 vapor-liquid equilibria (VLE) isotherms have been measured, at the temperatures 213, 223, 243, 263, 273, 283, and 299 K, including both dew and bubble points. 213 K is below the triple point of CO_2, and here also phase equilibria including solids have been investigated: liquid-solid equilibria (LSE) above the three-phase line and vapor-solid equilibria (VSE) below the three-phase line.

LSE and VSE measurements have been performed by measuring the pressure and composition of the liquids (freezing points) and vapor (frost points), respectively, in equilibria with solid CO_2. Finally, the three-phase line itself (VLSE) has been investigated. All measurements have been performed with great accuracy, and a thorough uncertainty analysis has been performed. The total, combined accuracy in terms of mole fraction is for a large part of the data estimated to be 0.015 % for bubble point measurements and 0.014 % for dew point measurements. In the critical regions and for phase equilibria involving solids, the estimated uncertainties are higher, up to 0.1 %. The relative measurement uncertainty estimates in pressure varies between 0.014 and 0.06%. Estimated temperature measurements uncertainty ranges from 1 to 13 mK. The new data have been compared with existing data where relevant, but the isotherms at 213, 243, and 263 have not previously been covered by a self-consistent data set, and the new data set extends further towards the critical point for all isotherms than previously reported work. The only previous report involving solids for CO_2 + Ar equilibria was on two freezing points 100 K below the 263 K isotherm of the current work.

Based on the new data accurate estimates of the critical points at each investigated temperature are provided by fitting a scaling law-model to the VLE data in the critical region, with uncertainties ranging from 0.02 to 0.2 % in composition and 1 to 7 kPa in pressure. The data have also been used to fit a Peng-Robinson equation of state with Wong Sandler mixing rules, the formulation of Mathias and Copeman for the alpha correction, and the NRTL formulation for the Gibbs free energy. With temperature dependent fitting coefficients, this model provides good fit with the experimental data.

In addition to the Peng-Robinson-Wong-Sandler model, the new VLE data were used to develop an improved Helmholtz-energy-explicit mixture model. The fitting process was enhanced by other accurate and recently established data for homogeneous density, speed of sound, and dew-point pressure. The mathematical structure of this model enables the calculation of all types of highly-accurate thermodynamic data by combining derivatives of the functional form. The uncertainty of calculated VLE data is within 1 mol% except for temperatures below the triple point of pure CO_2 ($T_{t,CO2}$ = 216.59 K) and in the critical region at low temperatures ($T \leq$ 243 K). Homogeneous state properties are mostly described within the experimental uncertainty of the most accurate underlying data used to fit the model. The new model will be implemented in an extended multi-fluid mixture model for the description of carbon-dioxide-rich mixtures with various impurities as relevant for CCS applications, which is developed at RUB, Bochum.

Acknowledgments

This publication has been produced with support from the research program CLIMIT and the BIGCCS Centre, performed under the Norwegian research program Centres for Environment-friendly Energy Research (FME). The authors acknowledge the following partners for their contributions: Gassco, Shell, Statoil, TOTAL, ENGIE and the Research Council of Norway (193816/S60 and 200005/S60).

The research leading to these results has also received funding from the European Community's Seventh Framework Programme (FP7-ENERGY-20121-1-2STAGE) under grant agreement n^o 308809 (The IMPACTS project). The authors acknowledge the project partners and the following funding partners for their contributions: Statoil Petroleum AS, Lundin Norway AS, Gas Natural Fenosa, MAN Diesel & Turbo SE and Vattenfall AB.

The research leading to these results has received funding from the Norwegian Financial Mechanism 2009-2014 under Project Contract no. 7F14466.

The authors would like to thank Håvard Rekstad and Reidar Tellebon of NTNU, Brede Hagen of SINTEF Energy Research, and Caroline Einen, Ingeborg Treu Røe, and Ranisha Sitlapersad who were interns at SINTEF Energy Research, for their contributions. Special thanks go to Dr. Markus Richter and Dr. Gergana Tsankova of RUB and Dr. Robin Wegge of PTB, Braunschweig, for many fruitful discussions and important contributions to the evaluation of the experimental database used to develop the Helmholtz-energy-explicit mixture model. In addition, the authors thank Dr. Eric W. Lemmon and Dr. Ian H. Bell for the careful validation of this new model and helpful input during the fitting process.

Appendix A. Measurements of the three-phase line at 213.5 K

This appendix provide a more detailed description of the measurements of the three-phase line at 213.15 K of this work.

In Fig. A.1, the measured cell pressure and stirrer operation in most of the 100 hours preceding measurement V5 is shown. During this period, several sample series were extracted before the final samples included in V5, which where extracted at around the time 105 hours. Since the bellows was not in operation, each sampling series led to a drop in pressure, whereas the impact of the stirrer was not so systematic. As

usual, the pressure of the data point, $\bar{p}_f$, was measured right before the first sample of V5, whereas the unsystematic standard uncertainty in pressure set to 4.1 kPa, which includes all the extreme measured values in pressure during the last 40 hours before V5 was measured, with the exception of periods when the system was pushed away from equilibrium due to sampling.

In Fig. A.2, a similar plot is shown for the many hours leading to the liquid data point L1. The data point pressure and its unsystematic uncertainty is estimated like for V5. Even though the paths leading to V5 and L1 were quite different, the two measurements of pressure were in agreement taking into account their respective uncertainties.

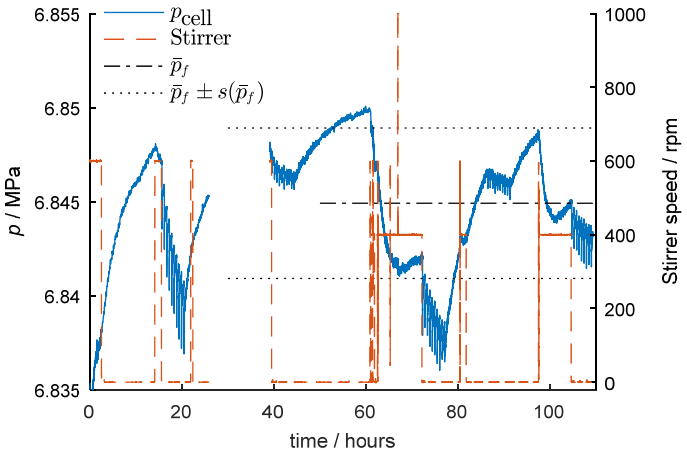

Fig. A.1: Estimation of pressure standard deviation for vapor data point V5 at the three-phase line at 213.146 K.

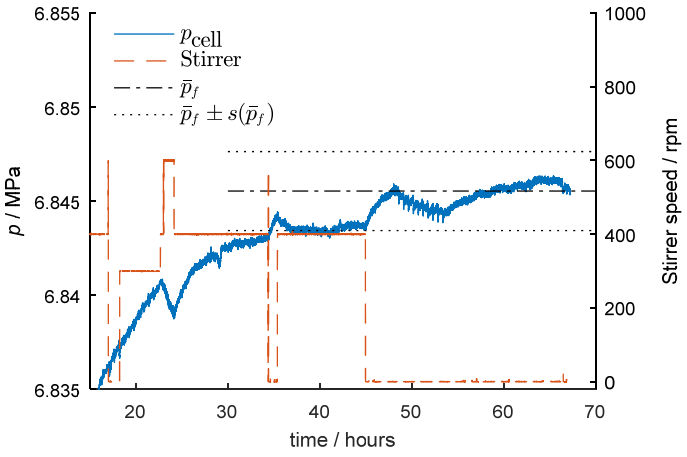

Fig. A.2: Estimation of pressure standard deviation for liquid data point L1 at the three-phase line at 213.146 K.

References

[1] Energy Technology Perspectives 2016 -- Towards Sustainable Urban Energy Systems, International Energy Agency, Paris, France, available at http://www.iea.org/etp/, 2016.

[2] Y. Tan, W. Nookuea, H. Li, E. Thorin, J. Yan, Property impacts on Carbon Capture and Storage (CCS) processes: A review, Energy Convers. Manage., 118 (2016) 204-222.

[3] A. Austegard, E. Solbraa, G.D. Koeijer, M.J. Mølnvik, Thermodynamic Models for Calculating Mutual Solubilities in H_2O–CO_2–CH_4 Mixtures, Chem. Eng. Res. Des., 84 (2006) 781–794.

[4] M. Ahmad, S. Gersen, Water Solubility in CO_2 Mixtures: Experimental and Modelling Investigation, Energy Proc., 63 (2014) 2402-2411.

[5] Y. Xiang, Z. Wang, X. Yang, Z. Li, W. Ni, The upper limit of moisture content for supercritical CO_2 pipeline transport, The Journal of Supercritical Fluids, 67 (2012) 14-21.

[6] M. Halseid, A. Dugstad, B. Morland, Corrosion and Bulk Phase Reactions in CO_2 Transport Pipelines with Impurities: Review Of Recent Published Studies, Energy Proc., 63 (2014) 2557-2569.

[7] G. de Koeijer, J. Henrik Borch, M. Drescher, H. Li, Ø. Wilhelmsen, J. Jakobsen, CO_2 transport–Depressurization, heat transfer and impurities, Energy Proc., 4 (2011) 3008-3015.

[8] K.Y. Song, R. Kobayashi, The water content of a carbon dioxide-rich gas mixture containing 5.31 Mol % methane along the three-phase and supercritical conditions, Journal of Chemical & Engineering Data, 35 (1990) 320-322.

[9] H. Li, J.P. Jakobsen, J. Stang, Hydrate formation during CO_2 transport: Predicting water content in the fluid phase in equilibrium with the CO_2-hydrate, Int. J. Greenh. Gas Control, 5 (2011) 549-554.

[10] G. Skaugen, S. Roussanaly, J. Jakobsen, A. Brunsvold, Techno-economic evaluation of the effects of impurities on conditioning and transport of CO_2 by pipeline, Int. J. Greenh. Gas Control, 54, Part 2 (2016) 627-639.

[11] S.W. Løvseth, G. Skaugen, H.G. Jacob Stang, J.P. Jakobsen, Ø. Wilhelmsen, R. Span, R. Wegge, CO_2Mix Project: Experimental Determination of Thermo Physical Properties of CO_2-Rich Mixtures, Energy Proc., 37 (2013) 2888-2896.

[12] J. Gernert, R. Span, EOS-CG: A Helmholtz energy mixture model for humid gases and CCS mixtures, J. Chem. Thermodyn., 93 (2016) 274–293.

[13] H. Li, J.P. Jakobsen, Ø. Wilhelmsen, J. Yan, PVTxy properties of CO_2 mixtures relevant for CO_2 capture, transport and storage: Review of available experimental data and theoretical models, Appl. Energy, 88 (2011) 3567-3579.

[14] H. Li, Ø. Wilhelmsen, Y. Lv, W. Wang, J. Yan, Viscosities, thermal conductivities and diffusion coefficients of CO_2 mixtures: Review of experimental data and theoretical models, Int. J. Greenh. Gas Control, 5 (2011) 1119-1139.

[15] M. Hammer, Å. Ervik, S.T. Munkejord, Method Using a Density–Energy State Function with a Reference Equation of State for Fluid-Dynamics Simulation of Vapor–Liquid–Solid Carbon Dioxide, Industrial & Engineering Chemistry Research, 52 (2013) 9965-9978.

[16] S.W. Løvseth, H.G.J. Stang, A. Austegard, S.F. Westman, R. Span, R. Wegge, Measurements of CO_2-rich mixture properties: status and CCS needs, Energy Proc., 86 (2016) 469-478.

[17] H. Jacob Stang, S.W. Løvseth, S.Ø. Størset, B. Malvik, H. Rekstad, Accurate Measurements of CO_2 Rich Mixture Phase Equilibria Relevant for CCS Transport and Conditioning, Energy Proc., 37 (2013) 2897-2903.

[18] S.F. Westman, H.G.J. Stang, S.W. Løvseth, A. Austegard, S.Ø. Størset, Vapor-liquid equilibrium data for the carbon dioxide and nitrogen (CO_2 + N_2) system at the temperatures 223, 270, 298 and 303 K and pressures up to 18 MPa, Fluid Phase Equilib., 409 (2016) 207-241.

[19] S.F. Westman, H.G.J. Stang, S.W. Løvseth, A. Austegard, I. Snustad, I.S. Ertesvåg, Vapor-liquid equilibrium data for the carbon dioxide and oxygen ($CO_2 + O_2$) system at the temperatures 218, 233, 253, 273, 288 and 298 K and pressures up to 14 MPa, Fluid Phase Equilib., 421 (2016) 67-87.

[20] E. Petropoulou, E. Voutsas, S.F. Westman, A. Austegard, H.G.J. Stang, S.W. Løvseth, Vapor - liquid equilibrium of the carbon dioxide/methane mixture at three isotherms, Accepted for publishing in Fluid Phase Equilibria, 2018.

[21] S.F. Westman, H.G.J. Stang, A. Austegard, S.W. Løvseth, Vapor-liquid phase equilibrium data for the carbon dioxide and carbon monooxide (CO_2 + CO) system at the temperatures 253, 273, 283, 298 K and pressures up to 12.5 MPa, Submitted to Fluid Phase Equilibria, 2017.

[22] R.T.J. Porter, M. Fairweather, M. Pourkashanian, R.M. Woolley, The range and level of impurities in CO2 streams from different carbon capture sources, Int. J. Greenh. Gas Control, 36 (2015) 161-174.

[23] S.T. Munkejord, M. Hammer, S.W. Løvseth, CO_2 transport: Data and models – A review, Appl. Energy, 169 (2016) 499-523.

[24] A. Jäger, R. Span, Equation of State for Solid Carbon Dioxide Based on the Gibbs Free Energy, J. Chem. Eng. Data, 57 (2012) 590-597.

[25] G.T. Preston, E.W. Funk, J.M. Prausnitz, Solubilities of hydrocarbons and carbon dioxide in liquid methane and in liquid argon, The Journal of Physical Chemistry, 75 (1971) 2345-2352.

[26] G. Tsankova, M. Richter, A. Madigan, P.L. Stanwix, E.F. May, R. Span, Characterisation of a microwave re-entrant cavity resonator for phase-equilibrium measurements and new dew-point data for a (0.25 argon + 0.75 carbon dioxide) mixture, J. Chem. Thermodyn., 101 (2016) 395-404.

[27] G. Tsankova, P.L. Stanwix, E.F. May, M. Richter, Densities, Dielectric Permittivities, and Dew Points for (Argon + Carbon Dioxide) Mixtures Determined with a Microwave Re-entrant Cavity Resonator, Journal of Chemical & Engineering Data, 62 (2017) 2521-2532.

[28] M. Ben Souissi, M. Richter, Yang, X, Kleinrahm, R, Span, R., Vapor-Phase (p , ρ, T , x) Behavior and Virial Coefficients for the (Argon + Carbon Dioxide) System, Journal of Chemical & Engineering Data, 62 (2016) 362-369.

[29] X. Yang, M. Richter, M.A. Ben Souissi, R. Kleinrahm, R. Span, Vapor-Phase (p , ρ, T, x) Behavior and Virial Coefficients for the Binary Mixture (0.05 Argon + 0.95 Carbon Dioxide) over the Temperature Range from (273.15 to 323.15) K with Pressures up to 9 MPa, Journal of Chemical & Engineering Data, 61 (2016) 2676–2681.

[30] R. Wegge, M.O. McLinden, R.A. Perkins, M. Richter, R. Span, Speed-of-Sound Measurements in (Argon + Carbon Dioxide) over the Temperature Range from (275 to 500) K at Pressures up to 8 MPa, J. Chem. Thermodyn., 99 (2016) 54–64.

[31] R. Span, W. Wagner, A new equation of state for carbon dioxide covering the fluid region from the triple-point temperature to 1100 K at pressures up to 800 MPa, J. Phys. Chem. Ref. Data, 25 (1996) 1509-1596.

[32] O. Kunz, R. Klimeck, W. Wagner, M. Jaeschke, The GERG-2004 wide-range equation of state for natural gases and other mixtures, VDI Verlag, Düsseldorf, Germany, 2007.

[33] O. Kunz, W. Wagner, The GERG-2008 Wide-Range Equation of State for Natural Gases and Other Mixtures: An Expansion of GERG-2004, J. Chem. Eng. Data, 57 (2012) 3032-3091.

[34] H. Li, J. Yan, Evaluating cubic equations of state for calculation of vapor–liquid equilibrium of CO_2 and CO_2-mixtures for CO_2 capture and storage processes, Appl. Energy, 86 (2009) 826-836.

[35] S. Lasala, P. Chiesa, R. Privat, J.-N. Jaubert, VLE properties of CO_2 – Based binary systems containing N_2, O_2 and Ar: Experimental measurements and modelling results with advanced cubic equations of state, Fluid Phase Equilib., 428 (2016) 18-31.

[36] D. Köpke, Verfahrenstechnik der CO_2-Abscheidung aus CO_2-reichen Oxyfuel-Rauchgasen, Dr.-Ing, Technischen Universität Hamburg-Harburg, 2010.

[37] D. Köpke, R. Eggers, Experimentelle Untersuchungen des Phasengleichgewichts des Systems Kohlendioxid/Argon und Literaturauswertung zum System Kohlendioxid/Schwefeldioxid, Chem. Ing. Tech., 79 (2007) 1235–1239.

[38] C. Coquelet, A. Valtz, F. Dieu, D. Richon, P. Arpentinier, F. Lockwood, Isothermal P, x, y data for the argon + carbon dioxide system at six temperatures from 233.32 to 299.21 K and pressures up to 14 MPa, Fluid Phase Equilib., 273 (2008) 38-43.

[39] G.-I. Kaminishi, Y. Arai, S. Saito, S. Maeda, Vapor-liquid equilibria for binary and ternary systems containing carbon dioxide, J. Chem. Eng. Jpn., 1 (1968) 109-116.

[40] M. Ahmad, J. Gernert, E. Wilbers, Effect of impurities in captured CO_2 on liquid–vapor equilibrium, Fluid Phase Equilib., 363 (2014) 149-155.

[41] W.W. Hines, D.C. Montgomery, Probability and Statistics in Engineering and Management Science, 3 ed., John Wiley & Sons, New York, USA, 1990.

[42] Evaluation of measurement data — Guide to the expression of uncertainty in measurement (GUM), JCGM, 2008.

[43] E. Sarashina, Y. Arai, S. Sasto, The p-v-t-x relation for the carbon dioxide-argon system, J. Chem. Eng. Jpn., 4 (1971) 379-381.

[44] O. Fandiño, J.P.M. Trusler, D. Vega-Maza, Phase behavior of (CO_2 + H_2) and (CO_2 + N_2) at temperatures between (218.15 and 303.15) K at pressures up to 15 MPa, Int. J. Greenh. Gas Control, 36 (2015) 78-92.

[45] A. Jäger, R. Span, Equation of State for Solid Carbon Dioxide Based on the Gibbs Free Energy, Journal of Chemical & Engineering Data, 57 (2012) 590-597.

[46] G. Soave, Equilibrium constants from a modified Redlich-Kwong equation of state, Chem. Eng. Sci., 27 (1972) 1197-1203.

[47] Ø. Wilhelmsen, A. Aasen, G. Skaugen, P. Aursand, A. Austegard, E. Aursand, M.A. Gjennestad, H. Lund, G. Linga, M. Hammer, Thermodynamic Modeling with Equations of State: Present Challenges with Established Methods, Industrial & Engineering Chemistry Research, 56 (2017) 3503-3515.

[48] D.Y. Peng, D.B. Robinson, A new two-constant equation of state, Ind. Eng. Chem. Fundam., 15 (1976) 59-64.

[49] D.S.H. Wong, S.I. Sandler, A theoretically correct mixing rule for cubic equations of state, AlChE J., 38 (1992) 671-680.

[50] P.M. Mathias, T.W. Copeman, Extension of the Peng-Robinson equation of state to complex mixtures: Evaluation of the various forms of the local composition concept, Fluid Phase Equilib., 13 (1983) 91-108.

[51] H. Renon, J.M. Prausnitz, Local compositions in thermodynamic excess functions for liquid mixtures, AlChE J., 14 (1968) 135-144.

[52] P.T. Boggs, R.H. Byrd, J.E. Rogers, R.B. Schnabel, User's Reference Guide for ODRPACK Version 2.01 Software for Weighted Orthogonal Distance Regression, National Institute of Standards and Technology (NIST), Gaithersburg, Maryland, USA, 1992.

[53] P. Ungerer, B. Tavitian, A. Boutin, Applications of molecular simulation in the oil and gas industry: Monte Carlo methods, Editions Technip, 2005.

[54] V. Lachet, T. de Bruin, P. Ungerer, C. Coquelet, A. Valtz, V. Hasanov, F. Lockwood, D. Richon, Thermodynamic behavior of the CO_2+SO_2 mixture: Experimental and Monte Carlo simulation studies, Energy Proc., 1 (2009) 1641-1647.

[55] I.H. Bell, A. Jäger, Calculation of critical points from Helmholtz-energy-explicit mixture models, Fluid Phase Equilib., 433 (2017) 159–173.

[56] E.W. Lemmon, R.T. Jacobsen, A Generalized Model for the Thermodynamic Properties of Mixtures, Int. J. Thermophys., 20 (1999) 825-835.

[57] C. Tegeler, R. Span, W. Wagner, A New Equation of State for Argon Covering the Fluid Region for Temperatures From the Melting Line to 700 K at Pressures up to 1000 MPa, J. Phys. Chem. Ref. Data, 28 (1999) 779–850.

[58] R. Span, Multiparameter Equations of State - An Accurate Source of Thermodynamic Property Data, 1. Auflage ed., Springer Verlag, Berlin, 2000.

[59] E.W. Lemmon, I.H. Bell, M.L. Huber, M.O. McLinden, NIST Standard Reference Database 23: Reference Fluid Thermodynamic and Transport Properties-REFPROP, Version 9.1.1, National Institute of Standards and Technology, Standard Reference Data Program, Gaithersburg, USA, 2014.

[60] R. Span, T. Eckermann, S. Herrig, S. Hielscher, A. Jäger, M. Thol, TREND. Thermodynamic Reference and Engineering Data 3.0, Lehrstuhl für Thermodynamik, Ruhr-Universität Bochum, Bochum, 2016.

[61] E.W. Lemmon, R.T. Jacobsen, A New Functional Form and New Fitting Techniques for Equations of State with Application to Pentafluoroethane (HFC-125), J. Phys. Chem. Ref. Data, 34 (2005) 69–108.

[62] I. Al-Siyabi, Effect of impurities on CO_2 stream properties, PhD, Heriot-Watt University, 2013.

[63] W.H. Abraham, C.O. Bennett, The Compressibility of Carbon Dioxide-Argon Mixtures, AlChE J., 6 (1960) 257–261.

[64] V.V. Altunin, O.D. Koposhilov, Thermal Properties of Gaseous Mixtures of Carbon Dioxide-Argon at Elevated Temperatures., Trudy Moskovskogo Energeticheskogo Instituta, 313 (1976) 20–23.

[65] V.V. Altunin, O.D. Koposhilov, An Experimental Investigation of the Thermal Properties of Gaseous Mixtures of Carbon Dioxide and Argon, Thermal Engineering (Engl.Transl.), 24 (1977) 66–70.

[66] J. Kestin, Y. Kobayashi, R.T. Wood, The viscosity of four binary, gaseous mixtures at 20° and 30°C, Physica, 32 (1966) 1065–1089.

[67] N.D. Kosov, I.S. Brovanov, Compressibility of a binary mixture of argon and nitrogen at different concentrations in the 59 - 590 bar pressure range, J.Eng.Phys., 36 (1979) 413–417.

[68] M. Mantovani, P. Chiesa, G. Valenti, M. Gatti, S. Consonni, Supercritical pressure–density–temperature measurements on CO_2–N_2, CO_2–O_2 and CO_2–Ar binary mixtures, The Journal of Supercritical Fluids, 61 (2012) 34–43.

[69] W. Schönmann, Messung der thermischen Eigenschaften und Aufstellung einer empirischen Zustandsgleichung gasförmiger Argon-Kohlendioxid-Gemische, Universität Karlsruhe (TH), 1971.

[70] J. Wang, Z. Wang, D. Ryan, C. Lan, A study of the effect of impurities on CO_2 storage capacity in geological formations, Int. J. Greenh. Gas Control, 42 (2015) 132-137.

[71] R. Wegge, Thermodynamic Properties of the (Argon + Carbon Dioxide) System: Instrument Development with Density and Speed-of-Sound Measurements: Dissertation, Ruhr-Universität Bochum, 2016.

[72] X. Yang, M. Richter, Z. Wang, Z. Li, Density measurements on binary mixtures (nitrogen+carbon dioxide and argon+carbon dioxide) at temperatures from (298.15 to 423.15)K with pressures from (11 to 31)MPa using a single-sinker densimeter, J. Chem. Thermodyn., 91 (2015) 17–29.

[73] J.P. Strakey, C.O. Bennett, B.F. Dodge, Joule-Thomson coefficients of argon-carbon dioxide mixtures, AlChE J., 20 (1974) 803–814.

[74] T.K. Bose, R.H. Cole, Dielectric and Pressure Virial Coefficients of Imperfect Gases. II. CO_2-Argon Mixtures, J. Chem. Phys., 52 (1970) 140–147.

[75] T.L. Cottrell, R.A. Hamilton, R.P. Taubinger, The second virial coefficients of gases and mixtures. Part 2.-Mixtures of carbon dioxide with nitrogen, oxygen, carbon monoxide, argon and hydrogen, Transactions of the Faraday Society, 52 (1956) 1310-1312.

[76] M.L. Martin, R.D. Trengove, K.R. Harris, P.J. Dunlop, Excess second virial coefficients for some dilute binary gas mixtures, Aust. J. Chem., 35 (1982) 1525-1529.

[77] H. Schmiedel, R. Gehrmann, B. Schramm, Die zweiten Virialkoeffizienten verschiedener Gasmischungen im Temperaturbereich von 213 bis 475 K, Berichte der Bunsengesellschaft für physikalische Chemie, 84 (1980) 721-724.

[78] B. Schramm, W. Müller, Messungen des zweiten Virialkoeffizienten von Gasen und Gasmischungen bei Zimmertemperatur mit einer Expansionsapparatur, Berichte der Bunsengesellschaft für physikalische Chemie, 86 (1982) 110-112.

[79] A. Jäger, V. Vinš, R. Span, J. Hrubý, Model for gas hydrates applied to CCS systems part III. Results and implementation in TREND 2.0, Fluid Phase Equilib., 429 (2016) 55–66.